# CYCLES AND INTERACTIONS:
A MATHEMATICIAN AMONG BIOLOGISTS

PABLO RODRÍGUEZ-SÁNCHEZ

Propositions

1. Most mechanical systems tend to equilibrium, while most alive systems tend to limit cycles
   (this thesis)

2. Apparently abstract mathematical concepts, such as chaos, are an essential ingredient to understand natural phenomena
   (this thesis)

3. The mathematical capacities and interests of biology students tend to be greatly underestimated

4. Mathematics is no more and no less than organized thought

5. The publication of non-reproducible computational research is slowly evolving from inconvenient to unacceptable

6. The popularity of wearable health-monitoring devices opens a great opportunity for the prediction of health conditions

7. Abstract models are essential for guiding research into the functioning of the complex systems on which humanity depends

8. Society has the right of having good science communicators

Propositions accompanying the PhD thesis:
Cycles and interactions: a mathematician among biologists

P. Rodríguez-Sánchez
Wageningen, 15 June 2020

Cycles and interactions: a mathematician among biologists

Pablo Rodríguez-Sánchez

Thesis committee

Promotor
Prof. Dr Marten Scheffer
Professor of Aquatic Ecology and Water Quality Management
Wageningen University & Research

Co-promotor
Dr Egbert H. van Nes
Associate Professor, Aquatic Ecology and Water Quality Management
Wageningen University & Research

Other members
Prof. Dr J Molenaar, Wageningen University & Research
Dr E Benincà, Rijksinstituut voor Volksgezondheid en Milieu, Bilthoven
Dr V Dakos, Sorbonne Université, Paris, France
Dr J Dubbeldam, Delft University of Technology

Cycles and interactions: a mathematician among biologists

Pablo Rodríguez-Sánchez

Thesis
submitted in fulfilment of the requirements for the degree of doctor
at Wageningen University
by the authority of the Rector Magnificus
Prof. Dr A.P.J. de Mol,
in the presence of the
Thesis Committee appointed by the Academic Board
to be defended in public
on June 15th 2020
at 1:30 p.m. in the Aula.

A mis colegas y amigos de *Naukas*.
Por empujarme.

Contents

Chapter 1

Introduction

1.1 Why cycles and biology?

Most of our daily experience with dynamical systems comes from the observation of movement. The vast majority of mechanical systems we experience in our everyday life are strongly dissipative systems, which simply means that objects tend to stop. As we'll see in section 1.2, this behaviour corresponds to a point attractor. Reaching a point attractor is thus the most common long-term behaviour for mechanical systems.

While points seem to be the most common attractor of mechanical systems, biological systems often reach limit cycles, the type of attractor corresponding with cyclic behaviour. Just to name a few: neuron firing, heartbeat, walking rhythm, breathing rhythm, intestinal peristalsis, body temperature cycle, sleep-wake cycle, menstruation, seasonal hibernation and seasonal leaf abscission in deciduous plants are all obviously rhythmic or quasi-rhythmic processes, and thus potentially related to limit cycles.

Ancient cultures were already fascinated by periodicity and cycles in nature. The regularity of astronomical cycles, such as the day-night or the seasons, has been known since ancient times. Herodotus' "Histories", written in 440 BC, already mentions the yearly flooding of the Nile basin as an important social and agricultural problem. This problem triggered some seminal early research on astronomy, geometry and topography (see ch. 2 in Boyer (1968)). Prediction of eclipses, seasons and other cyclic or almost-cyclic astronomical events account among some of the first documented successes of deterministic forecasting (Querejeta (2011)). Fast forwarding to modern times, we find cycles and synchronization at the very heart of electronics, laser technology and biomedical

sciences (see, for instance, Strogatz (2003)).

Cycles, and not to mention deterministic chaos, are obviously more complex than point attractors. After a short introduction about this richer behaviour of periodic systems, I will introduce the analysis tools that we need and that are not always covered in the biologist's syllabus.

1.2 Points, cycles and chaos

In theoretical studies, biological systems are often described by a system of deterministic differential equations. That is, equations of the form 1.1, where $\vec{x}$ is a vector containing each of the states, t is the time and $\vec{f}$ a flow function defining the dynamics.

$$\frac{d\vec{x}}{dt} = \vec{f}(\vec{x}, t) \tag{1.1}$$

If time is not explicitly present in the flow function (as in equation 1.2), we say that our system is autonomous. Autonomous systems are particularly easy to visualize and analyze, and are the only ones that we are going to deal with in the present thesis.

$$\frac{d\vec{x}}{dt} = \vec{f}(\vec{x}) \tag{1.2}$$

Although cyclic behaviour in biological models is often induced by explicitly time-depending external periodic forcings (typically representing an astronomical phenomenon such as the day/night cycle, the tides or the seasons), it is often possible to rewrite the equations

as autonomous by an appropriate choice of coordinates. We'll have to do this later, in the equation 4.1 of **chapter 4**.

One of the basic problems of dynamical systems theory is to determine the behaviour of such system in the long term. This concept is known by physicists and mathematicians as asymptotic behaviour. The states that are reached by the system are known as attractors (Strogatz, 1994).

In models of biological systems, three types of asymptotic behaviour appear very often: stabilization, periodic regimes and chaos. Each of them corresponds, respectively, to point, cyclic and chaotic attractors. A quick introduction to each of them is given in the next subsections.

1.2.1 Point attractors

The simplest possible case of asymptotic behaviour is to reach a stable steady state, typically corresponding to a point attractor. This corresponds with the intuitive idea of a system reaching an equilibrium. When a dynamical system is in a steady state, it remains on it indefinitely. If, additionally, the steady state is stable, then it has associated a basin of attraction around it. Any state contained in this basin of attraction will naturally return to the stable steady state. This property makes stable steady states resilient to perturbations, as long as they are not strong enough to make the state trespass the borders of the attraction basin. Unstable steady states lack this recovery capacity, and thus, are extremely sensitive to perturbations. The "attractor" corresponding to an unstable steady state receives the eloquent name of point repeller (Strogatz, 1994). An example of a point attractor is given in figure 1.1.
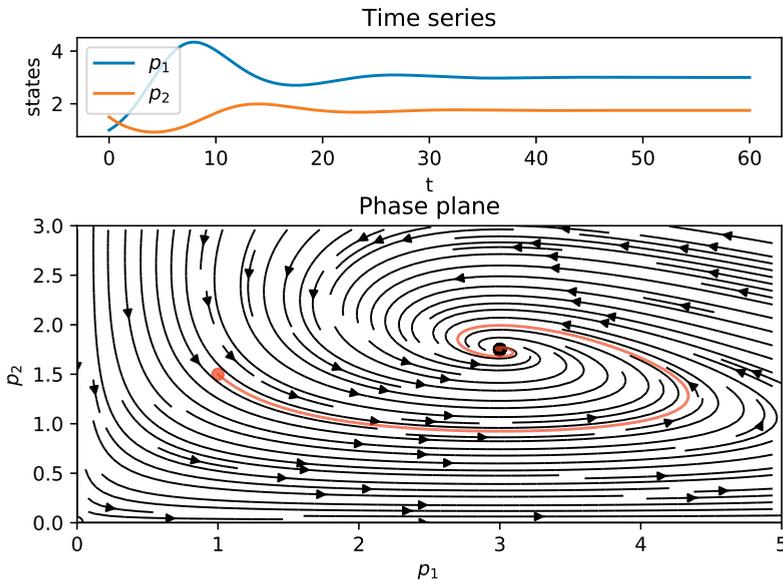
Figure 1.1: Example of a point attractor. The represented system is a Rosenzweig-MacArthur predator-prey model (Rosenzweig and MacArthur, 1963). p_1 and p_2 represent the populations a prey and a predator species, respectively. The time series shown in the upper panel corresponds to the red trajectory in the state space. Notice how the time series stabilize, and the trajectory in the state space spirals down to an attracting point.

Point attractors and point repellers are the two easiest examples of a fixed point. A fixed point is a state that doesn't experience any change under the dynamical equations. In the context of ordinary differential equations such as 1.2, the position of the fixed points is thus given by the roots of the dynamical equation (that is, the solutions to $\vec{f}(\vec{x}^*) = \vec{0}$).

Thanks to their relative simplicity, fixed points had a very impor-

tant role in the historical development of dynamical systems theory. As they are points (i.e., dimensionless objects) it is possible to analyze their behaviour using an infinitesimally small region around them. Inside this region, the dynamical equations can be replaced by a linear Taylor expansion (Simmons, 1996) centered around the attractor (Strogatz, 1994). Such a linear dynamical system is analytically solvable and, as always happens with linear functions, all its properties are summarized in the list of eigenvalues and corresponding eigenvectors (see Strang (2006) or any other introduction to linear algebra). One of those eigenvalues is particularly relevant: the one with the maximum real part. It is known as the dominant eigenvalue (λ_{max}), and can be used to measure the rate of divergence or convergence of nearby orbits (Strogatz, 1994; Sandri, 1996). λ_{max} contains relevant information about the stability of the limit point. Specifically, the sign of the real part of λ_{max} gives the overall attractiveness/repulsiveness of the point (negative for attractive, positive for repulsive). A λ_{max} with a real part exactly equal to zero is therefore not attractive nor repulsive: nearby trajectories may orbit around it without getting closer nor further. The imaginary part of any of the eigenvalues λ has the effect of introducing a rotational component to the trajectories in the phase plane. Fixed points with imaginary eigenvalues receive the eloquent name of spiral attractors or spiral repellers (Strogatz, 1994; Kuznetsov, 1998).

Gradient systems and stability landscapes

A particularly simple family of dynamical systems are those that can be expressed as the gradient of a scalar function $V(\vec{x})$ which is called the potential function or stability landscape (see equation

1.3).

$$\vec{f}(\vec{x}) = -\vec{\nabla}V \qquad (1.3)$$

The gradient $(\vec{\nabla})$ is a generalization of the concept of derivative in more than one dimension. It returns a vector that points in the direction of maximum steep of the potential function $V(\vec{x})$, and a null vector at a maximum or minimum (Marsden and Tromba, 2003). For a two dimensional function $V(x,y)$, the gradient is defined as in equation 1.4:

$$\vec{\nabla}V = \left(\frac{\partial V}{\partial x}, \frac{\partial V}{\partial y}\right) \qquad (1.4)$$

More details about the gradient are available in **chapter 3** of this thesis. The relationship 1.3 allows us to use the scalar field (typically a surface) defined by $V(\vec{x})$ instead of the vector field $\vec{f}(\vec{x})$, a more complicated mathematical object, to visualize the dynamical system. The negative sign in equation 1.3 has been introduced for historical and practical reasons: it makes stable equilibria correspond with local minima of V and unstable ones with local maxima or saddle points. This means that, if we plot the state on the surface defined by V, it will just "roll downhill" until it gets trapped in the bottom of a well. This visualization trick is often referred to as stability landscape or ball-in-a-cup diagram (see for instance Beisner et al. (2003)).

It can be proven that the only attractors that a gradient system can have are non-spiraling fixed points, either attractive or repulsive. As a consequence, any system showing spirals, cyclic or chaotic attractors will be automatically non-gradient (in the sense

that it cannot be written in the form of equation 1.3, and thus, it is not equivalent to a stability landscape V anymore). Several alternative approaches have been proposed to derive pseudo stability landscapes for non-gradient systems (a complete review can be found in Zhou et al. (2012a)), but are often misunderstood in communities without a strong mathematical background (Pawlowski, 2006).

In **chapter 3** I provide an accessible explanation of why a stability landscape could fail to exist. Additionally, I introduce a novel and simple computational tool to produce stability landscapes for gradient and also weakly non-gradient systems.

1.2.2 Cyclic attractors

A more complicated type of asymptotic behaviour happens if our system reaches a periodic regime. For systems like the one described in 1.2, limit cycles are only possible if the system is non-gradient and has two or more dimensions (Strogatz, 1994). Periodic behaviour typically corresponds to a limit cycle attractor. Just as happens with fixed points (cf. subsection 1.2.1), limit cycles can be attracting or repelling. The repelling ones are obviously no attractors, and are thus of limited interest in applied models. If a system's state is on an attracting limit cycle, it will remain periodic (and with the same frequency and amplitude profile) after a perturbation. An example of a limit cycle is shown in figure 1.2.

Limit cycles are curves, so we cannot surround them by an infinitesimally small region. This makes the linearization approach, successfully used with point attractors, less useful here. Interestingly enough, we can still make use of linearization to determine

the eigenvalues (which are now called Lyapunov exponents), but in this case we should sample several of them along the whole curve. In a limit cycle, the average real part of the dominant Lyapunov exponent converges to zero (Sandri, 1996).
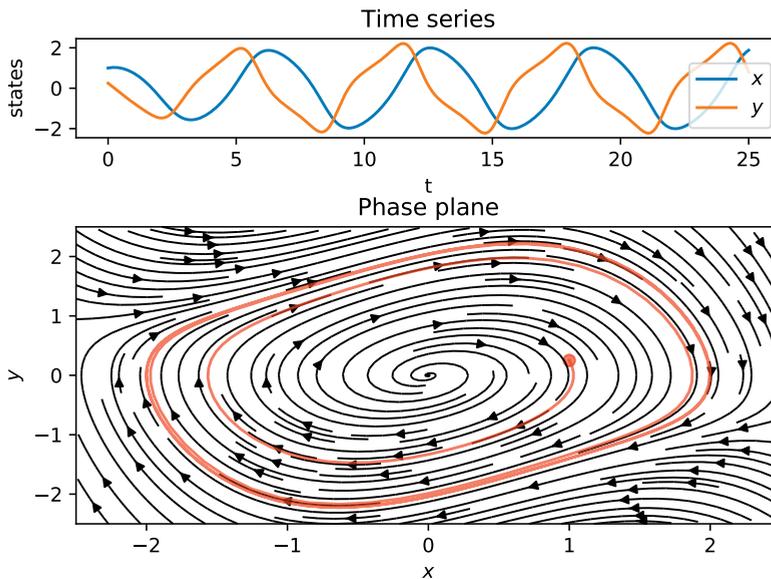

Figure 1.2: Example of a limit cycle. The represented system is a van der Pol oscillator. x and y represent two different voltages in a vacuum tube. The time series shown in the upper panel correspond to the red trajectory in the state space. Notice how the time series tends to a periodic regime, and the trajectory approaches a closed curve.

Limit cycles are easily noticed in time series by simple visual inspection. In case of requiring a more quantitative approach, several possibilities are available. The Lorenz map, for instance, is built measuring the peak-to-peak distances (Strogatz, 1994; Rinaldi et al.,

2001). If the system reaches a limit cycle, these distances should converge to the period of the system. The Poincaré map, built taking snapshots of the state of the system when the cycle intersects with an arbitrary cross section (Strogatz, 1994; Kuznetsov, 1998). This technique transforms the continuous dynamical problem in a discrete one. The stability of the limit cycle can be determined by analyzing the stability of this newly created discrete time dynamical system (Kuznetsov, 1998). A similar technique is that of the stroboscopic map (Guckenheimer and Holmes, 2002), where the state of the system is observed only in fixed time intervals $(x(t), x(t+T), x(t+2T), \dots)$. This is particularly useful in systems that are periodically forced by a perturbation of known period T. The interaction between self-sustained cycles with external periodic forcings gives rise to interesting phenomena such as chaos (Vandermeer, 1993; Doveri et al., 1993) and synchronization (Strogatz and Stewart, 1993; Pikovsky et al., 2003). Each phenomenon is treated, respectively, in subsection 1.2.3 and section 1.5 of the present chapter.

Fast Fourier transform (Press et al., 2007) can be used to identify the dominating frequencies of a time series and thus to establish if it is periodic. Methods designed to deal with chaotic time series, such as the *0-1* test (Gottwald and Melbourne, 2009), are also able to robustly detect periodic oscillations. More about the *0-1* method can be found in the subsection 1.2.3.

1.2.3 Chaotic attractors

An even more complicated type of asymptotic behaviour is deterministic chaos. If our system evolves towards a bounded region of the phase space (i.e.: if we can "build a box" around the state in

the state space, and the state never gets out of it) but, at the same time, its trajectory doesn't approach a point nor a limit cycle, then the system may have reached a chaotic attractor.

Although they may look as a theoretical construct of limited applied interest, chaotic attractors often appear in applied problems. Indeed, chaotic attractors were described for the first time in the context of a simple meteorological model (Lorenz, 1963). In biology, chaotic attractors are particularly common in population dynamics (see subsection 1.4).

Just as happened with cyclic attractors (cf. subsection 1.2.2), and for the same reasons, linearization is useless for studying chaotic attractors, but we can still get information from its Lyapunov exponents. When Lyapunov exponents are sampled along a trajectory in a chaotic attractor, the average of their real parts converge to a positive number, meaning that two neighboring trajectories will diverge exponentially in time. This leads to one of the most important properties of chaotic continuous systems: despite being deterministic, they are unpredictable in a practical sense due to their extreme sensitivity on initial conditions (see Strogatz (1994), section 9.3).

For autonomous ordinary differential equations such as 1.2, chaotic attractors are only possible in three or more dimensions (see section 7.3 of (Strogatz, 1994)). This makes their graphical representation on paper a bit challenging. In figure 1.3 we show a classical example of a chaotic attractor, the Lorenz attractor (Lorenz, 1963), projected from two different angles.
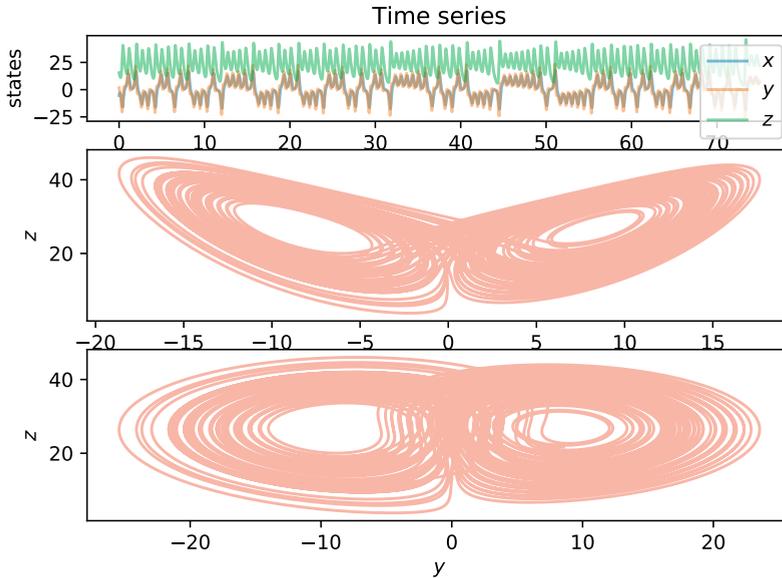
Figure 1.3: Classical example of chaotic behaviour, the Lorenz system (Lorenz, 1963). The time series shown in the upper panel corresponds to the red trajectory in the state space. In this case, the state space is three dimensional. We show two projections of the trajectory. This attractor has become part of the popular culture, and interactive 3D models can be easily found in the Internet.

A practical problem related to chaos is how to decide if an empirical time series is chaotic or not. The main challenges are to discriminate chaos from randomness and from long, complex transients. The problem with randomness doesn't exist if the time series is known to have been produced by a deterministic model, as stochasticity is automatically excluded. The problem with transients is usually solved by stabilization, i.e.: simulating for "long enough" compared to the typical time scales of the problem. The

chaoticity of an attractor in simple deterministic models can be proved analytically, but this approach is rarely feasible, and certainly never practical, in complex models (cf. section 9.4 in Strogatz (1994) to get an idea about how laborious this approach is even in a simple model). The same numerical approaches we mentioned in the context of limit cycles (subsection 1.2.2) can be used here, but they vary greatly in practical utility. Numerical estimation of Lyapunov exponents is computationally costly and requires exploring a significant portion of the attractor (Wolf et al., 1985), making it an unpractical method for systems with a high number of dimensions. The better suited numerical test for chaos detection in a time series is Gottwald-Melbourne's *0-1* test (Gottwald and Melbourne, 2009). It is remarkably easy and fast to run, and it robustly discriminates between stable equilibria, limit cycles and chaotic attractors. As with any other numerical method for assessing chaos, its performance relies on the assumptions that our time series has a deterministic source and any transient has faded away. An intuitive, geometrical explanation of Gottwald-Melbourne's *0-1* method can be found in appendix subsection 2.9.2 of chapter 2.

1.3 The dance of attractors: bifurcation theory

Applied dynamical models often contain parameters. Bifurcation theory is the branch of mathematics that deals with the effects of varying those parameters. Bifurcation theory is particularly relevant in biological systems, where most parameters in the dynamical models implicitly depend on external, variable factors such as the

temperature, the intensity of competition or the fishing pressure (Scheffer, 2009).

A change in the value of a parameter can affect the position, stability or number of attractors and, thus, the long term behaviour of the system. Small changes in a parameter most often will lead to small quantitative changes in the behaviour of the system (such as small displacements in the positions of the fixed points or small changes in a limit cycle's period and amplitude), but more complicated phenomena can appear in this dance of attractors around the phase space. A stable and an unstable point can collide and annihilate each other, giving rise to a saddle-node bifurcation. After a saddle-node bifurcation an ecosystem can evolve from bistability to monostability, giving rise to hysteresis and potentially irreversible shifts in the population composition (Scheffer et al., 2001). A stable point attractor can develop into a limit cycle (phenomenon known as Hopf bifurcation), or a limit cycle into a chaotic one. These processes that qualitatively change the dynamics are known as bifurcations, and there is a rich taxonomy of them (Crawford, 1991; Kuznetsov, 1998).

When a system is operating near a bifurcation, a small variation in its parameters and/or a small perturbation in the system's state can give rise to a transition to a completely different dynamical regime (Scheffer, 2009). The saddle-node bifurcation is particularly interesting for several reasons. To begin with, it often appears in biological models as diverse as water management (Van Nes et al., 2007) or coral reef growth (van de Leemput et al., 2016). As a straightforward side effect, those systems will show alternative stable states and, potentially, critical transitions and hysteresis (Van Nes et al., 2007; Scheffer, 2009). Last but not least, this bifurcation is preceded by the phenomenon of critical slowing down (Scheffer et al.,

2009; Dakos et al., 2012). This phenomenon can be numerically detected and quantified in a time series, opening the possibility of measuring the resilience of the system (understood as its capacity to return to the original equilibrium state after a perturbation).

1.4 Cycles, chaos and biodiversity

One of the subfields of biology where dynamical systems theory is intensively used is population dynamics. Experiments in ecology are particularly costly in time and resources. The theoretical and computational study of interactions between populations, that is, the field of population dynamics, represents a cheap alternative to fully experimental approaches. As often happens when buying cheap, this has a hidden cost: many of the ideas of population dynamics have not been experimentally confirmed. Evidence from models should thus not be given the same status as evidence from observations. Models in population dynamics should just be taken as tools to help us thinking. Interestingly enough, models proved also particularly useful when they led to the wrong predictions, as that shows that the models are too simple to describe reality. Such negative results may inspire many follow-up studies (see 1.4.1).

Population dynamics models are often written in the form of continuous differential equations, and can thus be written in the form of equation 1.2. Most of them describe many species, having thus many states. Additionally, the interactions are rarely linear. Consequently, they can show any of the asymptotic behaviours mentioned in section 1.2. A straightforward question is then: what is the probability for these different kinds of asymptotic behaviours,

given a certain model and an average interaction strength?

Observation and experiments show that the interaction between predators and prey may lead to cycles in nature (Elton and Nicholson, 1942; Veilleux, 1979). This type of systems has been described already by the famous model of Lotka and Volterra (Volterra, 1926) and more realistically by Rosenzweig and Macarthur (Rosenzweig and MacArthur, 1963). Another classical example worth mentioning is that of Ludwig (Ludwig et al., 1978) trying to shed some light on the cyclic outbreaks of spruce budworms (*Choristoneura fumiferana*), a fascinating phenomenon well known by field ecologists and naturalists.

Chaotic dynamics have been observed in models of plankton dynamics (May, 1974). Modelled ecosystems have been used to establish theoretical links between chaos and biodiversity (Huisman and Weissing, 1999) and between chaos and predictability (Huisman and Weissing, 2001). Although the role of chaos in real ecosystems has been a controversial topic in the past (Berryman and Millstein, 1989; Scheffer et al., 2003), the appearance of chaotic dynamics in simple ecosystems has been experimentally shown in chemostats (Benincà et al., 2008).

1.4.1 Attractors and the competitive exclusion principle

The methods of population dynamics resemble that of physics or mathematics, and often its results look like physical laws. The analysis of some early mathematical models, particularly those reaching point attractors, popularized the idea of the competitive exclusion principle, also known as Gause's law. It briefly states that

"complete competitors cannot coexist" (Hardin, 1960). Although it sounds as a general law of nature, a deeper read will make anyone with notions of epistemology raise her/his eyebrow: *"The statement given above has been very carefully constructed: every one of the four words is ambiguous. This formulation has been chosen not out of perversity but because of a belief that it is best to use that wording which is least likely to hide the fact that we still do not comprehend the exact limits of the principle"* (Hardin, 1960). The precise meaning of the words "principle" and "law" hardly apply here, and it seems that actually we are talking of a conjecture. Observational and experimental counterexamples to the "principle" were already known at the time it was published. Even more, later mathematical models showed that the principle of competitive exclusion can be easily violated if the system under study reaches an attractor other than a point attractor, such as a limit cycle (Armstrong and McGehee, 1980). The literature contains several other counterexamples showing violations of the principle, either theoretically or experimentally. The "paradox of the plankton" (Hutchinson, 1961), namely the enormous diversity of plankton species in such a remarkably uniform environment as lakes or open sea, deserves an honor position.

Principle or conjecture, the idea of competitive exclusion has been a useful cornerstone of ecological theory for more than half a century. Interestingly enough, the intentional ambiguous definition of the "principle" did its magic: the literature on potential mechanisms that could prevent competitive exclusion and explain the "paradox of the plankton" is very extensive (Scheffer et al., 2003). One of the main hypotheses is that some ecosystems are intrinsically out of equilibrium, either due to constantly varying external conditions (Hutchinson, 1959) or to intrinsic cyclic or chaotic

asymptotic behaviour (Huisman and Weissing, 1999; Benincà et al., 2008). Another interesting hypothesis is the so called "neutral theory of biodiversity" (Hubbell, 2003), proposing that species that are equivalent can coexist because they are unable to outcompete each other.

In **chapter 2** I contribute to this lively debate. Using numerical models, I show that both the neutral and the non-equilibrium hypotheses are not independent. Particularly, near-neutrality leads simultaneously to non-equilibrium dynamics (such as cycles or chaos) and to a higher biodiversity.

1.5 Cycles and biological synchronization

Predator prey cycles are not the only cyclic phenomena in biology. Several cyclic phenomena are of outmost importance for the physiology of living beings. Examples of such cycles of biomedical interest could be heartbeat, breathing, walking rhythms or sleep-wake patterns. Additionally, organisms are subject to cyclic external forcings. The astronomical cycles, such as the day/night and the yearly shift of seasons, are the most obvious examples of those forcings (Strogatz and Stewart (1993)).

The pioneering experiments of the French polymath Jean-Jacques d'Ortous de Mairan showed that organisms have an intrinsic capacity to generate rhythms (d'Ortous de Mairan (1729)). By intrinsic we mean that, in the absence of an external cue, they remain periodic. Those intrinsic cycles such as circadian rhythms show a similar frequency to the one imposed by the external influ-

ences. This synchronization capacity invites to think of an organism as an oscillator tuned to a given intrinsic frequency, and coupled with an external forcing (Strogatz (2003), Foster and Kreitzman (2017)).

The phenomenon of coupling the organism's inner cycles with the external forcing is known as synchronization. The ability to synchronize is, perhaps unsurprisingly, known to be a survival advantage (Foster and Kreitzman, 2017). Some health conditions, such as insomnia or arrhythmia, are related to a deficit in this synchronization capacity (Glass (2001)).

Examples from sleep research are particularly illuminating. Sleeping is a phenomenon that we are all familiar with, and the disadvantages of irregular sleep are obvious to anyone. Experiments performed with isolated individuals in caves (Siffre (1975)) and special soundproofed and window-less apartments (Czeisler (1979)) showed that most humans have an intrinsic sleep-wake period slightly longer than 24 h. An experiment performed by the U.S. Navy tried to force sleep-wake cycles of 18 h (6 of work, 6 of leisure and 6 of sleep) by taking advantage of the isolation of submarines' crews (Kelly et al. (1999)). The results were unsatisfactory, proving that there are limits to our capacity of synchronizing with an external cue if its frequency is too far from our intrinsic one.

Kuramoto's model (introduced in Kuramoto (1975)) captures all the key features of synchronization in a remarkably simple way. This minimal but surprisingly rich model has been successfully applied to several physical, biological and biomedical systems (see Strogatz (2000)). The mechanism of desynchronizing in such a model happens through a bifurcation known as saddle-node of cycles (Strogatz, 1994).

As the name suggests, the saddle-node of cycles is closely related to the saddle-node bifurcation. While dynamical indicators of resilience (DIORs) have been derived for the latter (Scheffer et al., 2009; Dakos et al., 2012), there are not DIORs for the saddle-node of cycles. In **chapter 4** I analyze Kuramoto's model and derive a method to assess the desynchronization risk from a time series.

1.6   Thesis overview

The backbone of this thesis is the interdisciplinary interaction between dynamical systems theory and a selection of problems of biological and biomedical interest. In the present chapter we introduced the basic mathematical tools that are going to be needed along the thesis. Ordinary differential equations of the form 1.2 are used to simulate food webs (**chapters 2 and 3**), circadian rhythms such as sleep-wake cycles (**chapter 4**) and simple models of regulatory gene networks and glycolysis (**chapter 3**).

In **chapter 2** we use a classical plankton predator-prey model to analyze the relationship between heterogeneity at the prey level and the probability of developing cyclic or chaotic dynamics. Due to the complexity and the dimensionality of the system under study, we rely on numerical simulations. In the spirit of bifurcation theory, we control the heterogeneity of the interactions between prey species with a single parameter. We generated a few thousands of *in silico* ecosystems differing in their neutrality parameter, and assessed the type of attractor reached using Gottwald-Melbourne's *0-1* test. We show that more heterogeneity significantly increases the chances of non-equilibrium dynamics and, additionally, of biodiversity.

In **chapter 3** we clarify some misunderstandings that exist around the concept of stability landscape in multidisciplinary research communities. We explain that such landscapes cannot be derived for non-gradient systems. In order to reach all audiences regardless of their interest/expertise in mathematics, we use spirals and cyclic dynamics, together with a metaphor from the artwork of M.C. Escher, as a transparent equation-free explanation. Additionally, we provide a novel and simple algorithm to calculate (pseudo)stability landscapes for systems that are only weakly non-gradient. The algorithm has a built-in safety protocol that warns the user with an error map indicating in which regions the stability landscape is reliable.

In **chapter 4** we use a two-oscillator Kuramoto model to represent a physiological variable potentially synchronized with the diurnal cycle. We explore the border between synchronized and desynchronized cycles and show that the phenomenon of loss of synchronization in this general model happens through a saddle-node bifurcation. We adapt the methods from Dakos et al. (2009) and derive two practical indicators to forecast desynchronization before it happens from time series data. We use sleep-wake models as a case study for proving the generality of our indicators.

In **chapter 5** I reflect on the potential of our results, and also on their limitations. In addition I discuss the more human side of performing the work presented in this thesis, sharing some of the lessons learned during my journey from physics to biology.

Chapter 2

Neutral competition boosts cycles and chaos in simulated food webs

Abstract

Similarity of competitors has been proposed to facilitate coexistence of species because it slows down competitive exclusion, thus making it easier for equalizing mechanisms to maintain diverse communities. On the other hand, previous studies suggest that chaotic ecosystems can have a higher biodiversity. Here we link these two previously unrelated findings, by analyzing the dynamics of food web models. We show that near-neutrality of competition of prey, in the presence of predators, increases the chance of developing chaotic dynamics. Moreover we confirm that chaotic dynamics correlate with a higher biodiversity.

2.1   Background

Ever since Darwin, the idea that species must be sufficiently different to coexist is deeply rooted in biological thinking. Indeed, the principles of limiting similarity (Macarthur and Levins, 1967) and competitive exclusion (Hardin, 1960; Armstrong and McGehee, 1980) are the cornerstones of ecological theory. Nevertheless, natural communities (such as plankton communities (Hutchinson, 1961)), often harbor far more species that may be explained from niche separation, inspiring G. Evelyn Hutchinson (Hutchinson, 1959) to ask the simple but fundamental question *"why are there so many kinds of animals?"*. Since then many mechanisms have been suggested that may help similar species to coexist. As Hutchinson (Hutchinson, 1961) already proposed himself, fluctuations in conditions may prevent populations to reach equilibrium at which species would be outcompeted. Also, natural enemies including pests and parasites tend to attack the abundant species more than rare species, and such a *"kill the winner"* (Winter et al., 2010) mechanism promotes diversity by preventing one species to become dominant.

In the extensive literature on potential mechanisms that could prevent competitive exclusion there are two relatively new ideas that have created some controversy: neutrality and chaos. The neutral theory of biodiversity introduced by Hubbell (Hubbell, 2003) proposes that species that are entirely equivalent can coexist because none is able to outcompete the other. In the case of near-neutral communities, although *sensu stricto* the exclusion will happen eventually, the exclusion process will take a very long time to finalize. The concept of equivalent species has met skepticism as it is incompatible with the idea that all species are different.

However, it turns out that also *"near-neutral"* competitors can co-exist in models of competition and evolution (Scheffer and van Nes, 2006; Scheffer et al., 2018). Support for such near-neutrality has been found in a wide range of communities (Segura et al., 2011, 2013; Vergnon et al., 2013). The second controversial mechanism that may prevent competitive exclusion is *"super-saturated coexistence"* in communities that display chaotic dynamics (Huisman and Weissing, 1999). This is in a sense analogous to the prevention of competitive exclusion in fluctuating environments, except that deterministic chaos is internally driven. Although there has been much debate about the question whether chaotic dynamics plays an important role in ecosystems (Berryman and Millstein, 1989; Scheffer, 1991; Schippers et al., 2001), several studies support the idea that chaos can be an essential ingredient of natural dynamics (Huisman and Weissing, 1999; Benincà et al., 2008, 2015).

In the present work, we used a multi-species food-web model to explore the effect of near-neutrality of prey on the probability of developing chaotic dynamics. We found a surprising link between both ideas: the closer to neutrality the competition is, the higher the chances of developing chaotic dynamics. Additionally, our results confirmed that there is a robust positive correlation between cyclic or chaotic dynamics and the number of coexisiting species.

2.2 Material and methods

2.2.1 Model description

We focused our attention on food webs with two trophic levels, competing prey and predators. The predators have a differentiated

preference of different prey species.

The dynamics were modelled using the Rosenzweig-MacArthur predator-prey model (Rosenzweig and MacArthur, 1963), generalized to a higher number of species (van Nes and Scheffer, 2004). Our model contains n_P prey species and n_C predator species. The prey's populations are under the influence of both intra and interspecific competition, whose intensities are defined by the competition matrix A. The relative preference that predators have for each prey is defined by the predation matrix S. Prey immigration from neighboring areas has been added to the classical model in order to avoid unrealistic dynamics, such as heteroclinic orbits giving rise to long-stretched cycles with near extinctions (van Nes and Scheffer, 2004). In mathematical notation, the system reads:

$$\begin{cases} \frac{dP_i}{dt} = r_i(P)P_i - \sum_{j=1}^{n_C} g_j(P)P_i S_{ji} C_j + f & : i = 1..n_P \\ \frac{dC_j}{dt} = -lC_j + e\sum_{i=1}^{n_P} g_j(P)P_i S_{ji} C_j & : j = 1..n_C \end{cases} \quad (2.1)$$

where $P_i(t)$ represents the biomass of prey species i at time t and $C_j(t)$ the biomass of predator species j at time t. The symbol P is used as a shorthand for the vector $(P_1(t), P_2(t), ..., P_{n_P}(t))$. The auxiliary functions $r_i(P)$ and $g_j(P)$ (see equations (2.2) and (2.3)) have been respectively chosen to generalize the logistic growth and the Holling type II saturation functional response (Edelstein-Keshet, 2005) to a multispecies system when inserted into equation (2.1).

$$r_i(P) = r\left(1 - \frac{1}{K}\sum_{k=1}^{n_P} A_{ik}P_k\right) \quad (2.2)$$

$$g_j(P) = \frac{g}{\sum_{i=1}^{n_P} S_{ji}P_i + H} \quad (2.3)$$

For details about the parameters used, please refer to subsection 2.2.2.

2.2.2   Parameterization

We parameterized our model as a freshwater plankton system based on Dakos' model (Dakos et al., 2009). Unlike Dakos, who uses seasonally changing parameters, our parameters were assumed to be independent of time (see table 2.1).

Table 2.1: Values and meanings of the parameters used in our numerical experiment. The elements of the predation (S) and competition (A) matrices are drawn from probability distributions described in subsection 2.2.2.

Symbol	Interpretation	Value	Units
r	Maximum growth rate	0.50	d^{-1}
K	Carrying capacity	10.00	$mg\ l^{-1}$
g	Predation rate	0.40	d^{-1}
f	Immigration rate	10^{-5}	$mg\ l^{-1}\ d^{-1}$
e	Assimilation efficiency	0.60	1
H	Saturation constant	2.00	$mg\ l^{-1}$
l	Predator's loss rate	0.15	d^{-1}
S	$n_C \times n_P$ predator preference matrix	See section 2.2.2	1
A	$n_P \times n_P$ competition matrix	See section 2.2.2	1

Competition and predation matrices

Our main purpose is to analyze the effect of different competition strengths on the long term dynamics exhibited. For this, we introduce the competition parameter ϵ to build a competition matrix A, whose non-diagonal terms are drawn from a uniform distribution centered at $1 + \epsilon$ and with a given width (here we chose $w = 0.05$). The diagonal terms are by definition equal to 1. Defined this way, the parameter ϵ allows us to move continuously from strong intraspecific ($\epsilon < 0$) to strong interspecific competition ($\epsilon > 0$), meet-

ing neutral-on-average competition at $\epsilon = 0$. For the rest of this paper, we will call ecosystems with $\epsilon = 0$ *near-neutral* (see figure 2.1).
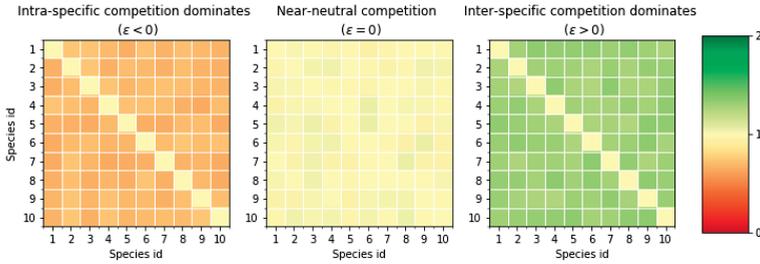

Figure 2.1: The competition matrix on the left is a clear case of dominant intraspecific competition. The central one represents a case of near-neutral competition. The matrix in the right panel shows a case of dominant interspecific competition. The difference between them is the relative size of the non-diagonal elements respective of the diagonal ones. This property of the competition matrices is controlled by the competition parameter ϵ.

Regarding the predation matrix S, we follow (Dakos et al., 2009) and draw each of its coefficients from a uniform probability distribution bounded between 0 and 1.

2.2.3 Numerical experiments

Depending on the parameters and initial conditions, our model (equation (2.1)) can have three kinds of dynamics, each of them roughly corresponding to a different kind of attractor (see figure 2.2). In a stable point attractor, species composition is constant. The limit cycle (and limit tori) attractor corresponds to periodically

(or quasiperiodically) changing species composition. The last category are chaotic attractors, where the species composition changes irregularly within bounds and there is extreme sensitivity to initial conditions.

Our target is to estimate the probability of reaching each type of attractor under different assumptions about competition. For this, we analyzed 25 values of the competition parameter ϵ (defined in section 2.2.2), ranging from $\epsilon = -0.8$ to $\epsilon = 0.8$. The lower value was chosen to ensure that the non-diagonal competition matrix elements were positive and non-negligible to exclude facilitation and non-competing species. The upper value was arbitrarily chosen to be symmetric with the lower one. For each value of the competition parameter, 200 different initial conditions, predation and competition matrices were generated. The intial conditions were drawn from a uniform distibution between 1 and 2 $mg \ l^{-1}$, while the predation and competition matrices were drawn from the probability distributions described in section 2.2.2. We used a Runge-Kutta solver (ode45) to simulate the model with each parameter set. A stabilizing run of 2000 days was executed to discard transient dynamics. Simulating for 5000 more days, we obtained a time series close to the attractor.

We determined the fraction of the 200 time series that were stable, cyclic or chaotic. For our multi-species models we compared the performance of three different methods: visual inspection, estimation of the maximum Lyapunov exponent (Sandri, 1996) and Gottwald and Melbourne's *0-1* test (Gottwald and Melbourne, 2009). We found the Gottwald-Melbourne test to be not only the most efficient, but also the most reliable test for performing this classification. Describing in detail Gottwald and Melbourne's *0-1* test is beyond the scope of this paper, and it has already been
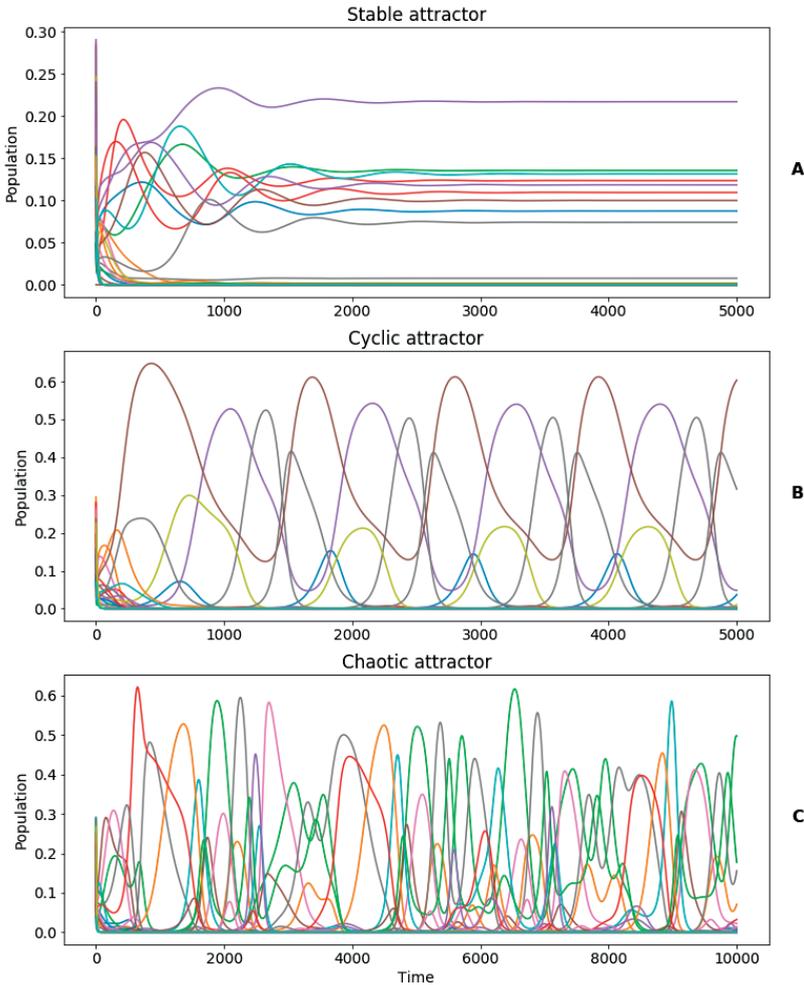
Figure 2.2: Our family of models generates time series of the population of each species. All of the three panels correspond to one simulation of an ecosystem initialized with 16 prey species and 12 predator species. Only the time series corresponding to prey populations are displayed. The time series can be classified in 3 qualitative types depending on their asymptotic behaviour: *stable*, *cyclic* and *chaotic*. In **panel A**, the system reaches a stable attractor after a transient time. In **panel B**, a periodic attractor, with an approximate period of 1000 days, is reached after the transient time. The system in **panel C** never reaches a stable nor a cyclic attractor, but a chaotic one.

done brilliantly in (Gottwald and Melbourne, 2009). Nevertheless, a quick introduction to this test and how we applied it is given in the appendix subsection 2.9.2.

Additionally, two different measures of biodiversity were applied to each simulated ecosystem: the average number of non-extinct prey species and the average biomass grouped by trophic level. We considered a species to be extinct when their population density remained below a threshold of 0.01 mg l^{-1} after the stabilization run. We determined the relationship between the competition strength, the probability of each dynamical regime and the biodiversity.

The numerical experiment was repeated for species pools of different sizes, ranging from a total of 5 to 50 species. In our simulations, we kept a ratio of 2:3 for the size of the species pool at the predator and the prey level.

In the spirit of reproducible research, we made available the code used to obtain our conclusions and generate our figures (Rodríguez-Sánchez, 2018).

2.3   Results

From figure 2.3 we conclude that, in our model, the likelihood of cyclic and chaotic dynamics reaches an optimum for near-neutral competition at the prey level. This result remains true for systems with a different number of species (see figures 2.5 and 2.6 in the Online Appendix). The likelihood of chaos also increases with the size of the food web. This effect should not be surprising: the more dimensions the phase space has, the easier is to fulfill the requirements of the complex geometry of a chaotic attractor (Stro-
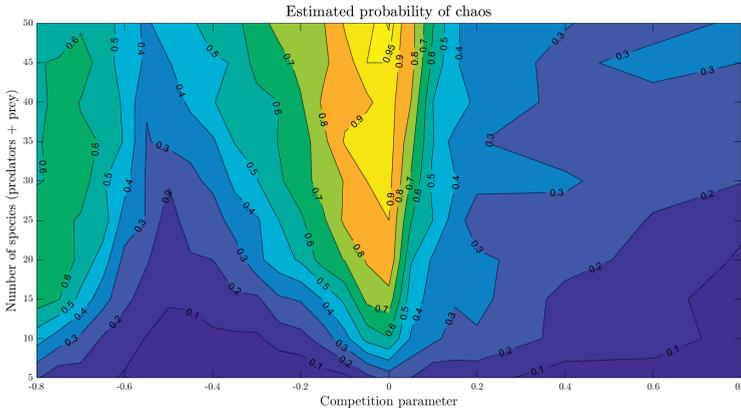
Figure 2.3: Contour map showing the probability of chaos for various competition parameters (horizontal axis) and initial number of species of the simulation (vertical axis). The predators' species pool is fixed as 2/3 of the prey's species pool. Notice that chaotic attractors appear more easily (i.e., for systems with less species) the closer is the competition to neutral (i.e., $\epsilon = 0$).

gatz, 1994). Even in those higher dimensional cases, there is still a clear maximum at near-neutral competition. The probability of chaos shows another local, lower maximum for weak competition coupling, while stable solutions are very rare (figure 2.4.A). Possibly due to the weaker coupling we get less phase locking of the predator prey cycles in this case.

Additionally, we found a clear correlation between the probability of chaos and the biodiversity. In all our cases the diversity in systems with chaotic dynamics were highest (figures 2.4 B,C) and the overall diversity peaked approximately at the near-neutral situation. Interestingly also the cyclic solutions were clearly much more diverse than cases with stable dynamics (figures 2.4 B,C).

In fact the difference in biodiversity of the situation with chaos and cycles was rather small (figure 2.4.C). This conclusion remains true for food webs of different sizes (figures 2.7 and 2.8 in the Online Appendix). From figure 2.4.D, we see that the prey biomass remains relatively stable for the whole range of competition parameters, with the exception of weak interspecific competition, where it reaches a maximum. The predator biomass grows almost linearly as the competition moves leftwards, from near-neutral to strong intraspecific, while the prey biomass remains constant. This also remains true for food webs of different sizes (see figure 2.9 in the Online Appendix) We think this can be understood from the effect of niche complementarity which causes an increase in their total prey biomass (Schnitzer et al., 2011). Like in a two-species model this increase in prey biomass results in an increase of predator biomass only (cf. (Rosenzweig and MacArthur, 1963)).

2.4 Discussion

We find that competition close to neutrality in simple food web models significantly increases the chances of complex dynamical behaviours (such as cycles and chaos), and also the biodiversity. These observations suggest that the hypothesis of non-equilibrium (Huisman and Weissing, 1999) and Hubbell's hypothesis of neutrality (Hubbell, 2003) are not completely independent. Our model shows another local maximum for the probability of chaos for weak competition coupling. We consider this a reasonable result, as predation is known to be the main driver of chaos in this kind of models (van Nes and Scheffer, 2004). Once again, this increase in the chances of complex dynamics is correlated with a higher biodiversity, but here
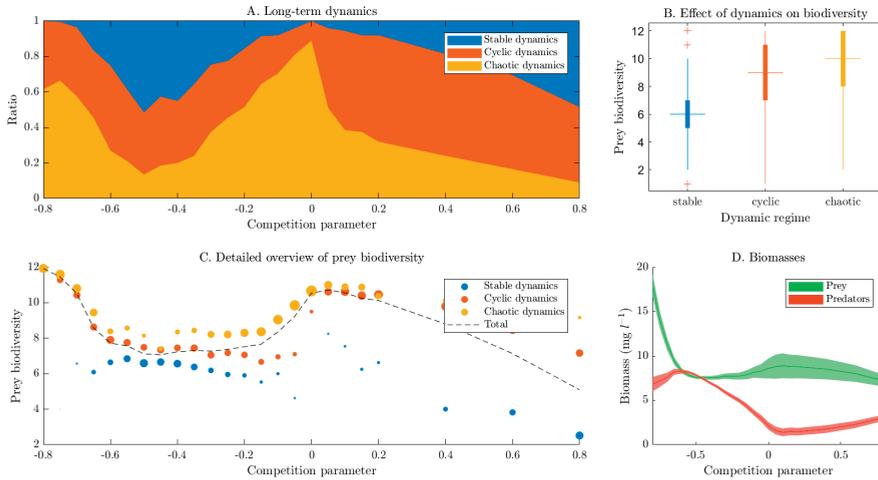
Figure 2.4: Results for food webs with a species pool of 8 predator and 12 prey species. Food webs of different sizes show similar results (see section 2.9.1 in Online Appendix). **Panel A**. Fraction of each dynamic regime as a function of the competition parameter. For each of the 25 parameter values we simulated 200 ecosystems. **Panel B**. Box and whisker plot of the average number of non-extinct prey species grouped by asymptotic regime. **Panel C**. Average prey biodiversity as function of competition parameter. The dashed line shows the average number of non-extinct prey species grouped by competition parameter. The colored circles represent the average prey biodiversity of the simulations, additionally grouped by dynamical regime (stable, cyclic and chaotic). The relative size of the circles represents the ratio of simulations that led to each kind of dynamics. **Panel D**. Average biomasses grouped by trophic level vs. competition parameter. The width represents standard deviation.

the high biodiversity is also due to the low interspecific competition which obviously increases species coexistence.

With these results in hand, it may be tempting to conclude that chaos causes diversity. But this will be a premature conclusion. For instance, we cannot exclude that near-neutrality leads to a higher diversity and that this higher number of species makes chaotic dynamics more likely to occur. Teasing apart the exact pathway of causation is beyond the scope of this paper.

Our research question requires a fine control of the ecosystems under study and keeping a long-term track of their development in time. The experimental realisation in a chemostat of a plankton ecosystem is very costly and time consuming even for a single run (cf. (Benincà et al., 2008)). To study our research question experimentally we would need many replicas and an experimental manipulation of the competition strengths. We think that such approach is unfeasible.

Our choice of the Rosenzweig-MacArthur model was based on the modeller's *mantra* of using the simplest possible model that shows the behaviour of interest. This model doesn't use Allee effects, nor noise, nor species-specific carrying capacities, nor advanced parameterization techniques (Massoud et al., 2018), and the functional form of each term has been chosen to account for satiation and saturation in the simplest possible ways. This opens the door to perform similar analyses in the future using more sophisticated models.

Both the competition and predation parameter sets were drawn from probability distributions. The interactions in our system can be interpreted as a weighted network with a high connectivity. In nature, trophic networks tend to show modular structure with var-

ious clusters (Thebault and Fontaine, 2010). Our simplified model could be interpreted as representing one of those densely connected modules. Moreover, while in the present paper our random parameters were drawn independently, the competition matrix can be chosen in a more advanced way (for instance, accounting for rock-paper-scissors competition). Studying the effect of different physiological scenarios (in the sense of (Huisman et al., 2001), that is, constrains between the parameters) on the probabilities of chaos could be a continuation to this paper.

Our result seemed to be robust against changes in the number of species. However, the exact probabilities of cyclic or chaotic dynamics are of course dependent on the model details and on the values of all parameters (Dakos et al., 2009). For a system with such a high number of parameters, a systematic exploration of the parameter space is unfeasible. In the present work we explored only the variation away from neutrality just by changing the competition strength and randomizing some of the parameters. We found no differences in the main qualitative results when our simulations were run under different sets of realistic parameters (*sensu* (Dakos et al., 2009)).

Due to the large number of simulations made (there were 5000 simulated time series for each of the 10 different food web sizes analyzed), we had to rely on automatic methods for detecting chaos. Automatic detection of chaos by numerical methods has fundamental limitations, especially for high dimensional systems like ours. Most of them can be boiled down to the fact that, in general, numerical methods cannot distinguish robustly between long, complicated transients and genuine chaos. Our motivation to choose the Gottwald - Melbourne test (Gottwald and Melbourne, 2009) was threefold: it discriminates between stable, cyclic and chaotic,

it scales easily to systems of higher dimensions, its computation is fast and it performs better than any other method we tried when compared to the visual inspection of the time series. Although we cannot exclude that we misinterpreted some of the generated time series due to long transients, we don't think this affected the overall patterns, as they were very robust in all our simulations.

Our results suggest a fundamentally new way in which near-neutrality may promote biodiversity. In addition to weakening the forces of competitive exclusion leading to long transients (Scheffer et al., 2018), our analyses reveal that near neutrality may boost the chances for more diverse chaotic and cyclic dynamics.

The results presented in this manuscript rely almost exclusively on simulations. Although they are beyond the scope of this manuscript, certain bridges with data from field ecology can be built. It is known that competition matrices can be estimated from field observations (Fort and Segura, 2018). Provided some studies point in the direction of neutrality (Scheffer and van Nes, 2006; Segura et al., 2011) and chaos (Massoud et al., 2018) being an emergent phenomenon, we find reasonable to expect near-neutral competition matrices to be common in real ecosystems. Assessing the interesting question of how frequent are near-neutral competition matrices in real ecosystems using data from field ecology represents a straightforward continuation of this manuscript.

2.5   Data accesibility

In the spirit of reproducible research, we made published the code used to obtain our conclusions and generate our figures in Zen-

odo, an open access repository. It is available at the reference (Rodríguez-Sánchez, 2018).

2.6 Authors' contributions

PRS designed and performed the numerical simulations, generated the figures and wrote the first drafts of the manuscript. EvN conceived the idea that gave rise to this manuscript and supervised the simulations. Both EvN and MS provided their expert knowledge of the literature in the field and contributed substantially to revisions. All authors gave final approval for publication.

2.7 Acknowledgements

2.8 Funding statement

2.9   Appendix

2.9.1   Results for species pools of different sizes

In the main body of the paper we focused our attention in families of food webs with species pools consisting of 12 prey and 8 predator species. In this section we show the results of the same analysis for food webs of different sizes.

Probability of chaos grouped by number of species
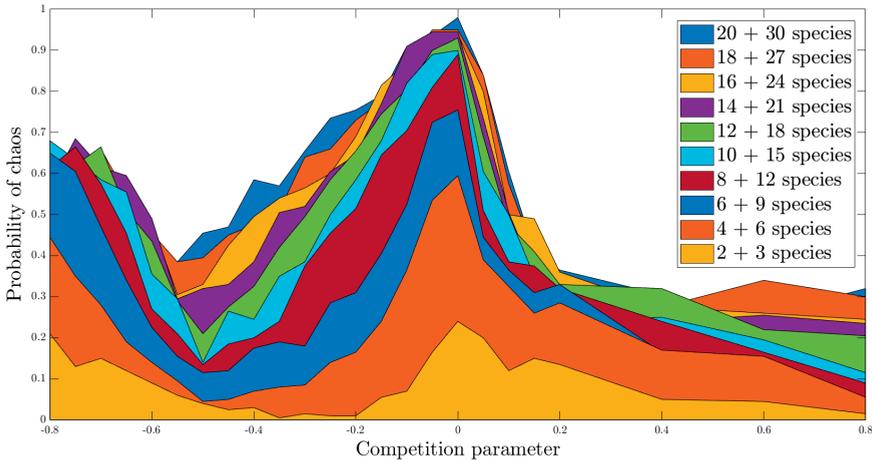
**Figure 2.5:** Probabilities of chaos vs. competition parameter for the whole set of simulations. The competition parameter ϵ is on the horizontal axis. The estimated probability of chaos is represented on the vertical one. Each panel corresponds to an ecosystem with a different number of interacting species. The exact number is shown in each box, as number of predator + number of prey species.

Probability of each dynamical regime
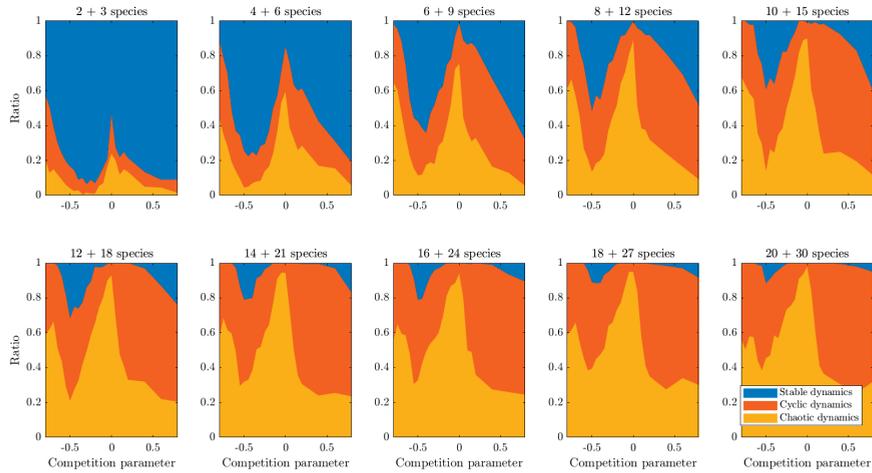
Figure 2.6: Ratio of each dynamical regime vs. competition parameter for the whole set of simulations. The competition parameter ϵ is on the horizontal axis. The size of the species pool is shown in each box, as number of predator + number of prey species.

Biodiversity measurements

For each simulation, a biodiversity index was estimated as the number of prey species whose population was higher than a minimum threshold of 0.01 $mg\ l^{-1}$, averaged respective to time.
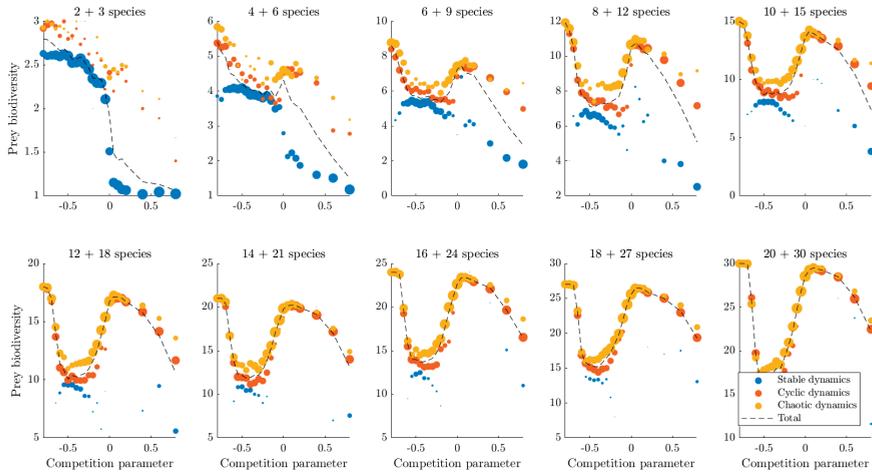
Figure 2.7: Average prey biodiversity vs. competition parameter. Each panel corresponds to a species pool of different size. For each value of the competition parameter, 200 randomly drawn ecosystems were simulated. The dashed line shows the average number of prey species of these 200 simulations. The yellow circles represent the average prey biodiversity of those simulations who had chaotic dynamics. The red and blue circles represent the same for, respectively, cyclic and stable dynamics. The relative area of the circles represents the ratio of each kind of dynamics.
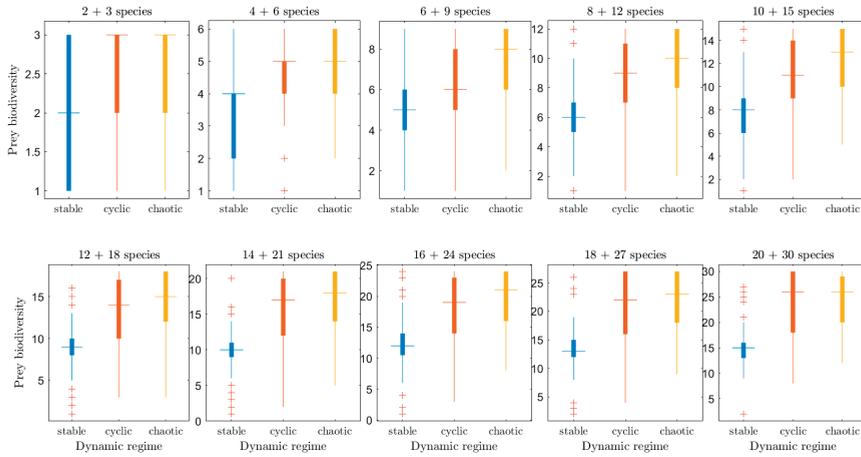
Figure 2.8: Box and whisker plot of the prey biodiversity, after being classified as stable, cyclic or chaotic. The size of the species pool is shown in each box, as number of predator + number of prey species.
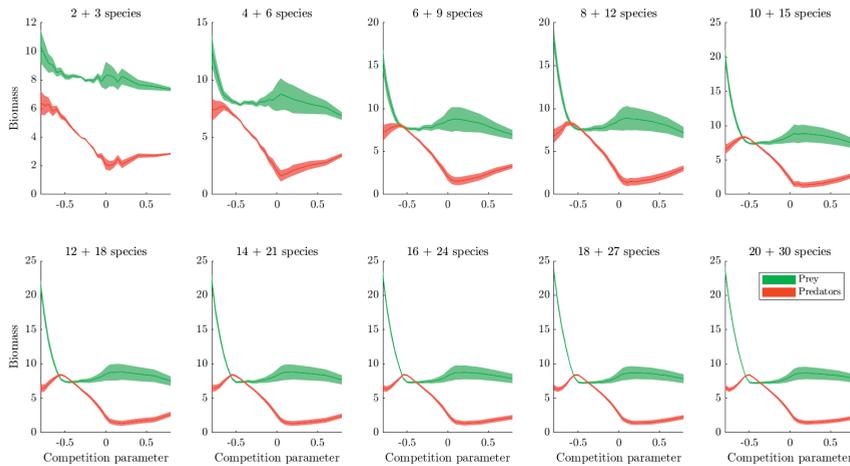

Figure 2.9: Average biomasses grouped by trophic level vs. competition parameter. The width represents standard deviation. The size of the species pool is shown in each box, as number of predator + number of prey species.

2.9.2 Gottwald-Melbourne 0-1 test in a nutshell

The *0-1* test for chaos is designed for distinguishing between regular
and chaotic dynamics in deterministic systems. It works directly
with the observed time series, so a prior knowledge of the under-
lying dynamics is not required (as long as we know that they are
deterministic). This short section is more a motivation than a rig-
orous proof. A minimal, geometrical approach to the method will
be outlined. For a detailed, complete explanation please refer to
(Gottwald and Melbourne, 2009).

The main input for the test is a one-dimensional time series of
observations, ϕ_k, where the integer k represents the time index.
This time series is used to build the functions of the parameter
θ:

$$\begin{cases} p_n(\theta) = \sum_{k=1}^{n} \phi_k cos(k\theta) \\ q_n(\theta) = \sum_{k=1}^{n} \phi_k sin(k\theta) \end{cases} \tag{2.4}$$

The summands in equation 2.4 are the horizontal and vertical com-
ponents of a vector of length ϕ_k pointing in the direction $k\theta$. Con-
sequently, each observation in our time series can be understood
as the size of a step in the plane, being $k\theta$ its direction (see table
2.2).

Table 2.2: Example showing a step by step geometrical construction of the elements inside the summation operator in equation (2.4). In this example we use a time series whose first elements are $\phi_j = \{2, 1, 0.5, 0.25, ...\}$. The parameter θ has been set to $\frac{\pi}{6}$.

k	0	1	2	3	...
$k\theta$	0	$\frac{\pi}{6}$	$\frac{2\pi}{6}$	$\frac{\pi}{2}$	...
$e^{ik\theta}$		$\frac{\pi}{6}$	$\frac{2\pi}{6}$	$\frac{\pi}{2}$	...
ϕ_k	2	1	0.5	0.25	...
$\phi_k e^{ik\theta}$					...

Adding up the elements in table 2.2 as indicated by equation (2.4) can be interpreted geometrically as vector addition, i.e., performing one "step" after another (see figure 2.10).
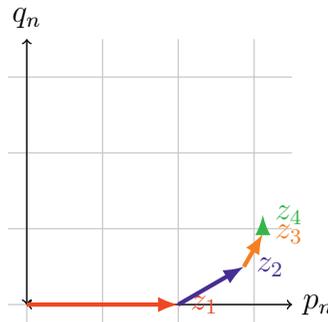

Figure 2.10: Geometrical calculation of z_1, z_2, z_3 and z_4 for $\phi_j = \{2, 1, 0.5, 0.25, ...\}$ and $\theta = \frac{\pi}{6}$.

With this picture in mind, it is easy to understand the kind of paths that different types of time series will give rise to (see figure 2.11). Constant time series generate cyclic paths (polygons) or

pseudocyclic paths (polygons that do not close after a first round). Periodic or pseudoperiodic time series generate periodic or pseudoperiodic paths. Random time series generate brownian-motion-like paths. Provided that our system is deterministic, the apparent stochasticity of our path is a strong indicator of chaos.
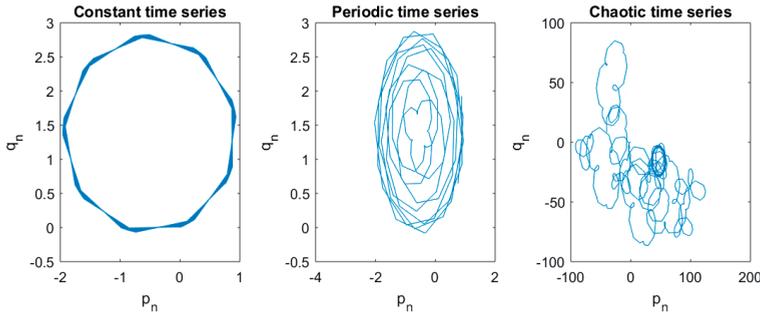
Figure 2.11: First and second panels show the paths generated by the *0-1* test when applied to constant and periodic time series. The third panel shows the case with a chaotic time series (notice the different scale). While in the first two cases the paths remain inside a bounded domain, in the chaotic case the path drifts away from the starting point in a brownian-motion-like fashion.

The case of an underlying chaotic time series is the only one that generates a path that doesn't stay inside a bounded domain around the starting point (compare the third panel in figure 2.11 with the other two). The *0-1* test uses the mean square displacement as a measure of this drift. The system is considered to be chaotic if the square displacement keeps growing for large times. If, on the contrary, it stays bounded, the test will consider the system not chaotic.

In the current manuscript, we used the time series corresponding to a non-extinct prey as input (ϕ_k) to the *0-1* test. The test parame-

ters θ were chosen from a uniform random distribution between $\frac{\pi}{3}$ and $\frac{2\pi}{3}$.

Chapter 3

Climbing Escher's stairs: a way to approximate stability landscapes in multidimensional systems

Abstract

Stability landscapes are useful for understanding the properties of dynamical systems. These landscapes can be calculated from the system's dynamical equations using the physical concept of scalar potential. Unfortunately, it is well known that for most systems with two or more state variables such potentials do not exist. Here we use an analogy with art to provide an accessible explanation of why this happens and briefly review some of the possible alternatives. Additionally, we introduce a novel and simple computational tool that implements one of those solutions: the decomposition of the differential equations into a gradient term, that has an associated potential, and a non-gradient term, that lacks it. In regions of the state space where the magnitude of the non-gradient term is small compared to the gradient part, we use the gradient term to approximate the potential as quasi-potential. The non-gradient to gradient ratio can be used to estimate the local error introduced by our approximation. Both the algorithm and a ready-to-use implementation in the form of an R package are provided.

3.1 Introduction

With knowledge becoming progressively more interdisciplinary, the relevance of science communication is rapidly increasing. Mathematical concepts are among the hardest topics to communicate to non-expert audiences, policy makers, and also to scientists with little mathematical background. Visual methods are known to be successful ways of explaining mathematical concepts and results to non-specialists.

One particularly successful visualization method is that of the stability landscape, also known as scalar potential, Waddington's epigenetic landscape, rolling marble diagram or ball-in-a-cup diagram (Edelstein-Keshet, 2005; Strogatz, 1994; Beisner et al., 2003; Pawlowski, 2006; Huang, 2012). In the rest of this work we define the stability landscape as a classical scalar potential, and thus we will use both terms as equivalents (for a precise mathematical definition, see subsection "Mathematical background" below). In stability landscapes (e.g.: figure 3.1) the horizontal position of the marble represents the state of the system at a given time. With this picture in mind, the shape of the surface represents the underlying dynamical rules, where the slope is proportional to the speed of the movement. The peaks on the undulated surface represent unstable equilibrium states and the wells represent stable equilibria. Different basins of attraction are thus separated by peaks in the surface. Stability landscapes, whose origin can be traced back to the introduction of the scalar potential in physics by Lagrange in the 18th century (Lagrange, 1777), have proven to be a successful tool to explain advanced concepts about dynamical systems theory in an intuitive way. Some examples of those advanced concepts are multistability, basin of attraction, bifurcation points and hys-

teresis (see Scheffer et al. (2001), Beisner et al. (2003) and figure 3.1).

The main reason for the success of this picture arises from the fact that stability landscapes are built as an analogy with our most familiar dynamical system: movement. Particularly, the movement of a marble along a curved landscape under the influence of its own weight. The stability landscape corresponds then with the physical concept of potential energy (Strogatz, 1994). This explains why our intuition, based in what we know about movement in our everyday life, works so well reading these type of diagrams. It is important to stress the fact that under this picture there's not such a thing as inertia (Pawlowski, 2006). The accurate analogy is that of a marble rolling in a surface while submerged inside a very viscous fluid (Strogatz, 1994).
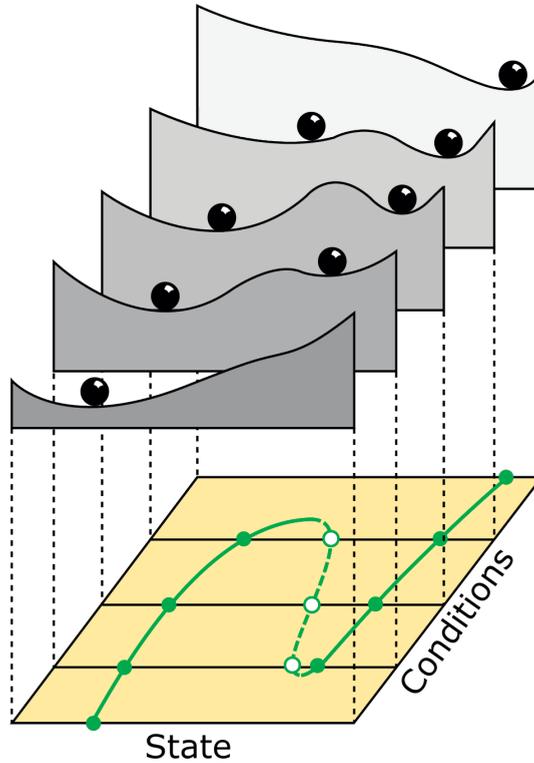
Figure 3.1: Example of a set of 5 stability landscapes used to illustrate bistability in ecosystems (e.g: forest/desert, eutrophicated lake/clear water, etc., see Scheffer et al. (2001)). The upper side of the figure shows the stability landscape of a one-dimensional system for 5 different values of a control parameter. The lower side shows the bifurcation diagram, where the filled points represent stable equilibria and the empty points unstable ones. This diagram proved to be a successful tool for explaining advanced concepts in dynamical systems theory such as bistability and fold bifurcations to scientific communities as diverse as ecologists, mathematicians and environmental scientists.

Like with any other analogy, it is important to be aware of its lim-

itations. The one we address here is the fact that, for models with more than one state variable, such a potential doesn't exist in general. To get an intuitive feeling of why this is true, picture a model with a stable cyclic attractor. As the slope of the potential should reflect the speed of change, we would need a potential landscape where our marble can roll in a closed loop while always going downhill. Such a surface is a classical example of an impossible object (see figure 3.2 and Penrose and Penrose (1958) for details).
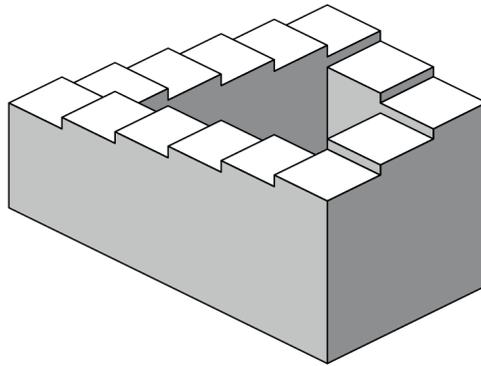
Figure 3.2: The Penrose stair (Penrose and Penrose, 1958) is a classical example of an impossible object. In such a surface, it is possible to walk in a closed loop while permanently going downhill. The scalar potential of a system with a cyclic attractor, if existed, should have the same impossible geometry. This object was popularized by the Dutch artist M.C. Escher (for two beautiful examples, see Escher (1960) and Escher (1961)).

As this is a centuries-old problem, it is perhaps not surprising that several methods have been proposed to approximate stability landscapes for general, high-dimensional systems. Helmholtz, in his pioneering work on fluid dynamics in the 19th century, de-

composes the dynamical equations into a gradient and a curl term (von Helmholtz, 1858; Zhou et al., 2012b). Helmholtz uses the gradient term to compute a well defined scalar potential. The curl term cannot be associated to a scalar potential, and requires computing a more complicated mathematical object, namely a vector potential. Vector potentials, although useful in fluid dynamics and electromagnetism (see for instance chapters 5 and 16 of Wangsness (1986)), do not correspond with the idea of a stability landscape. A similar approach is followed in the normal decomposition (Zhou et al., 2012b), where the dynamical equations are decomposed into two perpendicular directions, being one of them the gradient of a potential and the other interpreted as a perpendicular force. Another possible decomposition was introduced by Ao (Ao et al., 2007; Tang et al., 2017), consisting in applying the sum of a symmetric and an antisymmetric linear transformation to the dynamical equations. Some interesting alternatives are presented in Pawlowski (2006), like potentials for second-order systems or the use of Lyapunov functions as stability landscapes.

Alternative approaches based on probabilistic considerations have achieved great success. The underlying idea is that those states who are more stable have a higher chance to be found in the state space. The corresponding quasi-potential is then a function of the probability density function associated with the stochastic model. This is the approach followed by the Wang's potential landscape (Wang, 2011) and by the Freidlin-Wentzell potential (Freidlin and Wentzell, 2012) (a good review comparing both can be found in Zhou et al. (2012b)). Particularly, the Freidlin-Wentzell potential has become the standard for the derivation of quasi-potentials of stochastic systems. Its direct links with transition rates makes it particularly useful to understand and visualize relative stabilities

(Nolting and Abbott, 2015). Other quasi-potential approaches, and even the exact potential corresponding to a stochastic differential equation with a purely gradient deterministic part, are just limit cases of it (Zhou et al., 2012b, Zhou and Li (2016)). It is important to note that these probability-based quasi-potentials don't admit, in general, the straightforward interpretation of a "rolling marble". Additionaly, they require heavy mathematical weaponry, such as partial and stochastic differential equations. For a complete review about this topic, please refer to Zhou et al. (2012b).

In the present work we introduce a simple method to deal with the fundamental problem of approximating stability landscapes for high dimensional deterministic systems. Specifically, we introduce an algorithm to easily perform an approximation of the above-mentioned Helmholtz decomposition, i.e., to decompose differential equations as the sum of a gradient and a non-gradient, divergence-free part. Each part can be used, respectively, to compute an associated scalar potential and to measure the local error introduced by our picture. In order to reach those interested readers with little background in mathematics, we limited our mathematical weaponry. Knowledge of basic linear algebra and calculus will suffice to understand the paper to its last detail. Additionally, we provide a ready to use, tested and documented R package that implements the algorithm this paper describes (Rodríguez-Sánchez, 2019).

3.1.1 Mathematical background

Conditions of the potential to exist

Consider a coupled differential equation with two state variables x and y (equation (3.1)).

$$\begin{cases} \frac{dx}{dt} = f(x, y) \\ \frac{dy}{dt} = g(x, y) \end{cases}$$
(3.1)

If, in addition, we are able to find a two-dimensional function $V(x, y)$ whose slope is proportional to the change in time of both states, then V represents the stability landscape of the system (see equation (3.2), and compare it with (3.1)).

$$\begin{cases} \frac{dx}{dt} = f(x, y) = -\frac{\partial V(x,y)}{\partial x} \\ \frac{dy}{dt} = g(x, y) = -\frac{\partial V(x,y)}{\partial y} \end{cases}$$
(3.2)

It can be shown that such a function $V(x, y)$ only exists if the crossed derivatives of functions $f(x, y)$ and $g(x, y)$ are equal for all x and y (equation (3.3)). Systems satisfying equation (3.3) are known as conservative, irrotational or gradient fields (cf. section 8.3 of Marsden and Tromba (2003)). Function V is known as scalar potential in the physical and mathematical literature.

$$\frac{\partial f}{\partial y} = \frac{\partial g}{\partial x}$$
(3.3)

If condition (3.3) holds we can use a line integral (Marsden and Tromba (2003), section 7.2) to invert (3.2) and calculate $V(x, y)$ using the functions $f(x, y)$ and $g(x, y)$ as an input. An example of this inversion is equation (3.4), where we have chosen an integration path composed of a horizontal and a vertical line.

$$V(x, y) = V(x_0, y_0) - \int_{x_0}^{x} f(\xi, y_0)d\xi - \int_{y_0}^{y} g(x, \eta)d\eta$$
(3.4)

The attentive reader may have raised her or his eyebrow after reading the word *chosen* applied to an algorithm. In fact, we can introduce this arbitrary choice without affecting the final result. The condition for potentials to exist (3.3) implies that any line integral between two points in this vector field should be independent of the path (cf. section 7.2 of Marsden and Tromba (2003)). Going back to our rolling marble analogy, we can gain some intuition about why this is true: in a landscape the difference in potential energy between two points is proportional to the difference in height, and thus stay the same for any path. If the condition (3.3) is not fulfilled, the potential calculated with (3.4) will depend on the chosen integration path. As this is an arbitrary choice, the computed potential will be an artifact with no natural meaning.

A generalization to more dimensions of these ideas is presented in the online appendix.

Linearization of dynamical systems

It is known that under very general circumstances (particularly, local differentiability), a dynamical system can be approximated in the vicinity of a point (x_0, y_0) by using a first order Taylor expansion (equation (3.5)). This process is known as linearization (cf. section 6.3 of Strogatz (1994)).

$$
\begin{cases}
f(x,y) \approx f(x_0, y_0) + \frac{\partial f(x_0, y_0)}{\partial x}(x - x_0) + \frac{\partial f(x_0, y_0)}{\partial y}(y - y_0) \\
g(x,y) \approx g(x_0, y_0) + \frac{\partial g(x_0, y_0)}{\partial x}(x - x_0) + \frac{\partial g(x_0, y_0)}{\partial y}(y - y_0)
\end{cases}
\tag{3.5}
$$

Equation (3.5) can be written more compactly in matrix form (see equation (3.6)), where the square matrix contains the partial deriva-

tives evaluated at the point (x_0, y_0). This matrix is known as the Jacobian $J(x_0, y_0)$.

$$\begin{bmatrix} f(x, y) \\ g(x, y) \end{bmatrix} \approx \begin{bmatrix} f(x_0, y_0) \\ g(x_0, y_0) \end{bmatrix} + \begin{bmatrix} \frac{\partial f}{\partial x} & \frac{\partial f}{\partial y} \\ \frac{\partial g}{\partial x} & \frac{\partial g}{\partial y} \end{bmatrix}_{(x_0, y_0)} \cdot \begin{bmatrix} x - x_0 \\ y - y_0 \end{bmatrix} \qquad (3.6)$$

It is easy to see that condition (3.3) is equivalent to requiring the Jacobian matrix in equation (3.6) to be symmetric at all linearization points (x_0, y_0).

A few concepts about square matrices

In the rest of this work we will use a few concepts from basic linear algebra. Here we briefly review them, for the convenience of the reader.

The transpose of a matrix is obtained by exchanging rows and columns or, equivalently, by "mirroring" it around its diagonal (see equation (3.7) for an example).

$$\begin{bmatrix} a & b \\ c & d \end{bmatrix}^T = \begin{bmatrix} a & c \\ b & d \end{bmatrix} \qquad (3.7)$$

A symmetric matrix is equal to its transpose (see matrix S in (3.8)). A skew-symmetric matrix is equal to minus its transpose (see matrix K in (3.8)). The diagonal elements of a skew-symmetric matrix are always zero.

$$S = \begin{bmatrix} a & b \\ b & d \end{bmatrix} \quad K = \begin{bmatrix} 0 & b \\ -b & 0 \end{bmatrix} \qquad (3.8)$$

A basic result from linear algebra states that any square matrix can be univocally expressed as the sum of a symmetric and a skew symmetric matrix. Particularly, the symmetric and skew parts are given by equation (3.9).

$$M = M_{symm} + M_{skew} \text{ where: } \begin{cases} M_{symm} &= \frac{1}{2}\left(M + M^T\right) \\ M_{skew} &= \frac{1}{2}\left(M - M^T\right) \end{cases} \quad (3.9)$$

3.2   Material and methods

For the sake of a compact and easy to generalize notation, in the rest of this paper we will arrange the equations of our system as a column vector (equation (3.10) shows an example for a two-dimensional system).

$$\begin{bmatrix} f(x,y) \\ g(x,y) \end{bmatrix} = \vec{f}(\vec{x}) \quad (3.10)$$

The method for deriving a potential we propose is based on Helmholtz's idea of decomposing a vector field in a conservative or gradient part and a non-gradient part (see equation (3.11)).

$$\vec{f}(\vec{x}) = \vec{f_g}(\vec{x}) + \vec{f_{ng}}(\vec{x}) \quad (3.11)$$

The gradient term $\vec{f_g}(\vec{x})$ captures the part of the system that can be associated to a potential function, while the non-gradient term $\vec{f_{ng}}(\vec{x})$ represents the deviation from this ideal case. We'll use $\vec{f_g}(\vec{x})$ to compute an approximate or quasi-potential. The absolute error

of this approach is given as the euclidean size of the non-gradient term $\mid \vec{f}_{ng}(\vec{x}) \mid$. In regions where the gradient term is stronger than the non-gradient term, the condition (3.3) will be approximately fulfilled, and thus the calculated quasi-potential will represent an acceptable approximation of the underlying dynamics. Otherwise, the non-gradient term is too dominant to approximate a potential landscape.

In order to achieve a decomposition like (3.11), we begin by linearizing our model equations. Any sufficiently smooth and continuous vector field $\vec{f}(\vec{x})$ can be approximated around a point $\vec{x_0}$ using equation (3.12), where $J(\vec{x_0})$ is the Jacobian matrix evaluated at the point $\vec{x_0}$ and $\Delta \vec{x}$ is defined as the distance to this point, that is, $\Delta \vec{x} = \vec{x} - \vec{x_0}$, written as a column vector. Note that equation (3.12) is just the generalized version of the two dimensional case shown in (3.6).

$$\vec{f}(\vec{x}) \approx \vec{f}(\vec{x_0}) + J(\vec{x_0})\Delta \vec{x} \qquad (3.12)$$

As usual in linearization, we have neglected the terms of order 2 and higher in equation (3.12). This approximation is valid for $\vec{x}$ close to $\vec{x_0}$.

Using the skew-symmetric decomposition described in equation (3.9), we can rewrite the Jacobian as in equation (3.13):

$$J = J_{symm} + J_{skew} \qquad (3.13)$$

When inserted in equation, (3.12) it becomes (3.14):

$$\vec{f}(\vec{x}) \approx \vec{f}(\vec{x_0}) + J_{symm}(\vec{x_0})\Delta \vec{x} + J_{skew}(\vec{x_0})\Delta \vec{x} \qquad (3.14)$$

The first two terms in the left hand side of equation (3.14) represent a gradient system, being the third and last term the only nongradient term in the equation (see "Mathematical background"). Equation (3.14) represents thus a natural, well-defined and operational way of writing our vector field $\vec{f}(\vec{x})$ decomposed as in equation (3.11) (see (3.15)).

$$\begin{cases} \vec{f_g}(\vec{x}) & \approx \vec{f}(\vec{x_0}) + J_{symm}(\vec{x_0})\Delta\vec{x} \\ \vec{f_{ng}}(\vec{x}) & \approx J_{skew}(\vec{x_0})\Delta\vec{x} \end{cases} \tag{3.15}$$

The non-gradient term $\vec{f_{ng}}(\vec{x})$ is a divergence-free field (see Marsden and Tromba (2003) and/or online appendix), so our proposed decomposition is an approximation of the Helmholtz decomposition (Zhou et al., 2012b) (in that sense, our decomposition is more akin to that of Wang (2011) than to Ao et al. (2007), as may be wrongly suggested by the fact that Ao also uses the concepts of symmetry / anti-symmetry). The gradient term $\vec{f_g}(\vec{x})$ can thus be associated to a potential $V(\vec{x})$. This potential can be computed analytically for this linearized model using a line integral (see equation (3.4) for the two dimensional case, or the online appendix for the general one). The result of this integration yields an analytical expression for the potential difference between the reference point $\vec{x_0}$ and another point $\vec{x_1} \equiv \vec{x_0} + \Delta\vec{x}$ separated by a distance $\Delta\vec{x}$ (see equation (3.16)).

$$\Delta V(\vec{x_1}, \vec{x_0}) \equiv V(\vec{x_1}) - V(\vec{x_0}) \approx -\vec{f}(\vec{x_0}) \cdot \Delta\vec{x} - \frac{1}{2}\Delta\vec{x}^T J_{symm}(\vec{x_0})\Delta\vec{x} \tag{3.16}$$

Provided we know the value of the potential at one point $\vec{x}_{previous}$, equation (3.16) allows us to estimate the potential at a different

point $\vec{x}_{next}$ (cf.: equation (3.17)).

$$V(\vec{x}_{next}) \approx V(\vec{x}_{previous}) + \Delta V(\vec{x}_{next}, \vec{x}_{previous}) \qquad (3.17)$$

Equation (3.17) can be applied sequentially over a grid of points to calculate the approximate potential on each of them. In two dimensions, the resulting potential is given by the closed formula (3.18). The cases with 3 and more dimensions can be generalized straightforwardly. For a step by step example, see online appendix. For a flowchart overview of the algorithm, please refer to figure 3.3.

$$V(x_i, y_j) = V(x_0, y_0) + \sum_{k=1}^{i} \Delta V(x_k, y_0; x_{k-1}, y_0) + \sum_{l=1}^{j} \Delta V(x_i, y_l; x_i, y_{l-1})$$
$$(3.18)$$

As with any other approximation we need a way to estimate and control its error. The stability landscape described in (3.16) has two main sources of errors:

1. It has been derived from a set of linearized equations, sampled over a grid
2. It completely neglects the effects of the non-gradient part of the system

The error due to linearization in equation (3.14) is roughly proportional to $|\Delta \vec{x}|^2$, where $|\Delta \vec{x}|$ is the euclidean distance to the reference point. By introducing a grid, we expect the linearization error to decrease with the grid's step size.

The more fundamental error due to neglecting the non-gradient component of our system cannot be avoided by reducing the grid's

step choice. From equation (3.11) it is apparent that the absolute error of our decomposition is given by $\vec{f}(\vec{x}) - \vec{f}_g(\vec{x}) = \vec{f}_{ng}(\vec{x})$. That is, we can use the euclidean norm of $\vec{f}_{ng}(\vec{x})$ as an approximation of the local absolute error introduced by our algorithm. The relative error introduced by our approximation can be estimated using equation (3.19), where we use equation (3.15) to relate with the skew and symmetric parts of the Jacobian matrix.

$$err(\vec{x}) \approx \frac{\mid \vec{f}_{ng}(\vec{x}) \mid}{\mid \vec{f}_g(\vec{x}) \mid + \mid \vec{f}_{ng}(\vec{x}) \mid} \approx \frac{\mid J_{skew}(\vec{x}) \mid}{\mid J_{symm}(\vec{x}) \mid + \mid J_{skew}(\vec{x}) \mid}$$
(3.19)

The norms of the symmetric and skew Jacobians can be understood as the "weights" of each of those matrices. The relative error described in (3.19) quantifies how dominant the non-gradient term is in each region of the phase space, being 0 in those regions where the system is fully gradient (i.e.: $\mid J_{skew} \mid = 0$), and 1 where it is fully non-gradient (i.e.: $\mid J_{symm} \mid = 0$). The figures in the Results section show that the error maps calculated with equation (3.19) are a good estimator of the local quality of our quasi-potential approximation.

3.2.1 Implementation

As an application of the above-mentioned ideas, and following the spirit of reproducible research, we developed a transparent R package we called *rolldown* (Rodríguez-Sánchez, 2019). Our algorithm accepts a set of dynamical equations and a grid of points defining our region of interest as an input. The output is the estimated

potential and the estimated error, both of them calculated at each point of our grid (see figure 3.3 for details).
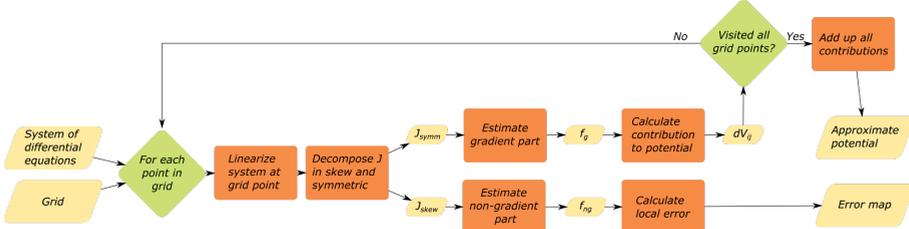
Figure 3.3: Flowchart showing the basic functioning of our implementation of the algorithm described in this paper.

3.3 Results

3.3.1 Synthetic examples

A four well potential

We first tested our algorithm with a synthetic model of two uncoupled state variables. Uncoupled systems are always gradient as all non-diagonal values of the Jacobian are zero everywhere. We added the interaction terms p_x and p_y to be able to make it gradually non-gradient (see equation (3.20)).

$$\begin{cases} \frac{dx}{dt} = f(x,y) = -x(x^2 - 1) + p_x(x,y) \\ \frac{dy}{dt} = g(x,y) = -y(y^2 - 1) + p_y(x,y) \end{cases} \quad (3.20)$$

When we choose those non-gradient interactions to be zero, the system is purely gradient and corresponds with a four-well potential.

Our algorithm rendered it successfully and with zero error (cf. figure 3.4, row A). In order to test our algorithm, we introduced a non-gradient interaction of the form $p_x(x, y) = 0.3y \cdot m(x, y)$ and $p_y(x, y) = -0.4x \cdot m(x, y)$, with $m(x, y) = e^{(x-1)^2 + (y-1)^2}$. $m(x, y)$ serves as a masking function guaranteeing that our interaction term will be negligible everywhere but in the vicinity of $(x, y) = (1, 1)$. After introducing this non-gradient interaction a four-well potential is still recognizable (cf. figure 3.4, row B). As expected, the error was correctly captured to be zero everywhere but in the region around $(x, y) = (1, 1)$. The error map warns us against trusting the quasi-potential in the upper right region, and guarantees that elsewhere it will work fine. Notice that, accordingly, the upper right stable equilibrium falls slightly outside its corresponding well. The rest of equilibria, to the contrary, fit correctly inside their corresponding wells.
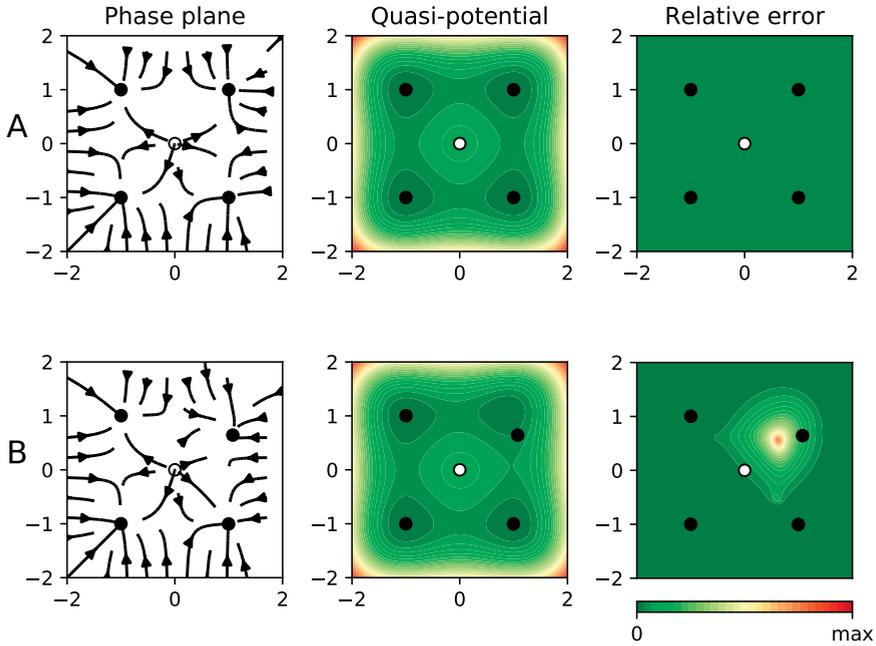
Figure 3.4: Results for two synthetic examples. In all panels the dots represent equilibrium points (black for stable, otherwise white). The left panel shows the phase plane containing the actual "deterministic skeleton" of the system. The central panel shows the quasi-potential. The right panel shows the estimated error. **Row A** shows the application to a gradient case (equation (3.20) with interaction terms equal to zero). As expected, the error is zero everywhere. In **row B** our algorithm is applied to a non-gradient case (equation (3.20), with non-zero interaction terms).

A fully non-gradient system

In order to stress our algorithm to the maximum, we tested it in a worst case scenario: a system with zero gradient part everywhere. Particularly, we fed it with equation (3.21). All solutions (but the unstable equilibrium point at $(0,0)$) are cyclic (cf. 3.5, left panel)). As we discussed in the introduction, calculating a potential for a system with cyclic trajectories is as impossible as Escher's paintings (and for similar reasons). This fact is captured by our algorithm, that correctly predicts a relative error of 1 everywhere (see figure 3.5, right panel). In this case, the quasi-potential (figure 3.5, left panel) is not even locally useful.

$$\begin{cases} \frac{dx}{dt} = -y \\ \frac{dy}{dt} = x \end{cases} \tag{3.21}$$
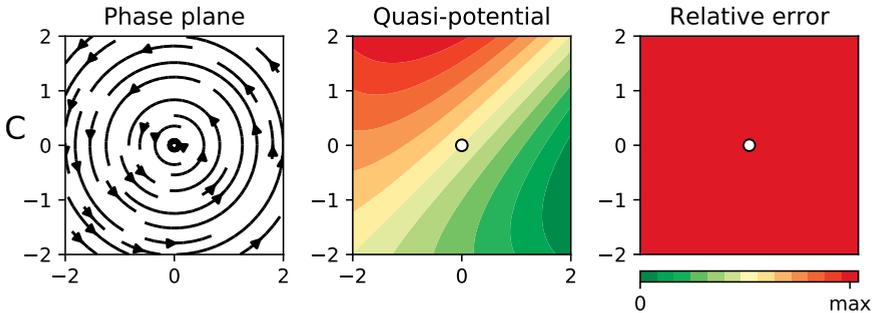
Figure 3.5: Results for a fully non-gradient system (equation (3.21)). In all panels the dots represent center equilibrium points. The left panel shows the phase plane containing the actual "deterministic skeleton" of the system. The central panel shows the quasi-potential. The right panel shows the estimated error.

3.3.2 Biological examples

A simple regulatory gene network

Waddington's epigenetic landscapes (Gilbert, 1991; Huang, 2012) are a particular application of stability landscapes to gene regulatory networks controlling cellular differentiation. When applied to this problem, stability/epigenetic landscapes serve as a visual metaphor for the branching pathways of cell fate determination.

A bistable network cell fate model can be described by a set of equations like (3.22). Such a system represents two genes (x and y) that inhibit each other. This circuit works as a toggle switch with two stable steady states, one with dominant x, the other with dominant y (see Bhattacharya et al. (2011)).

$$\begin{cases} \frac{dx}{dt} = b_x - r_x x + \frac{a_x}{k_x + y^n} \\ \frac{dy}{dt} = b_y - r_y y + \frac{a_y}{k_y + x^n} \end{cases} \tag{3.22}$$

Our parameter choice ($a_x = 0.4802$, $a_y = 0.109375$, $b_x = 0.2$, $b_y = 0.3$, $k_x = 0.2401$, $k_y = 0.0625$, $r_x = r_y = 1$ and , $n = 4$) corresponds with equations 6 and 7 of Bhattacharya et al. (2011), where we modified two parameters ($By = 0.3$, $foldXY = 1.75$, in their notation) in order to induce an asymmetry in the the dynamics. Although this system is non-gradient, our algorithm correctly yields a pseudopotential with two wells (see figure 3.6, row D). Observe that the bottom of those potentials corresponds with a stable equilibrium. The relative error, despite being distinct from zero in some regions, is not very high. This means that our quasi-potential is a reasonable

approximation of the underlying dynamics. Indeed, the equilibria correspond to the wells (stable) and the peak (unstable).

Predator prey dynamics

The Lotka-Volterra equations (3.23) are a classical predator-prey model (Volterra, 1926). In this model x and y represent, respectively, the prey and predator biomasses.

$$\begin{cases} \frac{dx}{dt} = ax - bxy \\ \frac{dy}{dt} = cxy - dy \end{cases} \tag{3.23}$$

This model is known to have cyclic dynamics. As we discussed in our analogy with Escher's paintings, we cannot compute stability landscapes in the regions of the phase plane where the dynamics are cyclic. When we apply our method to a system like equation (3.23), the error map correctly captures the fact that our estimated potential is not trustworthy (see figure 3.6, row E).
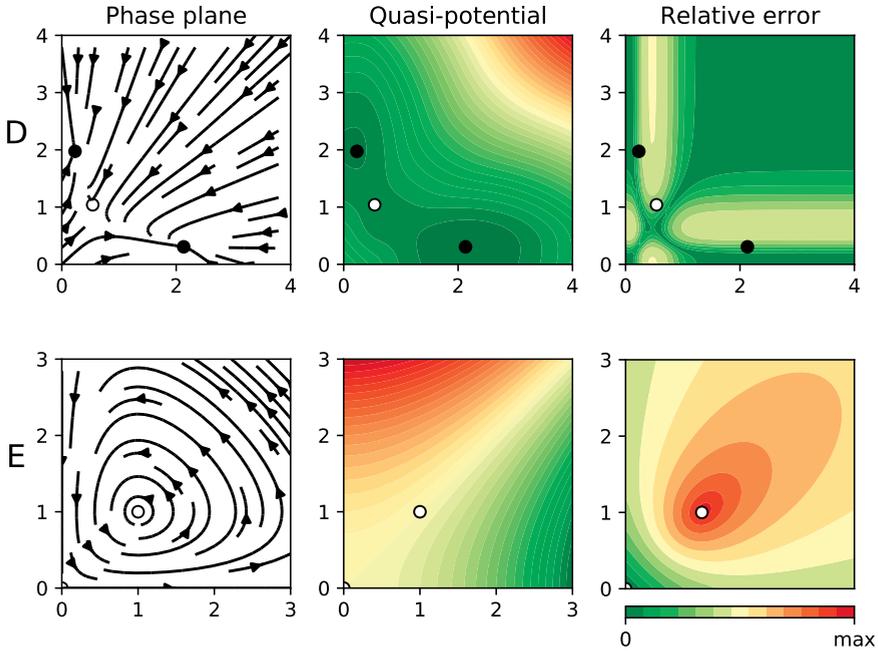
Figure 3.6: Results for two biological systems. In all panels the dots represent equilibrium points (black for stable, otherwise white). The left panel shows the phase plane containing the actual "deterministic skeleton" of the system. The central panel shows the quasi-potential. The right panel shows the estimated error. In **row D** we applied our algorithm to the simple gene regulatory network described in equation (3.22). In **row E** we apply our algorithm to a Lotka-Volterra system (equation (3.23), with $a = b = c = d = 1$).

Selkov model for glycolysis

The Selkov model for glycolysis reads like equation (3.24), where x and y represent the concentrations of two chemicals.

$$\begin{cases} \frac{dx}{dt} & = -x + ay + x^2y \\ \frac{dy}{dt} & = b - ay - x^2y \end{cases} \tag{3.24}$$

The Selkov model is a classical example of a dynamical equation motivated by a biochemical problem that can develop a limit cycle under certain circumstances. Particularly, if we fix $a = 0.1$, such a system is known to have a limit cycle for $b \in [0.42, 0.79]$ (figure 3.7, row G), and otherwise it reaches an equilibrium solution (figure 3.7, row F). This system is particularly interesting from the pedagogical point of view because the Jacobian doesn't depend on b, so the error map remains the same.

In the configuration showed in row F, we see that the trajectories corresponding to low concentrations of any of both chemicals (i.e.: $x \ll 1$ or $y \ll 1$) remain in the "safe zone" according to the error map. Our estimated potential can be used in that region and, accordingly, the equilibrium point lies in the bottom of a potential well. On the other hand, in the configuration showed in row G, even those trajectories that start inside the "safe zone" are forced to "explore" the "unsafe" area outside it. Such a configuration leads to a limit cycle and thus, unsurprisingly, doesn't admit a potential representation.
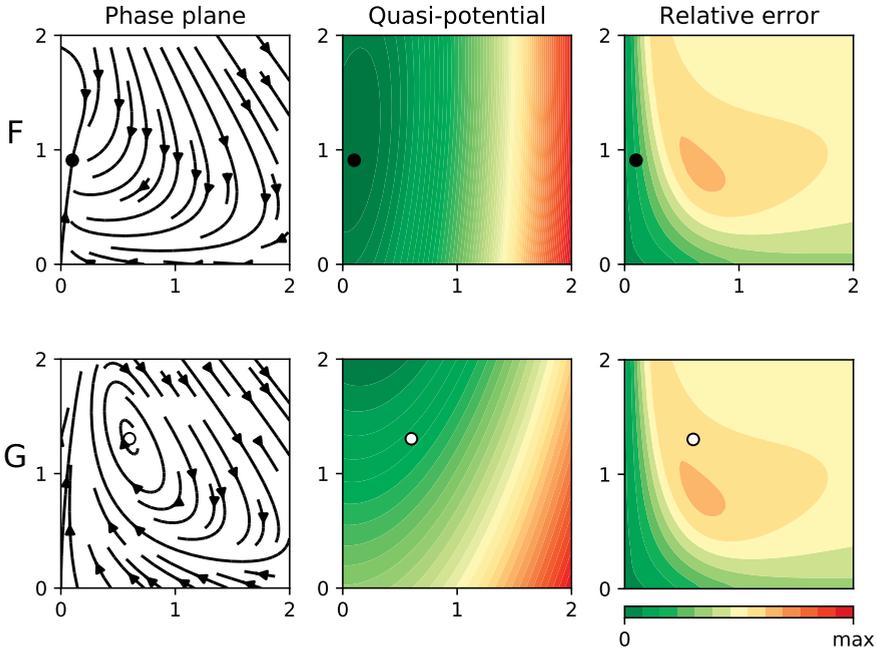
Figure 3.7: Results for two parameter settings of the Selkov equation (3.24). In all panels the dots represent equilibrium points (black for stable, otherwise white). The left panel shows the phase plane containing the actual "deterministic skeleton" of the system. The central panel shows the quasi-potential. The right panel shows the estimated error. In **row F** we applied our algorithm to a Selkov system with $b = 0.1$, so the solutions reach a stable point. In **row G** we set $b = 0.6$, so the system has a limit cycle.

3.4 Discussion

The use of stability landscapes as a helping tool to understand one-dimensional dynamical systems achieved great success, especially in

interdisciplinary research communities. A generalization of the idea of scalar potential to two-dimensional systems seemed to be a logical next step. Unfortunately, as we have seen, there are reasons that make two (and higher) dimensional systems fundamentally different from the one-dimensional case. The generalization, straightforward as it may look, is actually impossible for most dynamical equations. A good example of this impossibility is any system with cyclic dynamics, whose scalar potential should be as impossible as the Penrose stairs in Escher's paintings. As a consequence, any attempt of computing stability landscapes for non-gradient systems should, necessarily, drop some of the desirable properties of classical scalar potentials.

For instance, the method proposed by Bhattacharya (Bhattacharya et al., 2011) smartly tries to avoid the fundamental problem of path dependence of line integrals by integrating along trajectories, removing thus the freedom of path choice. A problem of this approach is that there is generally no continuity along the borders of the basins of attraction in the resulting quasi-potential, and that the results depend on the choice of the initial point. Our approach is, in some sense, the opposite. We embrace the fact that some systems do not have a reliable scalar potential landscape in some (or even all) regions of the phase space, and we show this fundamental limitation explicitly via the error map.

Methods based on probabilistic considerations such as occupancy probabilities at the steady-state distribution (Wang, 2011; Li and Wang, 2014) or transition rates between states (Ao et al., 2007; Zhou et al., 2012b; Freidlin and Wentzell, 2012; Tang et al., 2017), provide a continuous landscape where deep areas correspond with states with a high probability of occurrence. When applied to a limit cycle, they give rise to "Mexican hat" shaped surfaces (Wang,

2011). However, these surfaces cannot be interpreted straightforwardly as classical potentials where the state just "slides" to the bottom of the wells. That is, the "rolling-marble" analogy has to be used very carefully. Two transparent examples appear in fig. 3A in Wang (2011) or fig. 2B in Li and Wang (2014). While the slope correctly captures the attracting property towards the limit cycle, once inside of it the trajectories eventually go uphill. Additionally, these methods require familiarity with advanced mathematical concepts such as stochastic and partial differential equations, both of them more complex and computationally expensive than our approach.

We share the perception with other authors (Pawlowski, 2006) that the concept of potential is often misunderstood in research communities with a limited mathematical background. The algorithm we introduce here is an attempt to preserve as much as possible from the classical potential theory while addressing explicitly its limitations and keeping the mathematical complexity as low as possible. A more detailed summary about what our algorithm provides is:

- Integrity. At each step the strength of the non-gradient term is calculated. If this term is high, it is fundamentally impossible to calculate a scalar potential with any method. If this term is zero, our solution converges to the classical potential.
- Safety. The relative size of the non-gradient term can be interpreted as an error term, mapping which regions of our stability landscape are dangerous to visit.
- Speed. The rendering of a printing quality surface can be performed in no more than a few seconds in a personal laptop.
- Simplicity. The required mathematical background is covered by any introductory course in linear algebra and vector

calculus.

- Generality. The core of the algorithm is the skew-symmetric decomposition of the Jacobian. This operation can be easily applied to square matrices of any size, generalizing our algorithm for working in 3 or more dimensions.
- Usability. We provide the algorithm in the form of a ready to use, fully documented and tested R package Rodríguez-Sánchez (2019).

It is important to notice that, although our algorithm provides us with a way of knowing which regions of the phase plane can be "safely visited", we cannot navigate the phase plane freely but only along trajectories. This interplay between regions and trajectories limits the practical applicability of our algorithm to those trajectories that never enter regions with high error (good examples of this can be found in figures 3.4 row B and 3.7 row F). If our algorithm works in the region of interest, there is no need to use more advanced (and thus, more difficult to implement and to interpret) methods, as we expect them to converge to the same solution. As a rule of thumb, we found that any relative error below 0.2 can be considered small for visualization purposes, but this is a subjective criterion. For higher errors, or in case of doubt, we suggest to visually compare the calculated quasi-potential with the phase plane (as we did in all the figures in the Results section). If required, a more detailed assessment of the absolute error can be performed by calculating the difference between the flow containing the original dynamical equations and the flow corresponding to the quasi-potential (i.e., by direct evaluation of $\vec{f}(\vec{x}) - \vec{f}_g(\vec{x})$, see Methods section). Note that the absolute error should not be calculated using the quasi-potential itself, but the flows derived from it.

If we conclude that the system doesn't admit our quasi-potential, then the most reasonable alternative is to use a Freidlin-Wentzell potential, but keeping in mind that its interpretation is not so straightforward as that of a scalar potential.

The concept of potential is paramount in physical sciences. The main reason for the ubiquity of potentials in physics is that several (idealized) physical systems are known to be governed only by gradient terms (e.g.: movement in friction-less systems, classical gravitatory fields, electrostatic fields, ...). As physical potentials can be related with measurable concepts like energy, its use goes way further than visualization. From the depth and width of a potential we can learn about transition rates and resilience to pulse perturbations. The height and shape of the lowest barrier determines the minimum energy to transition to an alternative stable state, which relates to the probability of a noise-driven jump in a stochastic environment (Zhou et al., 2012b; Nolting and Abbott, 2015; Hänggi et al., 1990). All these results remain true for non-physical problems that happen to be governed exclusively by gradient dynamics, and, we claim, should remain approximately true for problems governed by weakly non-gradient dynamics. This is the situation our algorithm has been designed to deal with.

Regarding visualization alone, it may be worth reconsidering why we prefer the idea of stability landscape over a traditional phase plane figure, especially after pointing out all the difficulties of calculating stability landscapes for higher-dimensional systems. It is true that the phase plane is slightly less intuitive than the stability landscape, but it has a very desirable property: it doesn't require the imagination of a surrealist artist to exist.

3.5 Acknowledgements

3.6 Additional information

3.6.1 Gradient conditions for a system with an arbitrary number of dimensions

Dynamics in equation (3.2) and the condition for the crossed derivatives (3.3) can be straightforwardly generalized (see equations (3.26) and (3.25) to systems with an arbitrary number of state variables $\vec{x} = (x_1, ..., x_n)$. Particularly, if and only if our system of equations $\frac{dx_i}{dt} = f_i(\vec{x})$ satisfies the condition for all i:

$$\frac{\partial f_i}{\partial x_j} = \frac{\partial f_j}{\partial x_i} : i \neq j \tag{3.25}$$

then a potential $V(\vec{x})$ exists related to the original vector field:

$$\frac{dx_i}{dt} = f_i(\vec{x}) = -\frac{\partial V}{\partial x_i} : i = 1..n \tag{3.26}$$

and such a potential can be computed using a line integral:

$$V(\vec{x}) = V(\vec{x}_0) - \int_\Gamma \sum_{i=1}^n f_i(\vec{x}) dx_i \qquad (3.27)$$

3

where the line integral in (3.27) is computed along any curve Γ joining the points $\vec{x}_0$ and $\vec{x}$.

It is important to note that the number of equations (N) described in condition (3.25) grows rapidly with the dimensionality of the system (D), following the series of triangular numbers $N = \frac{1}{2}(D - 1)D$. Thus, the higher the dimensionality, the harder it may get to fulfill condition (3.25). As a side effect, we see that one-dimensional systems have zero conditions and their stability landscape is thus always well-defined.

3.6.2 Correspondence with the Helmholtz decomposition

Our decomposition (3.15) is an approximation of the Helmholtz decomposition. The Helmholtz decomposition is defined as the decomposition of the field in a gradient term and a curl, or divergence-free term. This decomposition is known to be unique.

The gradient nature of $\vec{f}_g(\vec{x})$ has already been established in the Methods section. Thus, in order to prove the correspondence, we only need to show that $\vec{f}_{ng}(\vec{x})$ is a divergence-free field, that is, $\vec{\nabla} \cdot \vec{f}_{ng} = 0$. The divergence represents one of the many generalizations of the concept of derivative in systems with 2 and more dimensions, and it is a central concept from vector calculus (Marsden and Tromba, 2003). The divergence operator $\vec{\nabla} \cdot$ of a field in cartesian coordinates is defined as the sum of the derivative of each element respective the corresponding coordinate

(see equation (3.28) for an example using the two-dimensional field $\vec{F}(x,y) = (F_x(x,y), F_y(x,y)))$.

$$\vec{\nabla} \cdot \vec{F} = \frac{\partial F_x}{\partial x} + \frac{\partial F_y}{\partial y} \qquad (3.28)$$

When applied to $\vec{f}_{ng}$, defined as in equation (3.15), the divergence equals the sum of the diagonal elements of J_{skew}. The diagonal elements of any skew matrix are all zero (see (3.8)), and thus, the divergence of $\vec{f}_{ng}$ is zero too.

3.6.3 Detailed example of application

To calculate the value of V at, for instance, the point (x_3, y_2) of a grid, we should begin by assigning 0 to the potential at our arbitrary starting point (i.e.: $V(x_0, y_0) = 0$ by definition). Then, we need a trajectory that goes from (x_0, y_0) to (x_3, y_2), iterating over the intermediate grid points (see figure 3.8).
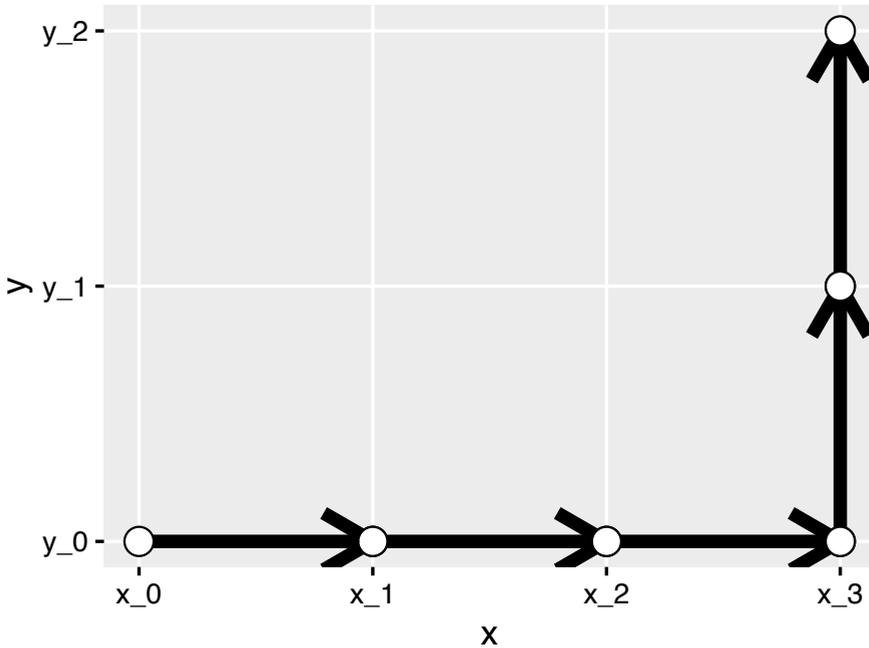
Figure 3.8: Path used to go from point (x_0, y_0) to (x_3, y_2). Note that this is not the only possible path. Our algorithm converges to the same potential regardless of the path chosen thanks to neglecting the skew part of the Jacobian in our linearization process.

In the first step we go from (x_0, y_0) to (x_1, y_0). The new potential is thus (using (3.17)):

$$V(x_1, y_0) \approx V(x_0, y_0) + \Delta V(x_1, y_0; x_0, y_0)$$

The next two steps continue in the horizontal direction, all the way to (x_3, y_0). The value of the potential there is:

$$V(x_3, y_0) \approx V(x_1, y_0) + \Delta V(x_2, y_0; x_1, y_0) + \Delta V(x_3, y_0; x_2, y_0)$$

Now, to reach our destination (x_3, y_2) we have to move two steps in the vertical direction:

$$V(x_3, y_2) \approx V(x_3, y_0) + \Delta V(x_3, y_1; x_3, y_0) + \Delta V(x_3, y_2; x_3, y_1)$$

Generalizing the previous example we see that we can compute the approximate potential at a generic point (x_i, y_j) using the closed formula (3.18). Both our example (3.6.3) and formula (3.18) have been derived sweeping first in the horizontal direction and next in the vertical one. Of course, we can choose different paths of summation. Nevertheless, because we are building our potential neglecting the non-gradient part of our vector field, we know that our results will converge to the same solution regardless of the chosen path.

Chapter 4

Early warning signals for desynchronization in periodically forced systems

Abstract

Conditions such as insomnia, cardiac arrhythmia and jet-lag share a common feature: they are all related to the ability of biological systems to synchronize with external cues such as the the day-night cycle. When organisms lose resilience, this ability of synchronizing can become weaker till they eventually become desynchronized in a state of malfunctioning or sickness. It would be useful to measure this loss of resilience before the full desynchronization takes place. Several dynamical indicators of resilience (DIORs) have been proposed to account for the loss of resilience of a dynamical system. The performance of these indicators depends on the underlying mechanism of the critical transition, usually a saddle-node bifurcation. Before such bifurcation the recovery rate from perturbations of the system becomes slower, a mechanism known as critical slowing down. Here we show that, for a wide class of biological systems, desynchronization happens through another bifurcation, namely the saddle-node of cycles, for which critical slowing down cannot be directly detected. Such a bifurcation represents a system transitioning from synchronized (phase locked) to a desynchronized state, or vice versa. We show that after an appropriate transformation we can also detect this bifurcation using dynamical indicators of resilience. We test this method with data generated by models of sleep-wake cycles.

4.1   Introduction

The phenomenon of endogenous circadian rhythms, first observed by the French polymath Jean-Jacques d'Ortous de Mairan in 1729 (d'Ortous de Mairan (1729)), has transcended science to become part of the popular culture, often referred to as *the inner clock*. The evolutionary convenience of synchronizing such *inner clocks* with the external cues, usually provided by regular astronomical events such as day-night periods and seasons, is well established (Foster and Kreitzman (2017)). Synchronization, thus, proves useful for living systems and a difficulty to synchronize (and sometimes also to desynchronize) can be an indicator of sickness or malfunctioning. Some synchronization-related conditions include insomnia, jet-lag, arrhythmia or epilepsy (Glass (2001)).

The transition from a synchronized to a desynchronized regime is discontinuous. The system is either synchronized or not. Therefore it could be that synchronization is a special kind of critical transition (Scheffer (2009)). This is relevant as there have been developed ways to foresee whether at critical transition is likely to occur (Scheffer et al. (2009)). These dynamic indicators of resilience (DIORs) are based on the phenomenon of "critical slowing down" (Wissel (1984), Van Nes and Scheffer (2007)). According to this theory, the recovery rate from perturbations decreases if systems are close to a critical transition. In time series we can measure critical slowing down using different indicators, such as increased autocorrelation and variance (Dakos et al. (2012)).

In the present work we illustrate with simple models that some transitions from synchronized to desynchronized states indeed can be related to a special kind of critical transition, namely a saddle-node

bifurcation of cycles. We show that after an appropriate transformation of the data, we can still use critical-slowing down indicators to see if one of these transitions is likely to happen.

4.2   Methods

4.2.1   Case study model

Our goal is to develop generic indicators for the risk of desynchronization of biological cycles such as the sleep-wake cycle. To understand the properties of this system, we analyze a generic model of such periodically forced cyclic systems. This minimal model consists of two oscillators: a master (representing the external forcing, for instance of a diurnal rhythm) and a slave (representing the organism's state, for instance its sleep/awake status). We represent each oscillator by its most basic feature: phase ($\theta_\odot$ for the master and θ for the slave) The master's frequency is constant (i.e. the phase grows steadily from 0 to 2π in 24 h), and it is not affected by the slave's dynamics. The slave's dynamics are more complex: in the absence of coupling it has a natural frequency, and an increasing tendency to synchronize with the master if the coupling gets more intense. These features are captured by model (4.1).

$$\begin{cases} \frac{d\theta}{dt} & = \omega - k \cdot f(\theta - \theta_\odot) \\ \frac{d\theta_\odot}{dt} & = \omega_\odot \end{cases} \qquad (4.1)$$

In model (4.1) each oscillator shows a natural frequency (ω and $\omega_\odot$). The first oscillator shows a tendency to slow-down if θ is ahead of $\theta_\odot$, and to speed-up otherwise. The function f measures

the difference between θ and $\theta_\odot$. Note that f has to be a periodic function (in the sense of $f(x + 2\pi) = f(x)$). This is a consequence of the cyclic nature of phases: by definition phases θ and $\theta + 2\pi$ represent the same point in a cycle, and thus, the same physical reality. In most applications f is also continuous and smooth. The strength of the coupling is given by the positive constant parameter k. If the coupling is not strong enough (relative to the difference in natural frequencies), synchronization doesn't happen.

The system (4.1) becomes simpler (and even analytically tractable) if we use the phase difference $\phi(t) \equiv \theta(t) - \theta_\odot(t)$ as a new state variable. With this change of state variable, the system takes the form (4.2), where, for convenience, we made $\Omega \equiv \omega - \omega_\odot$.

$$\frac{d\phi}{dt} = \Omega - k \cdot f(\phi) \tag{4.2}$$

For the sake of clarity, we will use $f(\phi) = \sin(\phi)$ in the rest of this work. As we discuss in the online appendix, we can do this without loss of generality. With this choice, our model becomes a simple subcase of the classical Kuramoto model (see Kuramoto (1975), Strogatz (2000)). Equating (4.2) to zero, the stable and unstable equilibria of our system are easily found to be $\phi_s^* = \Delta$ and $\phi_u^* = \pi - \Delta$, where $\Delta \equiv \arcsin \frac{\Omega}{k}$. It is important to note that, for those equilibria to exist, condition (4.3) should be satisfied. Intuitively, this means that our system can only synchronize cycles whose difference in natural frequencies (Ω) have at most the same order of magnitude as the coupling term (k).

$$| \frac{\Omega}{k} | \leq 1 \tag{4.3}$$

When condition (4.3) is satisfied, the system (4.2) tends naturally to the stable solution. In this case, the phase difference ϕ is constant, so both oscillators have the same frequency ($\omega_\odot$) and are thus synchronized. If, on the contrary, condition (4.3) is not satisfied, the phase difference ϕ never stabilizes and consequently synchronization is not possible.

But, what happens at the border between both cases, that is, when Ω/k approaches 1? In such a situation, the stable and unstable solutions collide and annihilate each other at $\phi^* = \frac{\pi}{2}$ (see first row of panel 4.1). This mechanism of losing stability is known as a saddle-node bifurcation (Kuznetsov (1998), Strogatz (1994)). For an extensive discussion about the choice of this system, please refer to the appendix.

We'll take advantage of the periodicity of our system by plotting its trajectories over a $2\pi \times 2\pi$ square with periodic boundary conditions (or, equivalently, on the surface of a torus). When the phase hits any border, it reappears at the opposite side (just like in old-school video games such as *Pac Man* or *Asteroids*). In figure 4.1 we see three different configurations of such a system. As our parameter approaches the saddle-node bifurcation, both the stable and unstable cycles get closer. When we introduce additive noise to the dynamics, transitions can happen before the bifurcation is reached if the noise is strong enough to make the state jump the gap between both cycles (figure 4.1, column B). Note that due to the periodic boundaries the system is only momentarily desynchronized as it "collapses" back to the synchronized dynamics.
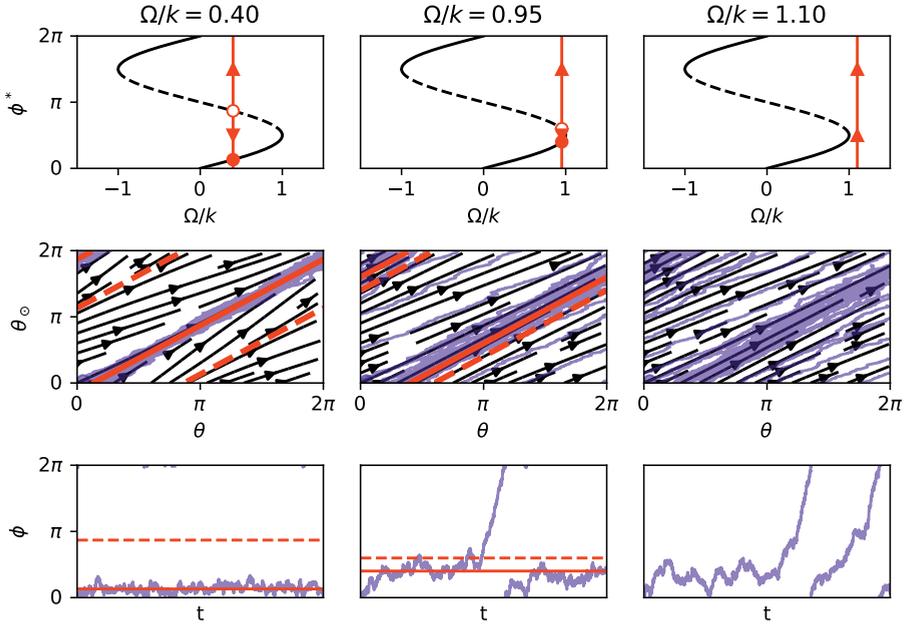
Figure 4.1: Each of the columns corresponds to a different configuration for system (4.1), identified by the value of the bifurcation parameter Ω/k, which represents the synchronization capacity. From left to right, each column represents less coupling strength. Each of the rows corresponds to a different representation of the dynamics. In the first row we see the bifurcation diagram of the phase difference (ϕ). The red arrows in the first row represent the flow on the line. In the second and third rows, the continuous red line represents the stable branch, and the dotted one the unstable branch. Saddle-node bifurcations happen at $\frac{\Omega}{k} = \pm 1$. If $|\frac{\Omega}{k}| > 1$ the system has no equilibrium solution and, thus, represents a desynchronized system. In both the second and third rows, the continuous red lines represent the stable cycle, and the dashed line, the unstable one. We plot in blue one simulated trajectory, under the influence of stochastic noise (modelled as a Wiener process with a variance of $\sigma^2 = 0.04$). The second row uses $(\theta, \theta_\odot)$ as coordinates (phase space) and the third row uses (t, ϕ) coordinates (time series). Notice that in the second column, even if $\frac{\Omega}{k} < 1$, a noise induced transition may happen due to the proximity of the stable and unstable cycles.

4.2.2 How to extract phase differences from data?

From the previous subsection it should be clear that synchronization is related to a fold bifurcation that occurs in the phase difference of the internal clock of a system respective to that of the forcing. This phase difference is usually not directly measurable. Instead, experimental data of periodic phenomena usually gives us indirect information about the phase. The angle of the Sun respective to the local meridian, the height of the tide or even the subjective feeling of sleepiness or hunger along the day are obviously affected by the phase of the cycle under study (see figure 4.2). But, can we use these indirect measurements to robustly infer the phase?

In order to answer this question, we will translate the ideas illustrated in the previous paragraph and figure 4.2 to mathematical language. Particularly, we'll assume, as a working hypothesis, that there is a certain functional relationship M between the phase of the cycle $\theta(t)$ and our observations $y(t)$ (equation (4.4)). Due to the periodic nature of our problem, we expect M to have a period of 2π.

$$y(t) = M[\theta(t)] \tag{4.4}$$

We define a reference cycle $y^{ref}(t)$ based in our knowledge about the system under study. For instance, if we are studying sleep cycles and $y(t)$ represents the asleep state, a reasonable choice for $y^{ref}(t)$ could be $y^{ref}(t) = 0$ (awake) if t is between 8 and 24 h, and 1 (asleep) otherwise. Such a function represents the idealized sleeping cycle of a healthy individual. We assume the reference cycle to be the result of applying the unknown function M to the

4
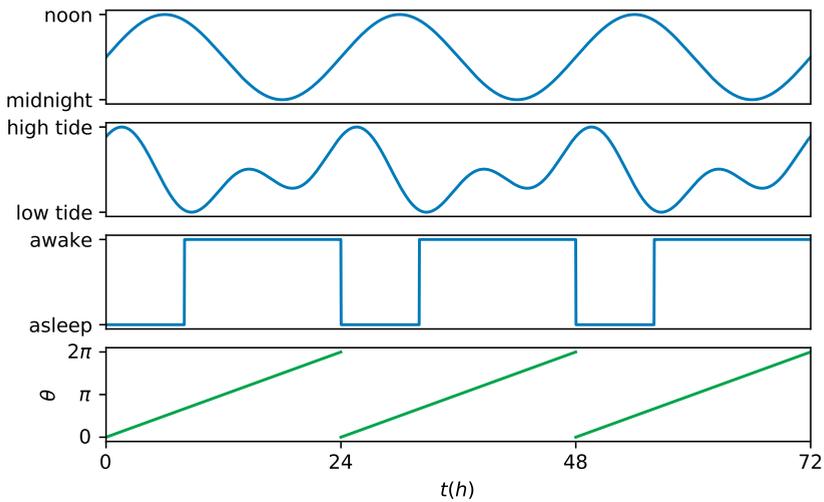
**Figure 4.2:** The first row shows the Sun's angular height from a local horizon. Second row represents the height of the tide. Third row shows a sleep wake cycle of a healthy individual. The fourth and last row shows a common phase for the three above-mentioned phenomena (thus, the time series in all rows can be expressed in the form given in equation (4.5)). All series have been plotted for three whole periods.

phase of the external forcing $\theta_\odot$ (equation (4.5)).

$$y^{ref}(t) = M[\theta_\odot(t)] \tag{4.5}$$

If our system is either synchronized or subject to slow variations in its external conditions, we can consider the phase difference $(\phi(t) \equiv \theta(t) - \theta_\odot(t))$ approximately constant over a given time span $[t_a, t_b]$. It can be shown (see appendix section 4.6.1) that under this circumstances we can expect that $y(t)$ is just shifted in time respective to $y^{ref}(t)$ by a certain time delay λ (equation (4.6)).

$$y(t) = y^{ref}(t + \lambda) \tag{4.6}$$

We find the time delay λ that best fits our data by minimizing the sum of squares between the time-shifted reference cycle and our measurements (see figure 4.3 and equation (4.7)). This time delay λ_{min} is proportional to the phase difference. In section 4.6.1 of the appendix, we show that, specifically, $\phi = \omega_\odot \lambda_{min}$.

$$D^2(\lambda) = \sum_{i=a}^{b} (y_i - y^{ref}(t_i + \lambda))^2 \tag{4.7}$$

Applying the method described above to different time windows allows us to use data to estimate a time series of the phase differences $(\phi(t_j))$ even if the precise analytical form of M is unknown (see first row in figure 4.5 and second row in figure 4.6). See appendix section 4.6.1 for details.

4
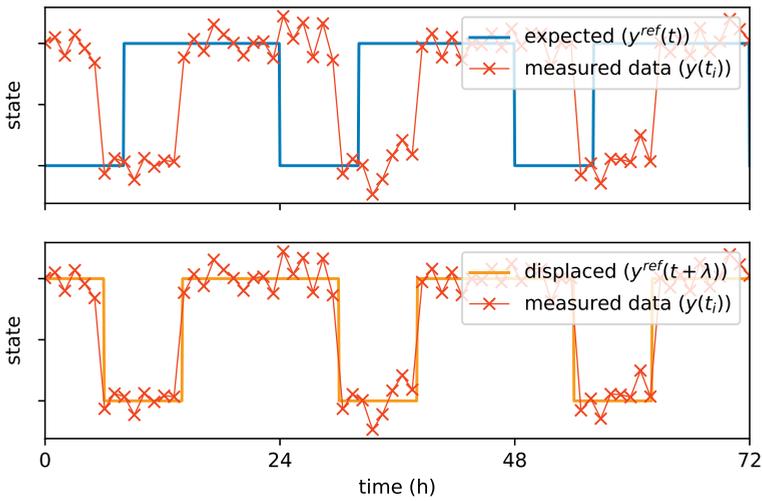
Figure 4.3: In both panels the red crosses represent the hypothetical activity of a human being experiencing a jet lag, measured every 60 minutes during 3 days. In the upper row we see the expected daily activity in blue (no activity while sleeping between 0 and 8 hours, and activity the rest of the day). In the lower row we see, in orange, the expected daily activity, but now displaced $6h$ in the time axis. This displacement provides the best fit for the data, and is calculated by minimizing the function $D^2(\lambda)$ given in equation (4.7).
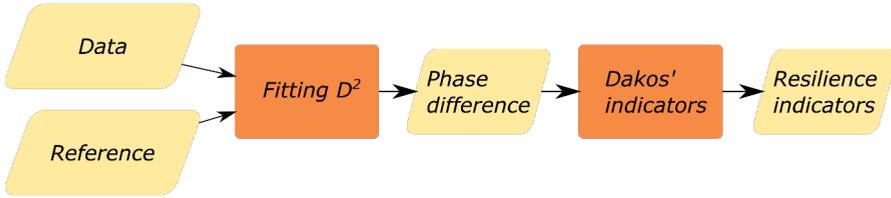
Figure 4.4: Schematic outline of our method.

4.2.3 Resilience indicators

Saddle-node bifurcations are often preceded by the phenomenon of critical slowing down (Scheffer et al. (2009)). Such a phenomenon can be directly observed in the time series even if the underlying dynamics are unknown. In the present manuscript we used the above-mentioned minimization algorithm along a moving window of typically 1-day width to extract the phase difference. Then, we applied the methods proposed by Dakos (Dakos et al. (2012)) to analyze this time series. Particularly, we first detrended the time series by simply subtracting the average value over non-intersecting windows of 1 day length. Afterwards, we calculated the standard deviation and autocorrelation of the residuals, using a rolling window with a length around 25-50% of the original time series' length. The optimal parameters (window length, autocorrelation lag, etc.) depend on the time scale and characteristics of the data under study. For more details about this method, see Dakos et al. (2012). For an extended discussion about the limitations of these methods, see Dakos et al. (2015).

Figure 4.4 summarizes all the steps, inputs and outputs of our method.

4.2.4 Model-generated time series

We tested our method with two model-generated time series.

The first time series was generated with the help of the sleep-wake model of Strogatz (Strogatz (1987)). We configured the system so the time series represents the sleep-wake dynamics of an individual that is becoming progressively more prone to insomnia. The insomnia effect was simulated by allowing the coupling term k to linearly decrease to zero along a period of 135 days. This makes the individual's inner clock progressively less capable of coupling with the day-night cycle, and eventually completely unable to do so. Strogatz's model (Strogatz (1987)) can be understood as a Kuramoto oscillator followed by a postprocessing function M that transforms the inner clock's phase θ into a sleep-wake time series. Particularly, $M(\theta)$ returns 1 (awake) if the inner clock's phase θ is between $2\pi/3$ and 2π radians (corresponding to 8 and 24 hours in the inner clock), and 0 otherwise (asleep). We used the generated time series to estimate the phase difference. As this model contains an explicit phase, we can use it as a control, and compare it with our estimated phase as a verification of our method for extracting phases from data (see first row of figure 4.5).

To show the generality of our method, we applied it to a second time series generated with a more realistic model, the Phillips-Robinson model (Phillips and Robinson (2007)). The Phillips-Robinson model is a deterministic sleep-wake model based on neurological considerations, and it doesn't contain an explicit phase. It describes the time evolution of three state variables: V_v the activity of the ventrolateral preoptic area (prompting the body to stay asleep), V_m the activity of the mono aminergic group (prompting the body to stay awake) and H the homeostatic pressure (an aux-

iliary variable that quantifies the need for sleep). The dynamics of the model are given by the equations (4.8), where $F(V)$ is a saturation function given by (4.9) and $C(t)$ (defined in equation (4.10)) is a time-dependent external forcing, representing the astronomical light/dark cycle. The remaining elements in equation (4.8), including the influence of the acetylcholine group (V_{a0}), are just constants. The parameters used are the same as in (Phillips and Robinson (2007)); see section 4.6.3 in the online appendix. Additionally, this appendix section provides a graphical representation of the relationships in equation (4.8).

$$
\begin{cases}
\tau_v \frac{dV_v}{dt} & = -V_v - \nu_{vm}S(V_m) + \nu_{vh}H - \nu_{vc}C(t) \\
\tau_m \frac{dV_m}{dt} & = -V_m - \nu_{mv}S(V_v) + \nu_{ma}S(V_{a0}) \\
\chi \frac{dH}{dt} & = -H + \mu S(V_m)
\end{cases}
\tag{4.8}
$$

$$
S(V) = \frac{Q_{max}}{1 + e^{-\frac{V-\theta}{\sigma}}}
\tag{4.9}
$$

$$
C(t) = \frac{1}{2}\left(1 + \cos(\omega t + \alpha)\right)
\tag{4.10}
$$

Once again, we simulated an individual whose sleep quality is slowly deteriorating. We achieved this effect by allowing the coupling parameter ν_{vc} to decrease linearly from its normal value of 6.3 mV to 0 mV along a period of three months. By doing this, the ability of the subject to synchronize his internal clock with the external time cues slowly disappears. The first episode of insomnia/desynchronization happens on the 83rd day (see first row in figure 4.6).

In order to simulate the fluctuations expected in any biological system we added noise to the integration of both our time series.

In particular, we modeled our systems as Wiener processes. The deterministic terms have been described in the previous paragraphs. The stochastic terms ($dW = \sigma dt$) for Strogatz's model where set to $\sigma = 0.05$ for the inner clock's phase, and to 0 for the driver. For the Phillips-Robinson model, the stochastic term was set to $\sigma = 1$ for the states V_v and V_m, and 0 for H. The integration was performed numerically with the Python package *sdeint*.

4.3 Application

We applied the minimization algorithm described in the methods section to the sleep-awake time series generated with Strogatz's model (see methods). As a reference of a healthy sleep-wake cycle, we used a simple assumption: a healthy individual is awake between 8 in the morning and 24 at night, and asleep otherwise. We managed to reconstruct correctly the phase difference. The reconstructed phase difference shows the classical signs of slowing down (namely, increase in standard deviation and autocorrelation) when the system is approaching the bifurcation (see figure 4.5).

Our method was also applied with success to the time series generated with the Phillips-Robinson model (equation (4.8)). We focused our attention only in the time series corresponding to the state variable H. We used the time series corresponding to day 1 as a reference to estimate the phase difference. Particularly, we built $y^{ref}(t)$ as a quadratic interpolator of the measurements corresponding to the first day. As we can see in figure 4.6, the first episode of insomnia (83rd day) is preceded by an increase in both standard deviation and autocorrelation of the estimated phase difference.
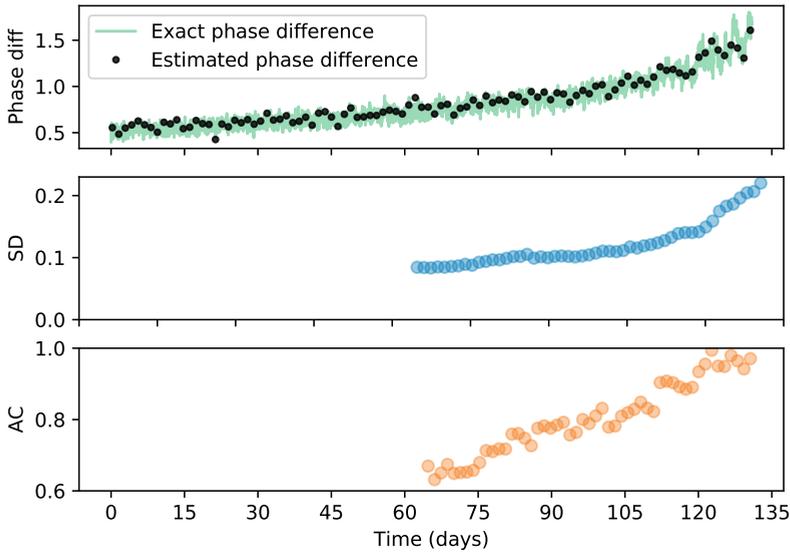
Figure 4.5: The black dots in the upper panel represent the phase difference, as approximated by our method. The exact phase difference is also shown (green line) as a reference of the method's accuracy. The central and lower panel show the standard deviation (in blue) and the autocorrelation with a 24 h lag (in orange) of the estimated phase difference, both of them calculated for a window 50% the length of the data. In both panels, as the time increases, the resilience of our system gets weaker.
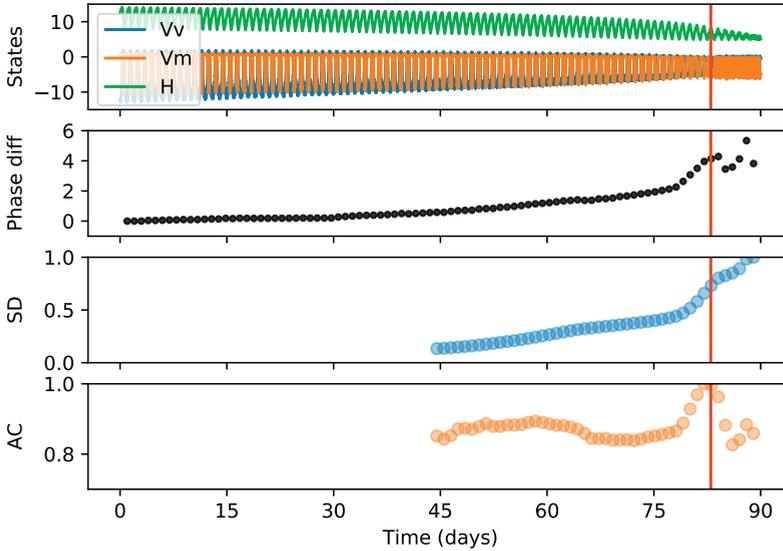
Figure 4.6: The upper panel shows a simulated time series obtained by integrating the Phillips-Robinson model under the influence of stochastic noise, and with the parameter ν_{vc} decreasing linearly in time to simulate an increasing difficulty in synchronizing. The simulation was initialized with non-transient values, to ensure the first days represent a healthy sleep wake cycle. The second panel shows the estimated phase difference (in hours) using the method described in our paper (sub-sampling the whole time series once per day, and using day 1 as reference). Our reference time series was chosen to be the somnogen level H during the first day. The two lower panels show the standard deviation (in blue) and the autocorrelation with a 48 h lag (in orange), calculated for a window of 45 days into the past, of the estimated phase differences. The red line the 83rd day marks the first episode of insomnia/desynchronization.

4.4   Discussion

In the current work we presented a way of deriving dynamic indicators of resilience (DIORs) for systems transitioning from synchronized to desynchronized states through the family of bifurcations known as saddle-node of cycles. Our method is designed for time series, and doesn't require detailed knowledge of the deterministic dynamics of the system. This makes it particularly suitable for biological systems where a loss of synchronization may have an undesired effect (such as insomnia or arrhythmia (Glass (2001))) or may be an indicator of a loss of resilience (such as the disruption in daily activity patterns in cows after calving (van Dixhoorn et al. (2018))).

It may be argued that our method rests on the particular choice of the model given in equation (4.1). As we discuss in the appendix, equation (4.1) represents the simplest, albeit non-trivial representative of a broader family of synchronization dynamics. Different choices yield different geometries in the bifurcation diagram (figure 4.1, first row), but the main characteristic, the fact that at least one saddle-node bifurcation exists, remains true. This, together with the method to extract phase differences for general time series of periodically forced systems, makes our approach valid under very general circumstances. Two application examples of time series that were generated with two different sleep-wake models, Strogatz's and Phillips-Robinson's are analyzed.

The method to extract phase differences requires an approximate reference time series. In the Strogatz's model application example we used the very simple assumption that a healthy individual sleeps from 0 h at night to 8 h in the morning. Some problems may benefit

from or even require more sophisticated assumptions. In the absence of any detailed knowledge of the system under study, another approach could be using the dynamics of an arbitrary day as a reference. This is what we did in the Phillips-Robinson application example.

Additionally, our method requires high quality time series. Those time series should be long (as we need many cycles to infer the indicators) and should have a high density of data points (typically of the order of 10 points measured per cycle, depending on the shape of the time series). This makes our method less suitable to be applied with success in fields where the data is difficult and/or expensive to collect. Luckily, data-rich systems such as the ones provided by wearable devices are becoming increasingly popular in medicine or veterinary sciences.

Even after extracting the phase difference, the critical slowing down may be difficult to detect under some circumstances. As already noted in Dakos et al. (2015), his method to forecast saddle-node bifurcations has some fundamental limitations. For instance, it is required that the time-scale of the changes in the external forcing to be slower than the natural time-scale of the system (that is, the transitions shouldn't be too sudden). The role of noise is also a delicate issue. On one hand, noise is required in order to observe the phenomenon of critical slowing down in the vicinity of a saddle-node bifurcation. On the other hand, it obscures the deterministic dynamics. Our analysis will prove weak for systems whose dynamics are strongly dominated by noise. Our method, based on Dakos' indicators, shares this set of limitations.

Even with those applicability challenges, we consider our method to be a step in the direction of forecasting transitions between syn-

chronized and desynchronized states. The fact that the disruption in certain physiological rhythms is associated with disease (Glass (2001)), together with the recent increase in the availability of high-quality biometric time series, makes the analysis and potential forecasting of these relevant kind of transitions a topic worth being explored.

4.5 Acknowledgements

4.6 Appendix

4.6.1 Detailed derivation of the phase extracting method

In order to justify the results of section 4.2.2, we will make use of equations (4.1), (4.4), (4.5) and (4.6). As a first step, we will write both sides of equation (4.6) in terms of M. We can do this by directly applying (4.4) and (4.5). The result is shown in equation (4.11).

$$
\begin{cases}
y(t) & = M[\theta(t)] \\
y^{ref}(t + \lambda) & = M[\theta_\odot(t + \lambda)]
\end{cases}
\tag{4.11}
$$

In order be able to compare the functions given by equations (4.4) and (4.5) we will change their coordinates. Using the phase difference $(\phi(t) \equiv \theta(t) - \theta_\odot(t))$, we can rewrite the equation (4.4) in terms of $\theta_\odot$ and ϕ (see first line in equation (4.12)). Introducing a leftwards shift λ in the time coordinate of equation (4.5) it takes the form $y^{ref}(t + \lambda) = M[\theta_\odot(t + \lambda)]$, where $\theta_\odot(t + \lambda)$ can be evaluated exactly by its first order Taylor expansion, that is, $\theta_\odot(t + \lambda) = \theta_\odot(t) + \omega_\odot \lambda$ (cf. second line of equation (4.1)). The results of both coordinate transformations appear in equation (4.12).

$$
\begin{cases}
y(t) & = M[\theta_\odot(t) + \phi(t)] \\
y^{ref}(t + \lambda) & = M[\theta_\odot(t) + \omega_\odot \lambda]
\end{cases}
\tag{4.12}
$$

Note that if the system is synchronized and/or if the adiabatic approximation (that is, that the external conditions vary slowly)

holds in our region of interest ($t \in [t_a, t_b]$), $\phi(t)$ can be approximated by a constant ϕ. We can estimate the value of ϕ by finding the shift λ^{min} that minimizes the square distance between both functions (equation (4.13)). By direct inspection of equation (4.12) we see that this optimal value corresponds to a phase difference of $\phi = \omega_{\odot} \lambda^{min}$.

$$D^2(\lambda) = \int_{t_a}^{t_b} (y(s) - y^{ref}(s + \lambda))^2 ds \qquad (4.13)$$

When faced with experimental data, we'll have a collection of N measured values y_i sampled at times t_i (that is, $y_i = y(t_i)$). The discrete equivalent of equation (4.13), representing the square distance between our measured and the expected points, is given in (4.7). By finding the value of the time displacement λ that minimizes $D^2(\lambda)$, we find the time delay that better fits our data (see figure 4.3).

4.6.2 Further generalization

By manipulating the parameter Ω/k in an equation like (4.2) with any non trivial continuous function $f(\phi)$ we are sure of encountering at least one saddle-node bifurcation. Even more, the saddle-node is the only kind of bifurcation that may happen.

This can be proven graphically. As we discussed in the methods section, the coupling function f in the model given by equation (4.2) can be any non-constant, continuous, smooth and periodic function, not necessarily a sine. A function f satisfying these properties will have at least one local minimum and one local maximum per period. This is also true for the right-hand side of equation (4.2). The effect
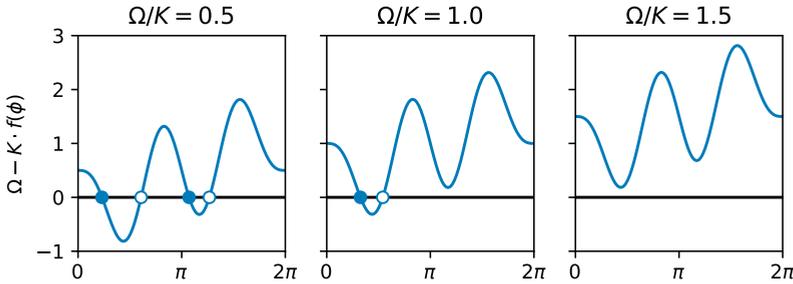
Figure 4.7: Here we plot the curve $y(\phi) = \Omega - kf(\phi)$ for a non-sinusoidal coupling function f. The function is non-constant, continuous, smooth and periodic. We plotted it for three different values of the bifurcation parameter $\frac{\Omega}{k}$. The roots of each curve represent the equilibria (filled dots if stable, white if unstable).

of the parameter Ω/k is to move up and down the curve defined by $y(\phi) = \Omega - kf(\phi)$, whose roots represent the equilibria. This rules out the pitchfork and the transcritical bifurcations, as those require a change in the shape of the curve $y(\phi)$ (Strogatz (2003)). By manipulating the parameter Ω/k, the only possible bifurcations are collisions of stable and unstable equilibria, that is, saddle-node bifurcations (Strogatz (2003)). Those bifurcations happen when a minimum or a maximum equals 0 (see figure 4.7).

Those readers familiar with analysis may prefer noticing that, in the vicinity of a minimum/maximum (ϕ_0), the second order Taylor expansion of the right-hand side of equation (4.2) can be written as the equation of a parabola (4.14).

$$\Omega - kf(\phi) \approx \Omega - kf(\phi_0) - \frac{kf''(\phi_0)}{2}(\phi - \phi_0)^2 \qquad (4.14)$$

By using the new variable $x \equiv \sqrt{\frac{-kf''(\phi_0)}{2}}(\phi - \phi_0)$ (representing a

shift and re-scale of the horizontal axis), and renaming $\Omega - kf(\phi_0)$ as r, the right-hand side of equation (4.14) adopts the canonical form of saddle-node bifurcation, i.e.: $r + x^2$ (Kuznetsov (1998)).

Due to the generality of the conditions requested to the coupling function f, we expect saddle-node bifurcations in the phase difference to be a widespread mechanism of synchronization and desynchronization. Consequently, we expect those bifurcations to be susceptible of being detected by the method described in this manuscript.

4.6.3 Parameters for Phillips-Robinson model

The parameters used in equation (4.8) are the same as in (Phillips and Robinson (2007)), with the exception of ν_{vc}, that decreases linearly from 6.3 mV to 0 mV along the period of 90 days. The time units have been changed to hours. The dynamics of the model are summarized in figure 4.8. A usable implementation of this model (in R) can be found at `https://github.com/PabRod/sleepR`.

Symbol	Value	Units
τ_m	10/3600	h
τ_v	10/3600	h
χ	10.8	h
ν_{vm}	1.9/3600	$mV \cdot h$
ν_{mv}	1.9/3600	$mV \cdot h$
ν_{vh}	0.19	$mV \cdot nM^{-1}$
μ	10^{-3}	$nM \cdot h$
ν_{vc}	$6.3 - 0$	mV
$\nu_{ma}S(V_{a0})$	1	mV
Q_{max}	$100 \cdot 3600$	h^{-1}

Symbol	Value	Units
θ	10	mV
σ	3	mV
ω	$2\pi/24$	h^{-1}
α	0	1

4
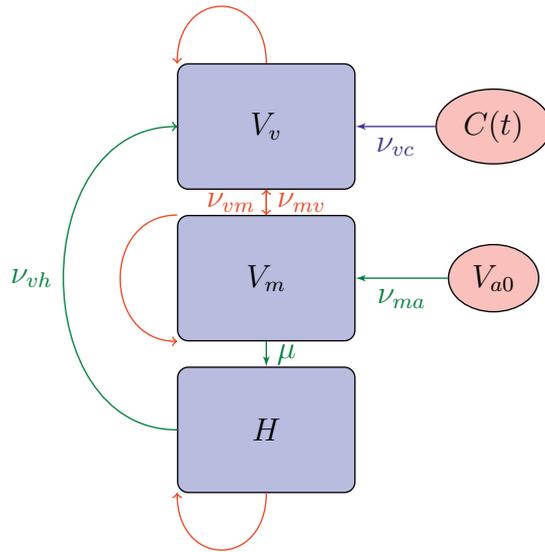
Figure 4.8: Schematic summary of the dynamics of the Phillips-Robinson model. The light blue nodes represent the system's states (V_v the activity of the ventrolateral preoptic area, V_m the activity of the mono aminergic group and H the homeostatic pressure). The pink nodes represent the external sources ($C(t)$, the astronomical light/dark forcing, and V_{a0}, the acetylcholine group constant influence). The positive effects are coded as green arrows. Negative ones as red arrows. Blue arrows represent oscillating effects.

Chapter 5

Afterthoughts

In this last chapter I briefly reflect on the potential and limitations of the results presented in this thesis. Subsequently, I reflect on some of the challenges of trans-disciplinary work that I experienced linking physics and biology for the work presented in this thesis.

5.1 Main conclusions and their main limitations

5.1.1 Neutrality and chaos are not independent drivers of diversity

In **chapter 2** we found that competition close to neutrality significantly increases the chances of non-equilibrium long-term behaviour. We also showed that the non-equilibrium dynamics of those simulated ecosystems were correlated with a higher biodiversity. This result adds some new arguments to the long-term ecological question: why are there so many species of plankton while there seem to be so few niches? (Hutchinson, 1961). Particularly, it provides a link between two hypotheses usually presented as independent: Hubbell's theory of neutrality (Hubbell, 2003) and the hypotheses of non-equilibrium (Armstrong and McGehee, 1980). I argue that perhaps those are indeed two sides of the same coin.

The results of **chapter 2** are based on the numerical analysis of a theoretical model. As in most models in mathematical biology, we cannot expect a high descriptive accuracy. They can only serve as a hypothesis that may be tested in experiments. Hopefully our work will inspire such experiments, but we are not optimistic about their

feasibility. A direct experimental confirmation of our results would be enormously challenging, as it is very difficult to show chaos in experimental data. For instance Benincà et al. (2008) needed data of an 8 year experiment to demonstrate that the populations in a chemostat had chaotic dynamics. To test our hypothesis would additionally require not only many replicates of such expensive experiments, but also a manipulation of the competition strengths between species. Despite the near-impossibility of performing such experimental tests, I feel that our modelling exercise may help seeing the relationship between two important, but previously unconnected mechanistic explanations of biodiversity.

5.1.2   Stability landscapes can rarely be accurate

Chapter 3 is an example of interdisciplinary interaction. Stability landscapes, a visual tool very popular in stem cell research (Gilbert, 1991) and other subfields of biological and social sciences (Beisner et al., 2003), are strongly based in the physical concept of scalar potential. We noticed that stability landscapes are surrounded by a lot of confusion and misuse in interdisciplinary research communities.

Stability landscapes have the virtue of simplifying the explanation of several advanced concepts in dynamical systems theory, such as multistability, resilience or tipping point (see for instance Scheffer et al. (2001)). But they also have an important limitation: they can only be defined for a family of dynamical systems known as gradient (Marsden and Tromba, 2003). In **chapter 3** we do not only explain the limitations of stability landscapes, but we also provide an algorithm to create approximated potentials for systems that are weakly and/or locally non-gradient. As the mathematical tools

involved are relatively advanced for non-mathematical audiences, a great amount of energy was invested in the readability and usability of the paper. An analogy with art was used to provide an intuitive illustration of the fundamental problem: the fact that sometimes stability landscapes cannot be defined.

Not our method, nor any other can derive a stability landscape if the system is strongly non-gradient. Software engineering protocols were used to develop and publish a fully working software package, in order to reach those users more interested in a solution than in the internal details. We made sure that the output always contains an error map, to explicitly address if and where the resulting stability landscape is reliable and, hopefully, avoid future confusion. This new approach may enlarge the realm of situations in which approximate stability landscapes can be produced. Nonetheless, I realize that it may remain challenging for most biologists to see the fundamental limitations of applying stability landscapes. This may not be a problem as long as the approach is loosely used as a heuristic only.

5.1.3 Resilience of synchronized states may be detected

In **chapter 4** we addressed the question of assessing the resilience of biological periodically forced systems, with respect to sudden loss of synchronization. By describing this problem in an abstract mathematical way (Kuramoto, 1975) we show that there is likely a fold bifurcation involved, but only when we consider the phase difference between the forcing and the cycle. We deliberately chose a very abstract model (Kuramoto, 1975) not only for pedagogical reasons, but also for deriving the most general indicators possible.

Resilience analysis (Dakos et al., 2009), particularly detection of critical slowing down, was used to derive two dynamical indicators for loss of resilience (DIORs) and to find them in simulated data. The generality of our method is justified by geometrical considerations. In order to check that our indicators work, we tested them against time series simulated using models from sleep science (Strogatz, 1987; Phillips and Robinson, 2007).

In addition to the fundamental requirements for detection of critical slowing down (Dakos et al., 2015) (such as having not too sudden changes in external conditions), the application of these indicators of resilience will require a long-term high quality data time series. The blooming wearable and remote sensing industries, particularly for medical and veterinary applications, are a possible source of data that we look at with great optimism. Unfortunately, not all fields of biosciences where synchronization seems to play a role are so lucky. Synchronization with seasons in plankton dynamics (Vandermeer et al., 2001), for instance, may be more challenging to study with the tools presented in **chapter 4** due to the difficulty of collecting enough data points.

Even with these practical challenges, we consider **chapter 4** a first step in the detection of early warning signals for desynchronization. Provided several conditions, such as insomnia or arrhythmia, are related with abnormal synchronization of physiological rhythms, our results may have a potentially important impact in health sciences.

I now turn to a series of more general reflections on the link between the different branches of science and engineering that I have encountered during the work presented in this thesis.

5.2 What can biology and physics learn from each other?

Maybe surprisingly, the seemingly distant scientific fields of physics and biology have many similarities. This is due to the most remarkable feature of mathematical knowledge: the power of abstraction. The underlying mathematical descriptions of apparently disconnected phenomena are often similar, and sometimes even exactly the same. The models used to pose and address questions in population dynamics (such as the one in **chapter 2**) are indeed quite similar to the ones used in chemical kinetics. Another example shown in this thesis is the problem of defining stability landscapes for multistate systems (addressed in **chapter 3**). In this case, the analysis is not only similar but the very same as a classical vector analysis problem known since the 19th century, that of the Helmholtz decomposition. A significant part of **chapter 3** is, indeed, a translation of Helmholtz's old ideas to multidisciplinary language.

Of course, there are also large differences between physics and biology. Maybe unexpectedly, dealing with biological models is often harder than with those from physics. This is a straightforward consequence of the higher complexity of biological systems when compared with most physical ones. For instance, even the simplest biological models show non-linear behaviour. This makes their resolution and analysis particularly challenging, and also gives rise to interesting phenomena such as limit cycles and chaos.

More importantly, most physical models are derived from a bunch of simple first principles known to be extremely accurate (such as Newton's laws of motion or Maxwell's equations for electromagnetism)

while biological ones cannot afford that luxury (there is no such a thing as Newton's laws of population dynamics). In other words: while most physical models are mechanistic, most biological ones are phenomenological (Edelstein-Keshet, 2005; Murray, 2002). The evolution from the Malthusian growth equation (Malthus, 1798; Bacaër, 2011) to the logistic growth one (Verhulst, 1838; Bacaër, 2011) is a good example of this phenomenological approach. The Malthusian growth model predicts unlimited population growth, something obviously not happening in nature. The logistic growth just adds an upper limit to the population, known as the carrying capacity, in the simplest mathematical manner: a linear decay in the growth rate with increasing biomass. Indeed different shapes of the decay curve in the growth rate may give better results in some populations, but the linear decay of the logistic growth often fits remarkably well (as seen in Driever et al. (2005)). As a side effect of this phenomenological character, the expected predictive power of a biological model is on average much lower than that of a physical one (Edelstein-Keshet, 2005; Murray, 2002).

None of the above means that biological or other phenomenological models are useless. Even an inaccurate biological model offers us new ways to think about biological phenomena. An example is the Kuramoto sleep-wake model (Strogatz, 1987) used in **chapter 4**. This model was built paying attention only to qualitative, gross properties of synchronized systems, and thus we cannot expect it to be highly accurate for specific cases. We show that this lack of accuracy can become an advantage: the model can be used as an approximation of any system with the same qualitative properties, that is, to a huge variety of different phenomena. Geometrical considerations also allow us to understand why the conclusions derived from this inaccurate model are expected to remain true

under very general circumstances, providing a formal theoretical basement.

When it comes to modelling, physicists have a powerful trait: they are used to follow a very structured bottom-up approach in problem solving. This is a consequence of the abundance of first principles in physics, without whom a bottom-up approach is just unfeasible. Two of the positive side effects of this trait are the increase of confidence and the improvement of the generalization capacity (in the sense of applying abstract concepts to apparently disconnected problems). Confidence is built each time the physicist solves a problem with the only help of a handful of first principles and a piece of paper. The generalization capacity is trained when the physicist solves several problems using the same first principle. Both together create the illusory feeling that any question can be solved with a small set of rules and a pocket calculator. This is of course dangerous and frustrating when the approach is not feasible anymore, as often happens with biological and other complex problems.

On the other hand, biologists are permanently exposed to the full complexity of their object of study: life. As a consequence, they are not scared at all by complex models. Biologists don't hesitate to use ambitious approaches in their models, combining all kind of inputs and interactions. Agent based models, that often require advanced calibration and validation methods to be parameterized are perhaps the most eloquent example (see for instance Grimm (2005)). Physicists, more used to neat, short and relatively simple models (they even use the words "elegant" and "beautiful"), tend to feel uncomfortable with such complex models. As nature is complex, the advantages of this trait biologists excel at are obvious. There are, nevertheless, a few disadvantages. The fact that almost no biological model can be solved with pen and paper usually invites the

biologist to rely too much on his/her computer, and increases the temptation of using third party methods and models as black boxes. Additionally, as a consequence of the lack of exposure to "elegant" models, most biologists may not pay much attention to the notation and readability of their equations (Edwards and Auger-Méthé, 2019). In some cases there is even no standard way to write down the model using mathematical notation (Grimm et al., 2006) but, as we'll see in subsection 5.3, tools such as literate programming represent a practical and natural alternative.

More exposure to complex problems from biology could help physicists to not forget how hard understanding nature can be as soon as one leaves the textbook examples. Conversely, more exposure to solvable problems from physics could increase biologists' appreciation of the power of abstract thinking and also improve the clarity of their explanations.

5.3 What can researchers learn from software engineering?

Most scientists make extensively use of computers in their research, and that is certainly the case for modelling studies such as this thesis. They often use self-made software or research scripts. Furthermore, there is an increasing concern about reproducibility of scientific results. At the same time software engineers have created various tools for developing their complex software in a more consistent way. For this reason, I plea for an integrated approach for writing scientific papers, combined with the data and software that may recreate the results.

Indeed, the standard of form of communication in science, the scientific paper, is also rather complex. This is true not only because the contents are complex: a scientific paper is complex from the point of view of information management. A scientific publication can be loosely defined as a piece of encapsulated information. It should be internally and externally consistent, convincing, reproducible and properly written. To make things even more complicated, scientific publications are usually written by a team of authors and have several versions in time.

Due to my experience in software engineering I noticed similarities between scientific writing and software development (see also Marwick et al. (2018)). Software is also a piece of encapsulated information that must fulfill similar requirements to those of scientific papers (see table below).

Software	Scientific paper
Consistent	Consistent
Working	Convincing and reproducible
Properly written and documented	Properly written
References and dependencies	References
Written by a team	Written by a team

Of course, there are also differences. For instance, due to code being less flexible than human language, consistency is harder to attain in code than in text. A minor typo on a paper, that in the worst case will make a reviewer raise her or his eyebrow, usually triggers a serious error when happens on a piece of code (or even worse: it doesn't trigger any and remains unnoticed). Software developers are very much aware of how hard to attain the list of requirements

in the table is, and they developed methods and protocols to deal with this set of problems, identified under the umbrella term of *best practices* (Wilson et al., 2014). These methods can be easily adapted to the scientific profession. Three of them are worth being explicitly mentioned in the context of this thesis:

Version control systems (VCS) record and store changes in the files contained in a project folder. Different "snapshots" can thus be stored. This is done manually, and each "snapshot" or version receives a meaningful name and description. This allows to compare and recover versions corresponding to different stages in time.

The most popular version control system nowadays is *git*. It provides integration with *GitHub*, a server that facilitates project discovery, coauthoring and publishing of projects.

Unit testing (UT) consists in writing and storing scripts that check the integrity of each component of a piece of software. In the case of scientific software, the battery of tests must check that each function written or used by the researcher produces the expected output when fed with a known input. This increases the robustness of the produced code, serves as additional documentation about the purpose of each function and makes error spotting in future editions (either by the same author or a coauthor) much easier.

Unit testing engines usually depend on the programming language used in the project. In **chapter 2** we used Matlab's script-based unit testing. In **chapter 3** we used the *R* package *testthat*. In **chapter 4** we used *Python's pytest*.

Literate programming (LP) tools use a combination of code and enriched text to produce a human-readable output. Most of this thesis has been written using *RMarkdown*, a format that combines enriched text with chunks of code. The R package *knitr* executes and exports these *RMarkdown* files to different human-readable formats such as *html*, *doc* or LaTeX.

LP is becoming progressively more popular for scientific writing, to the point that certain packages, such as *rticles*, automatically adapt the output to the requirements of different journals and conferences. The main reason for this popularity is the increasing concern about reproducibility of scientific results. While traditional papers are static descriptions of what the researcher has done, LP documents are living documents that not only describe, but actually perform the described operations.

Synergies

All the scientific research contained in this thesis has been structured in the form of a software engineering project. Code, text and figures have been managed together through a VCS, adding UT to check the consistency of our analyses. The code corresponding to all chapters has been registered via Zenodo in order to ensure permanent public access to the exact version used, a prerequisite to reproducibility. With no exception, each of our results can be reproduced with a single click. In **chapters 3 and 4** we took the parallelism between software and science writing even further: both chapters were written in the form of standard software packages (in R and Python, respectively), ready to be reused. The papers have been written using LP with calls to the packages themselves, in order to ensure reproducibility and robustness. This form of

publication, known as research compendium (Nüst et al., 2018), is increasingly gaining popularity.

The results couldn't have been more satisfactory. Some obvious advantages of this way of working are that our results are easily reproducible, and that our methods are ready to be found, used, adapted and even expanded by interested enough readers. More unexpected advantages were also found from the point of view of psychological well-being. The joint management of code and text using LP, together with the standardized folder structure of a software package and the use of a VCS kept the working environment remarkably tidy. The extensive use of UT also increased the consistency of the work and allowed for quick error spotting, making the anxiety produced by code crashes disappear completely. Following the classical, very structured software development workflow recommended by VCS (write, test, commit) naturally structured the author's everyday tasks in small, measurable steps, generating a rewarding feeling of daily progress. Additionally, VCS served naturally and effortlessly as a lab journal, being particularly helpful to gain momentum after having left a project aside for some time.

These methods and concepts are slowly finding their place in educational syllabi, often through the figure of *Data Competence Centers*. The increasing access to cheap computational power and the growing need of reproducible data analysis are making information literacy skills a must-have in any scientific discipline.

5.4 How can we improve the communication between mathematics and life sciences?

Mathematics is often perceived as a harsh subject both by scientific and non-scientific professionals. On the other hand, regardless of our personal preferences, mathematics are used in almost every field of knowledge and are must-have in any multidisciplinary project. The present thesis, written under the auspices of a consortium formed by mathematicians, physicists, biologists and economists, is an example. Such an environment represented the perfect ecosystem for experiencing multidisciplinarity, with both its advantages and difficulties.

Different disciplines have associated not only a set of background knowledge and methods, but a whole academic culture. When crossing the borders between disciplines, facts and methods can be learned, but accepting and adapting to another culture is much harder.

As with any other culture, mathematicians and biologists differ slightly in language, values, norms and interests. As usually happens in intercultural communication, there is plenty of opportunity for misunderstandings, and each subgroup cultivates myths and misconceptions about the other.

In the rest of this section, I will offer some advice for both biologists and mathematicians (understood here as mathematically oriented professionals, including physicists and engineers) interested in exploring "the other side".

Advice for biologists working with mathematicians

Invest in applied mathematics

Applied mathematics doesn't mean easy mathematics. The adjective "applied" or "pure", accompanying the word "mathematics", tells us something about the object under study, but nothing about its difficulty. Indeed, the mathematical tool will be as complex as the object under study is.

It may be frustrating to learn that, for instance, it is required to get familiar with second order tensors (a particularly hard tool rooted in differential geometry) in order to understand fluid dynamics. Mathematicians don't introduce this tool to torture the newcomers, but because tensors are the easiest available tool to study a complex phenomenon that cannot be avoided in the study of fluids: deformation. The difficulty is provided by the problem under study, not by the tool used to solve it.

This thesis contains some advanced mathematical concepts appearing more or less naturally in biological problems. The concepts of attractor and deterministic chaos appear in **chapter 2**, even after having built our model with very simple assumptions. The gradient theorem is the core of the misunderstanding around stability landscapes described in **chapter 3**. The concepts of fold bifurcation and critical slowing down are key for deriving the indicators for desynchronization in biological systems studied in **chapter 4**, and the generalization of our method is proved using continuity theorems.

Equations and rigor are not torture instruments

It is known that the mere sight of an equation can create anxiety. Even the physicist Stephen Hawking, in the preface of his best seller "A brief history of time" (Hawking, 1998), claims that each printed equation divides the potential audience by two.

Whether we like them or not, equations are often the best way to share complex information in a compact and practical manner. Invest time in learning how to read them. Rigorous and detailed analyses are often required, as some details can escape intuition. A good example is the calculation of 2 dimensional stability landscapes. Intuitivelly one may think that expanding the tool from 1 to 2 dimensions should be straightforward, but as we saw in **chapter 3** this is far from true.

Be also aware that the same equation can be written in different ways. Even if different ways of writing the same equation are correct, some of them can be clearer than others. A consistent use of upper and lower case (for instance, upper for states, lower for parameters), superscript and subscript, smart use of auxiliary definitions, proper alignment of related equations and other simple rules can significantly increase the readability of your scientific output (Edwards and Auger-Méthé, 2019).

Modelling is all about simplifying

Be prepared that the main task of modelling is simplifying as not all processes can usually be included in a model. This is the main challenge as here both knowledge of the system and of modelling is needed. In the design phase of a model lots of exchange is needed

between the biologists and the mathematicians. This may come as a surprise, but most mathematicians feel overwhelmed by biologists' talk. Biologists tend to provide too much information for them.

When communicating to mathematicians, focus more on the ideas than on the details you would provide for your peers. You can easily underestimate how difficult your own field is for outsiders. For instance, the experimental methods can be left out, as mathematicians will just assume that the data has been properly collected. Try also to think in terms of inputs, processes and outputs.

This exercise of thinking in terms of inputs, processes and outputs is not only good for interdisciplinary communication, but also for experimental design and even for structuring a report. This approach was followed in the present thesis, to the point that the core of each chapter can be summarized in a flow diagram.
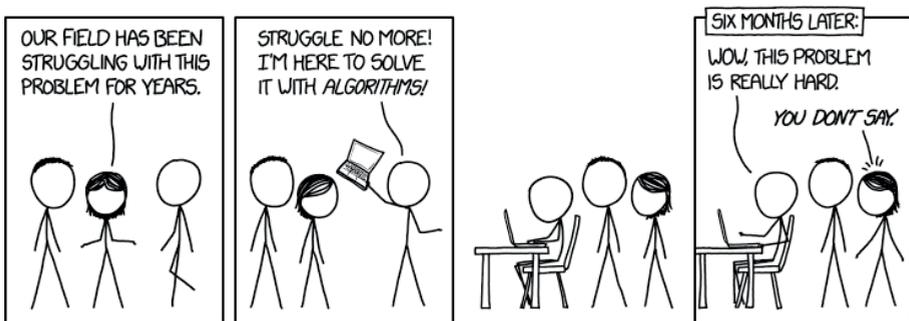

Figure 5.1: Dramatic recreation of the first months of a typical multidisciplinary collaboration. Source: (https://xkcd.com/1831/)

Advice for mathematicians working with biologists

Make peace with uncertainty

Due to the complexity of the subject of study, it is unrealistic to expect the same precision from biological models than from physical ones. Forget all you learned in math/physics/engineering school about discarding any result with an r^2 below 0.99. You are working with complex systems now. Models just do as good as possible. Additionally, you'll have to embrace the fact that most of these models rarely allow an elegant, analytical approach, and numerical methods will be required most of the time.

None of the models used in this thesis can be considered very accurate if compared with engineering or physical models. But our field of study, biological systems, is more unpredictable due to both practical and fundamental limitations. In the practical side, the difficulty of collecting biological data (particularly in ecology) makes almost impossible to even know the initial conditions of a given system. A more fundamental problem, that couldn't be resolved even if we had a magical tool to establish the initial conditions, is that our models are a strongly simplified description of a complex reality. Nevertheless, despite all these difficulties, qualitative conclusions can still be drawn from mathematical modelling.

Explain why you do what you do

When explaining a mathematical method, instead of starting with generic propositions and formal proofs, always explain why it is useful using simple examples. Biologists may quickly loose motivation if they are not convinced that the used mathematics are somehow

useful.

A particularly illuminating experience happened to me while teaching matrix multiplication to a group of biology students. The topic is particularly boring, and most often is just presented as a rule. In this case, I proceeded differently: I first let the students experience the *need* of a compact notation (by making them write down line by line increasingly larger competition models), and later I explained why the rule of matrix notation is what it is and how it solves their need for a compact notation.

Presented this way, the students notice that the mathematical tool is solving a problem they already have, instead of feeling that it creates a new one (that of having to learn a new tool). Additionally, the explanations about why the rule is how it is helps them learn and remember it.

Proofs are scary

Maybe you think mathematical proofs *shouldn't* be scary, but the fact is that for most biologists they are. A proof is somehow a journey, a journey from a set of assumptions to a conclusion, and your collaborators should enjoy the ride too.

Often, proofs can be substituted by a graphical or an intuitive approach. This substitution may come with some simplification when affordable, but often can be done without loss. Euclid's "Elements", probably the most influential mathematical book ever written, contains mostly visual proofs. More modern examples can be found in the collection "Proofs without words" (Nelsen, 1993).

If a proof is really needed, make an effort in explaining the notation

and all the steps. The quickest way of creating frustration in your audience is by using the word *trivial*, so avoid it always. When writing publications in non-mathematical journals, it is usually a good idea to write the proofs in an appendix and just state the results as a fact in the main body. Just like mathematicians feel they cannot judge experimental methods, most biologists will assume proofs are correct.

In the present thesis we present an informal proof of the generality of the results of **chapter 4** based exclusively in a graphical approach. We use an analogy with art in **chapter 3** to explain why some problems lack a stability landscape and, when we explain the details of the algorithm we introduced, we explicitly explained the meaning of any mathematical symbol not covered in high school.

Use visualization as much as possible

Take advantage of humans' most advanced information acquisition system: vision. Illustrate your ideas with graphs and figures, or even movies and animations when applicable. If they are good, they can even replace an equation.

Visualization has been used all around the present thesis. The example of **chapter 3** is particularly relevant, as the whole story is built around an analogy with a famous piece of art.

Advice for both

Get involved in science communication

If you think interdisciplinary communication is hard, just try to communicate science to a general public. Not only will you notice that science communication is even harder, but also you will learn a lot about how to improve your overall communication skills.

Despite science communication is receiving more attention than ever by universities and other scientific institutions, and although nowadays there are lots of ways of getting involved with it (from writing a blog to giving a talk at an event), science communication is still often perceived as a secondary task and rarely has any impact in the researcher's curriculum. Some steps have been performed in order to change this, such as the introduction of the Altmetrics index or the inclusion of a contractual obligation to involve in science communication in certain projects (such as the H2020).

The practice of science communication forces a deep understanding of the topic being communicated. It requires to remove the unnecessary, to identify what is hard and why and to advance the audience questions and doubts. It requires, in one word, understanding.

5.5 A mathematician among biologists: invasion or symbiosis?

Any thesis is strongly shaped by the interests, the skills and even the personality of its author. This one is of course no exception.

When I began writing it, I was a physicist, working as an engineer in a technological company, and who was hired as a mathematician by a group of aquatic ecologists. The question is straightforward: what is a mathematician doing there?

The symbiosis between mathematics and biology, although may seem improbable at first sight, is actually backed by a centuries old tradition of collaboration. It started with mathematicians that were inspired by biology such as Leonardo Pisano, *alias* Fibonacci. His famous sequence (namely: $1, 1, 2, 3, 5, 8, 13, ...$), a landmark in number theory very popular among amateur mathematicians, was first described in the context of a practical problem on rabbit breeding in such an early date as year 1202 (Bacaër, 2011).

Mathematical knowledge has improved greatly since the 13th century. The foundations of the tools used by modern mathematical biologists, namely, calculus and differential equations, were laid in the late 17th century by Isaac Newton and Gottfried Leibniz motivated by mechanical problems (Boyer, 1968; Simmons, 1991). The great mathematician Leonhard Euler and the economist and demographer Thomas R. Malthus, two of the pioneers of using differential equations to address biological problems, had both printed their seminal works in population dynamics before the fall of year 1800 (Bacaër, 2011).

This interdisciplinary collaboration between mathematics and biology is nowadays alive and in good shape. Some of the most influential names in ecology in the 20th and 21st century have, indeed, a background in mathematics (such as Robert MacArthur, Simon Levin or Alan Hastings) or in physics (such as Robert May).

The opportunity offered by cheap access to computing power, together with the unavoidable increase of required technical skills

such as programming, data analysis and advanced statistical methods, points to a future were the technical profiles expected from a research team in biology will not be so different to those of a team of physicists or applied mathematicians. It is reasonable to expect that this symbiosis between mathematicians and biologists will remain strong, and even get stronger, in the near future.

5

References

Ao, P., Kwon, C., and Qian, H. (2007). On the existence of potential landscape in the evolution of complex systems. *Complexity*, 12(4):19–27.

Armstrong, R. A. and McGehee, R. (1980). Competitive Exclusion. *The American Naturalist*, 115(2):151–170.

Bacaër, N. (2011). *A short history of mathematical population dynamics*. Springer.

Bathiany, S., van der Bolt, B., Rodríguez-Sánchez, P., and Mirza, U. (2018). *Tipping points, zo werken ze!* Netherlands Earths System Science Centre.

Beisner, B., Haydon, D., and Cuddington, K. (2003). Alternative stable states in ecology. *Frontiers in Ecology and the Environment*, 1(7):376–382.

Benincà, E., Ballantine, B., Ellner, S. P., and Huisman, J. (2015). Species fluctuations sustained by a cyclic succession at the edge of chaos. *Proceedings of the National Academy of Sciences*, 112(20):6389–6394.

Benincà, E., Huisman, J., Heerkloss, R., Jöhnk, K. D., Branco, P., Van Nes, E. H., Scheffer, M., and Ellner, S. P. (2008). Chaos

in a long-term experiment with a plankton community. *Nature*, 451(7180):822–825.

Berryman, A. and Millstein, J. (1989). Are ecological systems chaotic — And if not, why not? *Trends in Ecology & Evolution*, 4(1):26–28.

Bhattacharya, S., Zhang, Q., and Andersen, M. E. (2011). A deterministic map of Waddington's epigenetic landscape for cell fate specification. *BMC Systems Biology*, 5(1):85.

Boyer, C. B. (1968). *A history of mathematics*. John Wiley & Sons.

Crawford, J. D. (1991). Introduction to bifurcation theory. *Reviews of Modern Physics*, 63(4):991–1037.

Czeisler, C. A. (1979). *Human circadian physiology: Internal organization of temperature, sleep-wake and neuroendocrine rhythms monitored in an environment free of time cues.* PhD thesis, US.

Dakos, V., Beninca, E., van Nes, E. H., Philippart, C. J. M., Scheffer, M., and Huisman, J. (2009). Interannual variability in species composition explained as seasonally entrained chaos. *Proceedings of the Royal Society B: Biological Sciences*, 276(1669):2871–2880.

Dakos, V., Carpenter, S. R., Brock, W. A., Ellison, A. M., Guttal, V., Ives, A. R., Kéfi, S., Livina, V., Seekell, D. A., van Nes, E. H., and Scheffer, M. (2012). Methods for detecting early warnings of critical transitions in time series illustrated using simulated ecological data. *PloS one*, 7(7):e41010.

Dakos, V., Carpenter, S. R., van Nes, E. H., and Scheffer, M. (2015). Resilience indicators: Prospects and limitations for early warnings of regime shifts. *Philosophical Transactions of the Royal Society B: Biological Sciences*, 370(1659):1–10.

d'Ortous de Mairan, J.-J. (1729). Observation botanique. *Histoire*

de l'Academie Royale des Sciences, 31:35–36.

Doveri, F., Scheffer, M., Rinaldi, S., Muratori, S., and Kuznetsov, Y. (1993). Seasonality and Chaos in a Plankton Fish Model. *Theoretical Population Biology*, 43(2):159–183.

Driever, S. M., van Nes, E. H., and Roijackers, R. M. (2005). Growth limitation of Lemna minor due to high plant density. *Aquatic Botany*, 81(3):245–251.

Edelstein-Keshet, L. (2005). *Mathematical Models in Biology*. Society for Industrial and Applied Mathematics.

Edwards, A. M. and Auger-Méthé, M. (2019). Some guidance on using mathematical notation in ecology. *Methods in Ecology and Evolution*, 10(1):92–99.

Elton, C. and Nicholson, M. (1942). The Ten-Year Cycle in Numbers of the Lynx in Canada. *The Journal of Animal Ecology*, 11(2):215.

Escher, M. C. (1960). Klimmen en dalen.

Escher, M. C. (1961). Waterval.

Fort, H. and Segura, A. (2018). Competition across diverse taxa: quantitative integration of theory and empirical research using global indices of competition. *Oikos*, 127(3):392–402.

Foster, R. G. and Kreitzman, L. (2017). *Circadian rhythms. A very short introduction*. Oxford University Press.

Freidlin, M. I. and Wentzell, A. D. (2012). *Random Perturbations of Dynamical Systems*, volume 260 of *Grundlehren der mathematischen Wissenschaften*. Springer Berlin Heidelberg, Berlin, Heidelberg.

Gilbert, S. F. (1991). Epigenetic landscaping: Waddington's use of

cell fate bifurcation diagrams. *Biology & Philosophy*, 6(2):135–154.

Glass, L. (2001). Synchronization and rhythmic processes in physiology. *Nature*, 410(6825):277–284.

Gottwald, G. A. and Melbourne, I. (2009). On the Implementation of the 0-1 Test for Chaos. *SIAM Journal on Applied Dynamical Systems*, 8(1):129–145.

Grimm, V. (2005). Pattern-Oriented Modeling of Agent-Based Complex Systems: Lessons from Ecology. *Science*, 310(5750):987–991.

Grimm, V., Berger, U., Bastiansen, F., Eliassen, S., Ginot, V., Giske, J., Goss-Custard, J., Grand, T., Heinz, S. K., Huse, G., Huth, A., Jepsen, J. U., Jørgensen, C., Mooij, W. M., Müller, B., Pe'er, G., Piou, C., Railsback, S. F., Robbins, A. M., Robbins, M. M., Rossmanith, E., Rüger, N., Strand, E., Souissi, S., Stillman, R. A., Vabø, R., Visser, U., and DeAngelis, D. L. (2006). A standard protocol for describing individual-based and agent-based models. *Ecological Modelling*, 198(1-2):115–126.

Guckenheimer, J. and Holmes, P. (2002). *Nonlinear Oscillations, Dynamical Systems, and Bifurcations of Vector Fields*. Applied Mathematical Sciences. Springer New York.

Hänggi, P., Talkner, P., and Borkovec, M. (1990). Reaction-rate theory: fifty years after Kramers. *Reviews of Modern Physics*, 62(2):251–341.

Hardin, G. (1960). The Competitive Exclusion Principle. *Science*, 131(3409):1292–1297.

Hawking, S. (1998). *A Brief History of Time*. Bantam Books.

Huang, S. (2012). The molecular and mathematical basis of

Waddington's epigenetic landscape: a framework for post-Darwinian biology? *BioEssays : news and reviews in molecular, cellular and developmental biology*, 34(2):149–57.

Hubbell, S. P. (2003). The Unified Neutral Theory of Biodiversity and Biogeography. *Biological Conservation*, 110(2):305.

Huisman, J., Johansson, A. M., Folmer, E. O., and Weissing, F. J. (2001). Towards a solution of the plankton paradox: the importance of physiology and life history. *Ecology Letters*, 4(5):408–411.

Huisman, J. and Weissing, F. J. (1999). Biodiversity of plankton by species oscillations and chaos. *Nature*, 402(6760):407–410.

Huisman, J. and Weissing, F. J. (2001). Fundamental Unpredictability in Multispecies Competition. *The American Naturalist*, 157(5):488–494.

Hutchinson, G. E. (1959). Homage to Santa Rosalia or Why Are There So Many Kinds of Animals? *The American Naturalist*, 93(870):145–159.

Hutchinson, G. E. (1961). The Paradox of the Plankton. *The American Naturalist*, 95(882):137–145.

Kelly, T. L., Neri, D. F., Grill, J. T., Ryman, D., Hunt, P. D., Dijk, D.-J., Shanahan, T. L., and Czeisler, C. A. (1999). Nonentrained Circadian Rhythms of Melatonin in Submariners Scheduled to an 18-Hour Day. *Journal of Biological Rhythms*, 14(3):190–196.

Kuramoto, Y. (1975). Self-entrainment of a population of coupled non-linear oscillators. In *International Symposium on Mathematical Problems in Theoretical Physics*, pages 420–422.

Kuznetsov, Y. A. (1998). *Elements of Applied Bifurcation Theory, Second Edition*. Springer.

Lagrange, J.-L. (1777). Remarques générales sur le mouvement de plusieurs corps qui s'attirent mutuellement enraison inverse des carrés des distances.

Li, C. and Wang, J. (2014). Landscape and flux reveal a new global view and physical quantification of mammalian cell cycle. *Proceedings of the National Academy of Sciences of the United States of America*, 111(39):14130–5.

Lorenz, E. N. (1963). Deterministic Nonperiodic Flow. *Journal of the Atmospheric Sciences*, 20(2):130–141.

Ludwig, D., Jones, D. D., and Holling, C. S. (1978). Qualitative Analysis of Insect Outbreak Systems: The Spruce Budworm and Forest. *The Journal of Animal Ecology*, 47(1):315.

Macarthur, R. and Levins, R. (1967). The Limiting Similarity, Convergence, and Divergence of Coexisting Species. *The American Naturalist*, 101(921):377–385.

Malthus, T. R. (1798). *An Essay on the Principle of Population*. London.

Marsden, J. E. and Tromba, A. (2003). *Vector calculus*. W.H. Freeman.

Marwick, B., Boettiger, C., and Mullen, L. (2018). Packaging Data Analytical Work Reproducibly Using R (and Friends). *The American Statistician*, 72(1):80–88.

Massoud, E. C., Huisman, J., Benincà, E., Dietze, M. C., Bouten, W., and Vrugt, J. A. (2018). Probing the limits of predictability: data assimilation of chaotic dynamics in complex food webs. *Ecology Letters*, 21(1):93–103.

May, R. M. (1974). Biological Populations with Nonoverlapping Generations: Stable Points, Stable Cycles, and Chaos. *Science*,

186(4164):645–647.

Murray, J. D. (2002). *Mathematical Biology*, volume 17 of *Interdisciplinary Applied Mathematics.* Springer New York, New York, NY, 3 edition.

Nelsen, R. B. (1993). *Proofs Without Words: Exercises in Visual Thinking.* Classroom resource materials. Mathematical Association of America.

Nolting, B. C. and Abbott, K. C. (2015). Balls, cups, and quasi-potentials: quantifying stability in stochastic systems. *Ecology*, pages 15–1047.1.

Nüst, D., Boettiger, C., and Marwick, B. (2018). How to Read a Research Compendium. arXiv:1806.09525.

Pawlowski, C. W. (2006). Dynamic Landscapes, Stability and Ecological Modeling. *Acta Biotheoretica*, 54(1):43–53.

Penrose, L. S. and Penrose, R. (1958). Impossible objects: A special type of visual illusion. *British Journal of Psychology*, 49(1):31–33.

Phillips, A. and Robinson, P. (2007). A Quantitative Model of Sleep-Wake Dynamics Based on the Physiology of the Brainstem Ascending Arousal System. *Journal of Biological Rhythms*, 22(2):167–179.

Pikovsky, A., Rosenblum, M., and Kurths, J. (2003). *Synchronization A Universal Concept in Nonlinear Sciences.* Cambridge University Press.

Press, W. H., Teukolsky, S. A., Vetterling, W. T., and Flannery, B. P. (2007). *Numerical Recipes: The Art of Scientific Computing.* Cambridge University Press, USA, 3 edition.

Querejeta, M. (2011). On the Eclipse of Thales, Cycles and Probabilities. Culture and Cosmos, Vol. 15, no. 1, Fall 2011, pp. 3-32.

Rijpma, J., Scheffer, M., and Rodríguez-Sánchez, P. (2020a). Gravity waves. Presented at microconvention MIR - WUR Art and Science.

Rijpma, J., Scheffer, M., and Rodríguez-Sánchez, P. (2020b). Interacting cycles. Presented at microconvention MIR - WUR Art and Science.

Rinaldi, S., Candaten, M., and Casagrandi, R. (2001). Evidence of peak-to-peak dynamics in ecology. *Ecology Letters*, 4(6):610–617.

Rodríguez-Sánchez, P. (2018). PabRod/Chaos-and-neutrality: Analysis script for "Neutral competition boosts chaos in food webs". 10.5281/zenodo.1319590.

Rodríguez-Sánchez, P. (2019). PabRod/rolldown: a package for computing quasipotentials. 10.5281/zenodo.2591550.

Rodríguez-Sánchez, P., van Nes, E. H., and Scheffer, M. (2018). Neutral competition boosts chaos in food webs. arXiv:1807.06901.

Rodríguez-Sánchez, P., van Nes, E. H., and Scheffer, M. (2020). Climbing Escher's stairs: A way to approximate stability landscapes in multidimensional systems. *PLOS Computational Biology*, 16(4):e1007788.

Rodríguez-Sánchez, P., van Nes, E. H., and Scheffer, M. (2020). Early warning signals for desynchronization in periodically forced systems. arXiv:2003.11595.

Rosenzweig, M. L. and MacArthur, R. H. (1963). Graphical Representation and Stability Conditions of Predator-Prey Interactions. *The American Naturalist*, 97(895):209–223.

Sandri, M. (1996). Numerical calculation of Lyapunov exponents. *The Mathematica Journal*.

Scheffer, M. (1991). Should we expect strange attractors behind plankton dynamics – and if so, should we bother? *Journal of Plankton Research*, 13(6):1291–1305.

Scheffer, M. (2009). *Critical Transitions in Nature and Society*. Princeton University Press.

Scheffer, M., Bascompte, J., Brock, W. a., Brovkin, V., Carpenter, S. R., Dakos, V., Held, H., van Nes, E. H., Rietkerk, M., and Sugihara, G. (2009). Early-warning signals for critical transitions. *Nature*, 461(7260):53–59.

Scheffer, M., Carpenter, S., Foley, J. a., Folke, C., and Walker, B. (2001). Catastrophic shifts in ecosystems. *Nature*, 413(6856):591–596.

Scheffer, M., Rinaldi, S., Huisman, J., and Weissing, F. J. (2003). Why plankton communities have no equilibrium: solutions to the paradox. *Hydrobiologia*, 491(1-3):9–18.

Scheffer, M. and van Nes, E. H. (2006). Self-organized similarity, the evolutionary emergence of groups of similar species. *Proceedings of the National Academy of Sciences*, 103(16):6230–6235.

Scheffer, M., van Nes, E. H., and Vergnon, R. (2018). Toward a unifying theory of biodiversity. *Proceedings of the National Academy of Sciences*, 115(4):201721114.

Schippers, P., Verschoor, A. M., Vos, M., and Mooij, W. M. (2001). Does "supersaturated coexistence" resolve the "paradox of the plankton"? *Ecology Letters*, 4(5):404–407.

Schnitzer, S. A., Klironomos, J. N., HilleRisLambers, J., Kinkel, L. L., Reich, P. B., Xiao, K., Rillig, M. C., Sikes, B. A., Callaway,

R. M., Mangan, S. A., Van Nes, E. H., and Scheffer, M. (2011). Soil microbes drive the classic plant diversity-productivity pattern. *Ecology*, 92(2):296–303.

Segura, A. M., Calliari, D., Kruk, C., Conde, D., Bonilla, S., and Fort, H. (2011). Emergent neutrality drives phytoplankton species coexistence. *Proceedings of the Royal Society B: Biological Sciences*, 278(1716):2355–2361.

Segura, A. M., Kruk, C., Calliari, D., García-Rodriguez, F., Conde, D., Widdicombe, C. E., and Fort, H. (2013). Competition drives clumpy species coexistence in estuarine phytoplankton. *Scientific Reports*, 3(1):1037.

Siffre, M. (1975). Six months alone in a cave. *National Geographic*, 147(3):426–435.

Simmons, G. F. (1991). *Differential Equations With Applications and Historical Notes*. McGraw-Hill Education, 2 edition.

Simmons, G. F. (1996). *Calculus with analytic geometry*. McGraw-Hill.

Strang, G. (2006). *Linear algebra and its applications*. Thomson, Brooks/Cole, Belmont, CA.

Strogatz, S. H. (1987). Human sleep and circadian rhythms: a simple model based on two coupled oscillators. *Journal of Mathematical Biology*, 25(3):327–347.

Strogatz, S. H. (1994). *Nonlinear Dynamics And Chaos: With Applications To Physics, Biology, Chemistry And Engineering*.

Strogatz, S. H. (2000). From Kuramoto to Crawford: exploring the onset of synchronization in populations of coupled oscillators. *Physica D: Nonlinear Phenomena*, 143(1):1–20.

Strogatz, S. H. (2003). *SYNC: The Emerging Science of Spontaneous Order*. Penguin Books.

Strogatz, S. H. and Stewart, I. (1993). Coupled oscillators and biological synchronization. 10.1038/scientificamerican1293-102.

Tang, Y., Yuan, R., Wang, G., Zhu, X., and Ao, P. (2017). Potential landscape of high dimensional nonlinear stochastic dynamics with large noise. *Scientific Reports*, 7(1).

Thebault, E. and Fontaine, C. (2010). Stability of Ecological Communities and the Architecture of Mutualistic and Trophic Networks. *Science*, 329(5993):853–856.

van de Leemput, I. A., Hughes, T. P., van Nes, E. H., and Scheffer, M. (2016). Multiple feedbacks and the prevalence of alternate stable states on coral reefs. *Coral Reefs*, 35(3):857–865.

van Dixhoorn, I., de Mol, R., van der Werf, J., van Mourik, S., and van Reenen, C. (2018). Indicators of resilience during the transition period in dairy cows: A case study. *Journal of Dairy Science*, 101(11):10271–10282.

Van Nes, E. H., Rip, W. J., and Scheffer, M. (2007). A Theory for Cyclic Shifts between Alternative States in Shallow Lakes. *Ecosystems*, 10(1):17–28.

van Nes, E. H. and Scheffer, M. (2004). Large Species Shifts Triggered by Small Forces. *The American Naturalist*, 164(2):255–266.

Van Nes, E. H. and Scheffer, M. (2007). Slow recovery from perturbations as a generic indicator of a nearby catastrophic shift. *American Naturalist*, 169(6):738–747.

Vandermeer, J. (1993). Loose Coupling of Predator-Prey Cycles: Entrainment, Chaos, and Intermittency in the Classic Macarthur Consumer-Resource Equations. *The American Natu-*

ralist, 141(5):687–716.

Vandermeer, J., Stone, L., and Blasius, B. (2001). Categories of chaos and fractal basin boundaries in forced predator-prey models. *Chaos, solitons and fractals*, 12(2):265–276.

Veilleux, B. G. (1979). An Analysis of the Predatory Interaction Between Paramecium and Didinium. *The Journal of Animal Ecology*, 48(3):787.

Vergnon, R., Leijs, R., van Nes, E. H., and Scheffer, M. (2013). Repeated Parallel Evolution Reveals Limiting Similarity in Subterranean Diving Beetles. *The American Naturalist*, 182(1):67–75.

Verhulst, P. (1838). Notice sur la loi que la population poursuit dans son accroisse-ment. *Corresp. Math. Phys.*, 10:113–121.

Volterra, V. (1926). Variazioni e fluttuazioni del numero d'individui in specie animali conviventi. *Memorie della R. Accademia dei Lincei*, 6(2):31–113.

von Helmholtz, H. (1858). Über Integrale der hydrodynamischen Gleichungen, welcher der Wirbelbewegungen entsprechen. *Journal für die reine und angewandte Mathematik*, 55:25–55.

Wang, J. (2011). Potential Landscape and Flux Framework of Nonequilibrium Biological Networks. *Annual Reports in Computational Chemistry*, 7:3–37.

Wangsness, R. K. (1986). *Electromagnetic fields*. Wiley.

Wilson, G., Aruliah, D. A., Brown, C. T., Chue Hong, N. P., Davis, M., Guy, R. T., Haddock, S. H. D., Huff, K. D., Mitchell, I. M., Plumbley, M. D., Waugh, B., White, E. P., and Wilson, P. (2014). Best Practices for Scientific Computing. *PLoS Biology*, 12(1):e1001745.

Winter, C., Bouvier, T., Weinbauer, M. G., and Thingstad, T. F. (2010). Trade-Offs between Competition and Defense Specialists among Unicellular Planktonic Organisms: the "Killing the Winner" Hypothesis Revisited. *Microbiology and Molecular Biology Reviews*, 74(1):42–57.

Wissel, C. (1984). A universal law of the characteristic return time near thresholds. *Oecologia*, 65(1):101–107.

Wolf, A., Swift, J. B., Swinney, H. L., and Vastano, J. A. (1985). Determining Lyapunov exponents from a time series. *Physica D: Nonlinear Phenomena*, 16(3):285–317.

Zhao, Q., Van den Brink, P. J., Carpentier, C., Wang, Y. X. G., Rodríguez-Sánchez, P., Xu, C., Vollbrecht, S., Gillissen, F., Vollebregt, M., Wang, S., and De Laender, F. (2019). Horizontal and vertical diversity jointly shape food web stability against small and large perturbations. *Ecology Letters*, page ele.13282.

Zhou, J. X., Aliyu, M. D. S., Aurell, E., and Huang, S. (2012a). Quasi-potential landscape in complex multi-stable systems. *Journal of The Royal Society Interface*, 9(77):3539–3553.

Zhou, J. X., Aliyu, M. D. S., Aurell, E., and Huang, S. (2012b). Quasi-potential landscape in complex multi-stable systems. *Journal of The Royal Society Interface*, 9(77):3539–3553.

Zhou, P. and Li, T. (2016). Construction of the landscape for multistable systems: Potential landscape, quasi-potential, A-type integral and beyond. *Journal of Chemical Physics*, 144(9).

Summary

Cyclic phenomena in biology are enormously varied. The periods of biological cycles range from years, such as those of oscillating plankton populations, to less than a second, such as those of neuron firing. Despite those differences, the mathematical analysis of apparently disparate biological cycles can often be very similar. In **chapter 1** I present the mathematical tools and ideas used along this thesis, together with the different biological problems I applied them to.

In **chapter 2** we address a classical problem of ecology, that of the *paradox of the plankton*. Particularly, we show that there is a link between two of the proposed hypotheses out of the paradox, that of super-saturated coexistence due to non-equilibrium dynamics and Hubbell's neutral theory. We do this by analyzing a family of simulated ecosystems with two trophic levels, we show that near-neutrality of competition at the prey's level, in the presence of interactions with natural enemies, increases the chances of developing chaotic or cyclic dynamics. Additionally, we measured a correlation between the chances of developing chaotic dynamics and an increase in biodiversity.

In biological literature the potential, a concept from physics, is com-

monly used to explain the stability properties of dynamical systems. In biology potentials are commonly called stability landscapes, marble-in-a-cup diagrams or Waddington's landscapes. They have proven to be particularly useful to communicate complicated concepts from dynamical systems theory to non-expert audiences, such as bifurcation, basin of attraction or hysteresis. These diagrams work well in one-dimensional systems where the state is described by a single variable. Unfortunately, when we try to use these pictures for systems with two or more state variables we find a critical limitation: potentials cannot exist unless the system verifies certain constrains. This limitation rules out most multidimensional biological systems, and is particularly problematic in systems with cyclic dynamics and/or in systems with asymmetric interactions, a common situation in ecological models. In **chapter 3** we explain the reason why a potential may fail to exist without using heavy mathematical weaponry. We found a pedagogical analogy in the world of art, particularly in M.C. Escher's paintings of impossible objects. As a partial solution to the problem, we introduced a simple and efficient algorithm that takes into account the abovementioned limitations, providing the best quasi-potential candidate plus an error map indicating the regions of the phase space where it is safe to use it.

Biological phenomena so diverse as heartbeat, sleep or menstruation have a common characteristic: they all have the capacity of synchronizing to a rhythm imposed externally. Often this capacity is of paramount importance, and a lack of it can translate into disease or malfunctioning. Different conditions such as epilepsy, insomnia or arrhythmia are clearly related with a failure in synchronization. A straightforward biological question is: *can we forecast transitions between synchronized and desynchronized states in a bio-*

logical system? In **chapter 4** we developed forecasting methods for this kind of transitions. Particularly, we show that after an appropriate coordinate transformation, we can expect the phenomenon of critical slowing down to take place. Our method is complex, cannot predict too sudden regime shifts, and requires high-quality time series. Despite these limitations, we are optimistic about its potential. Particularly, we are looking at the growth in popularity of the health-monitoring wearables with great optimism.

In **chapter 5** I reflect on the results presented in this thesis and, inevitably, their limitations. In addition, I reflect on my experiences in this endeavor of multidisciplinary research, and highlight some of the challenges of communication and the role of software in science.

Acknowledgements

On 6th July 2015, Marten Scheffer and Egbert van Nes made a decision that deeply changed my life. They decided to trust the nerdy physicist I was (who do I want to fool?, I still am), and offered me a PhD position at their department. Two months later, I moved from Spain to The Netherlands carrying only the contents of a travel bag, and quite literally started a new life.

The transition and culture shock would have been hard without the kindness of my friends and colleagues at Wageningen University. Special mention to the infinite generosity of Sebastian Bathiany, who offered me a room at his apartment only after a 15 minutes coffee talk, and to Sanne van den Berg, the responsible of extending my plans to stay in The Netherlands from 4 years to indefinite. In normal circumstances (this includes the absence of a global pandemic), I would have asked them both to be my paranymphs.

The present thesis wouldn't have been possible without the enormous momentum gained during my undergraduate years at the Physics School of *Universidad Complutense de Madrid*. I was lucky enough to have lots of great teachers, so many, that trying to mention all of them would be a mistake. Nevertheless, it would also be a mistake not to mention two names who shone with blinding light:

Isabel Gonzalo Fonrodona and Gabriel Álvarez Galindo. They can really do magic with no more than a piece of chalk and a blackboard, and some of their lessons still resonate in my head more than a decade later.

Those undergraduate years, the most intense and challenging of my life, were also deeply influenced by the unique personalities of my friends Enrique Benito Matías, Alejandro Remeseiro Fernández, Fernando Gutiérrez Alonso and José Ramón Álvarez Layna. Our marathonian study sessions at the library could have become a traumatic memory without their stories about semiconductors, remote Pacific islands, Roman law or the Scottish Enlightenment.

The lessons learned during my stage as an engineer at *Indizen Optical Technologies* proved to be extremely valuable in these years of research. This thesis would have been very different without the mentorship provided by Eduardo Pascual Ramírez and Antonio Quiroga Mellado in the period 2012-2015.

Science communication had a crucial but hidden role during the writing of this thesis. It was the close contact with the science communication group *Naukas* what kept my passion for knowledge alive, and what ultimately motivated me to abandon a comfortable engineering position in Madrid and move back to academia. In the moments of frustration, an unavoidable part in the process of writing a thesis, it was this community that most effectively cheered me up. For these and many other reasons this thesis is dedicated to them. Thanks for so much.

About the author

Pablo Rodríguez-Sánchez was born in Guadalajara, Spain, in 1984. His childhood, marked by an interest in dinosaurs, sharks and monkeys, was as nerdy as one can imagine. Although he had lots of difficulties with math during high school, he studied theoretical physics at *Universidad Complutense de Madrid*. The fact that he graduated tells a lot about the power of education and the patience of his teachers. In the year 2012 he wrote his master's thesis on Artificial Vision. This master's thesis gave him the opportunity to work in the optical industry. Between 2012 and 2015, he worked as an engineer at the research and development department of *Indizen Optical Technologies*, a lens design company.

In the period between 2015 and 2019, Pablo was enrolled as a Marie Curie predoctoral researcher in the CRITICS[1] Innovative Training Network. Coordinated by Imperial College London, this network had nodes all around Europe, and Pablo was based at the one in Wageningen University, under the supervision of Marten Scheffer and Egbert van Nes. The present thesis is the main outcome of the work performed during this period.

Pablo is strongly involved with several science teaching and sci-

---

[1]CRItical Transitions In Complex Systems

ence communication projects. Since 2011, he has collaborated with newspapers, radio and TV shows, and gave multiple talks in theaters, ranging from musicals to stand-up comedy. He's a member of the GeoGebra Community, devoted to the development of interactive applets for teaching mathematics. He's also a very active member of Naukas.com, which with around 2 million visitors per month is one of the largest science communication platforms in Spanish language. With the patronage of Naukas, he has published more than 90 blog entries about science, most of them at his personal blog, *Fuga de cerebros* / Brain drain[2].

Since autumn 2019, Pablo works as a research engineer at the *Netherlands eScience Center*, where he combines three of his main interests: science communication, applied mathematics and scientific computing.

---

[2]fuga.naukas.com

Peer-reviewed journal publications

- Zhao, Q., Van den Brink, P. J., Carpentier, C., Wang, Y. X. G., Rodríguez-Sánchez, P., Xu, C., Vollbrecht, S., Gillissen, F., Vollebregt, M., Wang, S., and De Laender, F. (2019). Horizontal and vertical diversity jointly shape food web stability against small and large perturbations. *Ecology Letters*, page ele.13282

- Rodríguez-Sánchez, P., van Nes, E. H., and Scheffer, M. (2020). Climbing Escher's stairs: A way to approximate stability landscapes in multidimensional systems. *PLOS Computational Biology*, 16(4):e1007788

Submitted manuscripts

- Rodríguez-Sánchez, P., van Nes, E. H., and Scheffer, M. (2018). Neutral competition boosts chaos in food webs. arXiv:1807.06901

- Rodríguez-Sánchez, P., van Nes, E. H., and Scheffer, M. (2020). Early warning signals for desynchronization in periodically forced systems. arXiv:2003.11595

Book chapter

- Bathiany, S., van der Bolt, B., Rodríguez-Sánchez, P., and Mirza, U. (2018). *Tipping points, zo werken ze!* Netherlands Earths System Science Centre

Scientific software

- Rodríguez-Sánchez, P. (2018). PabRod/Chaos-and-neutrality: Analysis script for "Neutral competition boosts chaos in food webs". 10.5281/zenodo.1319590

- Rodríguez-Sánchez, P. (2019). PabRod/rolldown: a package for computing quasipotentials. 10.5281/zenodo.2591550

Artwork

- Rijpma, J., Scheffer, M., and Rodríguez-Sánchez, P. (2020a). Gravity waves. Presented at microconvention MIR - WUR Art and Science

- Rijpma, J., Scheffer, M., and Rodríguez-Sánchez, P. (2020b). Interacting cycles. Presented at microconvention MIR - WUR Art and Science

Science communication

I've produced around 50 blog entries and 5 public talks during my predoctoral period. The whole list can be accessed at `pabrod.github.io`.

SENSE

*Netherlands Research School for the
Socio-Economic and Natural Sciences of the Environment*

D I P L O M A

for specialised PhD training

The Netherlands research school for the
Socio-Economic and Natural Sciences of the Environment
(SENSE) declares that

Pablo Rodríguez-Sánchez

born on 13 October 1984 in Guadalajara, Spain

has successfully fulfilled all requirements of the
educational PhD programme of SENSE.

Wageningen, 15 June 2020

The Chairman of the SENSE board   the SENSE Director of Education

Prof. dr. Martin Wassen   Dr. Ad van Dommelen

The SENSE Research School has been accredited by the Royal Netherlands Academy of Arts and Sciences (KNAW)

K O N I N K L I J K E   N E D E R L A N D S E
A K A D E M I E   V A N   W E T E N S C H A P P E N

The SENSE Research School declares that **Pablo Rodríguez-Sánchez** has successfully fulfilled
all requirements of the educational PhD programme of SENSE with a
work load of 65.8 EC, including the following activities:

SENSE PhD Courses

o   Environmental research in context (2016)
o   A2: 'Outreach article: mappingignorance.org/2016/05/09/the-sound-of-chaos' (2016)

Other PhD and Advanced MSc Courses

o   Scientific publishing, Wageningen Graduate Schools (2016)
o   Dynamics Days 2016, National Technical University of Athens (2016)
o   High Performance and Advanced High Performance Cluster course (2017)
o   CRITICS schools and workshops (2016-2018)
o   From working code to software package, University Utrecht, The Netherlands (2019)

External training at a foreign research institute

o   CERES summer school, École Normale Supérieure, France (2016)
o   GeoGebra Global Gathering, Johannes Kepler University, Austria (2017)
o   Mathematics and industry, Imperial College London, United Kingdom (2018)

Selection of Management and Didactic Skills Training

o   Teaching in PhD seminars 'Crash course on linear algebra' (2016), 'An introduction to
    Unit Testing with Matlab' (2017), ' An introduction to Git and GitHub' (2017) and 'Quick
    introduction to partial differential equations' (2018)
o   Teaching in three MSc courses 'Ecology, classic and trends' (2016), 'Theoretical ecology'
    (2017), 'Practical aquatic ecology and water management' (2018)
o   Activities and promotion coordinator at Marie Curie Alumni Association (2016-2017)
o   Organization of the CRITICS spring workshop and school 2017

Selection of Oral Presentations

o   *Competition, diversity and the benefits of chaos. Innovations and applications.*
    Mathematics and industry. Jul 12th 2018. Imperial College London, United Kingdom.
o   *Neutral competition and chaos, an example of reproducible research.* CRITICS Summer
    workshop. Aug 29th 2018. University College Cork. Ireland.

Other societal impact

o   Published 47 blog entries about science (full list at pabrod.github.io)
o   Interviews in newspaper (Vozpópuli, 2015 and 2017) and radio (RNE, 2018 and 2019)

SENSE coordinator PhD education

Dr. ir. Peter Vermeulen